

Floating single-lift installation of WTGs equipped with C1 Wedge Connection

Modelling and assessment of stability
and operability during mating operation

Master Thesis
Stefan Hoogervorst

Floating single-lift installation of WTGs equipped with C1 Wedge Connection

Modelling and assessment of stability
and operability during mating operation

by

Stefan Hoogervorst

to obtain the degree of Master of Science
at the Delft University of Technology,
to be defended publicly on Monday July 8, 2024 at 14:00 PM.

Student Number

4720571

Committee Chair	A. Metrikine
TU Supervisor	J. Hoving
HMC Supervisor	T. Ouwehand
HMC Supervisor	M. Veldhuizen
C1 Supervisor	J. Winkes
Project Duration	Sep. 2023 - Jul. 2024
Faculty	Faculty of Mechanical Engineering, Delft

Cover: Single-lift WTG installation render by HMC (Modified)
Style: TU Delft Report Style, with modifications by Daan Zwaneveld

An electronic version of this thesis is available at <http://repository.tudelft.nl/>.

*“Es ist nicht genug, zu wissen, man muß auch anwenden;
es ist nicht genug, zu wollen, man muß auch tun.”
“In der Beschränkung zeigt sich erst der Meister.”*

Johann Wolfgang von Goethe

Freely translated as:

*“Knowing is not enough; we must apply.
Willing is not enough; we must do.”
“The master shows himself in his limitation”*

Johann Wolfgang von Goethe

Preface

This report is written as part of the Graduation Project (OE54035) at the Delft University of Technology (TU Delft) to fulfil the requirements for the MSc degree in Offshore and Dredging Engineering. This report is constructed as documentation of the master thesis project including the literature research, research setup, results, discussions, and conclusions. The writing of this master thesis was done with support of Heerema Marine Contractors and C1 Connections.

I would like to thank all the people involved in my guidance and supervision, including, but not limited to; my daily supervisors Ir. Tim Ouwehand (HMC), Ir. Maarten Veldhuizen (HMC) and Ir. Jasper Winkes (C1 Connections), my university supervisor Ir. Jeroen Hoving (TU Delft) and graduation committee chair Prof.dr. Andrei Metrikine (TU Delft). Thank you for the valuable insights and discussions over the last months.

Apart from my direct supervisors, I also would like to express my gratitude to all the people of HMC's Product Development team. It is astonishing to see how much knowledge there is within the team and company. It was interesting and educating to confer about the offshore industry and speculate about the future. Lastly, I would like to give a shout-out to my father, who, although he does not have an offshore background, was my most dedicated peer-reviewer. Whatever my future may hold, I really enjoyed working on a project related to the energy transition and look forward toward working in this business.

*Stefan Hoogervorst
Delft, July 2024*

Abstract

This master thesis proposes a method for assessment of the allowable sea states for the single-lift installation of a Wind Turbine Generator (WTG) with a Quick Connection System (QCS) on a bottom-founded support structure with focus on the landing (mating) operation. The thesis also determines the operability of this installation and examines how it could be optimised.

Due to an increase of WTG size, the current lifting height of state-of-the-art floating Heavy Lift Vessels (HLVs) is insufficient to lift the WTG components to the required installation height. To overcome this limitation, and to further reduce installation time, new installation techniques are being developed. The single-lift installation methodology; where the WTG is lifted at the bottom of the WTG and just above the combined Centre of Gravity, in combination with the C1 Wedge Connection; a newly developed connection with a high ULS and FLS strength and large installation tolerances, forms a promising setup for dual crane HLVs. The Quick Connection System (QCS) of the C1 Wedge Connection can create a temporary connection able to provide sufficient restoring moment, required to keep the WTG upright. In this thesis the operability of a floating single-lift installation of a WTG with a QCS is determined and optimised. The performance of the QCS is compared to alternative connections and design improvements for the operation are proposed.

Two computer simulation models are built and compared, where-after the most promising model is expanded and further developed. This OrcaFlex model includes wave and wind loading in in-plane directions (3 Degree of Freedom directions). Nine critical events and limiting parameters are identified, containing motion limits of the WTG and QCS limits.

The results show that the operability for the base case (no Heave Compensation and strict limiting parameters) is negligible. In all cases assessed, the time required to activate the QCS turned out to be the governing limit. If heave compensation is incorporated and some parameters are altered (e.g. increasing the allowed WTG rotation or the maximum C1 Wedge Connection gap between the flanges) the operability can be increased to become feasible for wave peak periods up to $T_p < 9s$ and significant wave heights $H_s < 2m$. In this optimised situation the activation of the QCS is the governing installation activity, with respect to the load transfer phase situation. Here, a minimum of 16 QCS Wedges are required for the load transfer phase and the pre-activation load transfer should be around 20% of the WTG static weight. For $H_s < 1.4m$, the mating operation was found to be feasible without a QCS. Here, it should be noted that optimal wind loading was assumed, and zero DP drift is incorporated.

It is recommended to expand the model to include all 6 DOF directions to verify if these results are still valid for non-optimal wind loading conditions. Furthermore, with these results, a study could be set up to determine the economic feasibility of this installation methodology. Such a study is essential as the economic viability determines the adoption of the technology.

Contents

Preface	ii
Abstract	iii
1 Introduction	1
1.1 Offshore wind energy market	1
1.2 Problem Statement	4
1.3 Research objective	5
1.3.1 Research Goal	5
1.3.2 Scope	6
1.3.3 Main Assumptions	6
1.4 Research Methodology	6
1.4.1 Approach	6
1.4.2 Assessment Criteria	7
1.4.3 Outline of Report	7
2 State of the Art Offshore Structures and Equipment	8
2.1 Offshore Wind Turbines	8
2.1.1 Bottom-Founded Support Structures	9
2.1.2 Floating Support Structures	9
2.2 Wind Turbine Installation Vessels	10
2.2.1 Jack-up Installation Vessel	10
2.2.2 Floating Installation vessel	12
2.3 Installation Methodology	12
2.4 Steel Rigging Wires	17
2.5 Structural Connections between Turbine Tower and Support Structure	18
2.5.1 Bolted L-flange Connection	18
2.5.2 Slip Joint Connection	20
2.5.3 C1 Wedge Connection	20
2.6 Heave Compensation for crane loads	22
2.6.1 Passive Heave Compensation (PHC)	22
2.6.2 Active Heave Compensation (AHC)	23
2.6.3 Comparison and variations of Heave Compensation	25
2.7 Intermediate Findings Offshore Structures and Equipment	27
3 State of the Art Modelling of Dynamics of WTG during Installation	28
3.1 Wind Loading	28
3.1.1 Variations in Time	28
3.1.2 Short-term Variations	29
3.1.3 Variations in Space	29
3.1.4 Lift and Drag	30
3.2 Wave Loading	31
3.2.1 Description of Waves	31
3.2.2 Wave Spectra	33
3.3 Vessel Motions	34
3.3.1 Hydromechanics	34
3.3.2 Response for Regular Waves	35
3.4 Operational Limits for Installations	36
3.5 Stability of the WTG	36
3.6 Modelling Software	38
3.7 Intermediate Findings Literature Research	38

4	Fundamental Models for WTG installation	42
4.1	Model Development	42
4.1.1	Installation Procedure	42
4.1.2	Lifting Configuration	43
4.1.3	Environmental Loading Incorporated	46
4.1.4	Dynamic Simulations	47
4.2	Python Model Setup	48
4.3	Python Model Results	50
4.4	Fundamental OrcaFlex Model Setup	53
4.5	Fundamental OrcaFlex Model Results	54
4.6	Comparison and Verification of Fundamental Models	57
5	Enhanced OrcaFlex Model	59
5.1	Expansions in Enhanced OrcaFlex Model	59
5.2	Limiting Parameters	61
5.3	Verification Techniques	64
5.4	Assumptions and Limitations	64
5.5	Model Design Summary	65
6	Results and Discussion of Enhanced Model	67
6.1	Results Situation 2 (before QCS activation)	67
6.2	Results Situation 3 (after QCS activation)	69
6.3	Sensitivity Study and Optimisation of Operability	75
6.3.1	Sensitivity of Limiting Parameters	75
6.3.2	Sensitivity of Input Parameters	77
6.3.3	Optimised Operability	84
6.4	Validity and Reliability	84
6.4.1	Enhanced OrcaFlex Model	84
6.4.2	Limiting Parameters	85
6.4.3	Operability Plotting	86
6.4.4	Comparison to Similar Research	87
7	Conclusions and Recommendations	88
7.1	Conclusions	88
7.2	Recommendations	89
7.2.1	Model Expansions	89
7.2.2	Elaborations besides Installation Modelling	90
	References	92
A	Heerema Marine Contractors	99
A.1	History	99
A.2	Fleet	99
A.3	Present day	101
B	LiftDyn description leaflet	102
C	Literature Analysis	104
C.1	Qualitative analysis	104
C.2	Quantitative analysis	104
D	Equation of Motion Python Model	106
E	LiftDyn input model	112
E.1	Model Input	112
E.2	Model Output	112
	Nomenclature	113
	List of Figures	119
	List of Tables	120

1

Introduction

This chapter provides an introduction to the offshore wind market and to this master thesis. The offshore wind energy market is described to set the scene under which the thesis is written. The introduction explains why the thesis is written and how. This includes the problem statement, research objectives, research questions, and the outline of the report.

1.1. Offshore wind energy market

Over the last decades wind energy has developed from a small local energy supplying technology to an energy source of global significance. With a Compound Annual Growth Rate (CAGR) of 38.5% for offshore wind between the years 2000 and 2018, the growth did not seem to have a limit [53]. But as inflation skyrocketed in 2022 and wind turbine costs increased by up to 40% over the last two years, investments stagnated [110]. Not a single commercial scale offshore wind farm reached a final investment decision (FID) in Europe in 2022 [109]. The increase in costs even resulted in Vattenfall to stop development of its British Norfolk Boreas offshore wind project [100], Orsted to cancel the offshore wind projects Ocean Wind 1 & 2 on the US east coast [69] and BP & Equinor to terminate the Empire Wind 2 offtake agreement [10].

This practice stands in sharp contrast to the vision of most western countries to heavily invest in offshore wind energy. The Netherlands, for example, almost doubled their offshore wind ambition for 2030 from 11.5 to 21 Gigawatt (GW) of installed capacity [66]. Since the beginning of the war in Ukraine in 2023, countries worldwide have aimed to increase energy independence. Producing clean energy locally is empowered by plans like the IRA and REPowerEU. The IRA is the largest piece of federal legislation in the United States (US) to ever address climate change and energy. The IRA contains a package worth 400 billion US dollars of stimulating measures to make the US economy and infrastructure sustainable [51, 83]. RePowerEU is a plan of the European Union (EU) to accelerate the energy transition and become completely independent of Russian energy supply. RePowerEU aims at an installed offshore wind capacity in the EU of 90 GW in 2030 and 300 GW in 2050 (compared to 28 GW in 2021) [82].

A quick calculation will show that the European goal is overly optimistic. The aim is to install 140.8 GW of offshore wind capacity between 2022 and 2031 [108]. This means an average of 14 1GW wind farms installed each year. With the current wind farm installation project timeline this will be a great challenge. If we choose a progressive turbine size of 15 MW on average and a water depth of 50 meters, we can estimate the current fleet able to install these turbines. Figure 1.1 shows an overview of the current fleet of crane vessels able to install large wind turbines. The vessels in the green area are expected to be able to install 15MW turbines. Currently there exist 13 of these and including the 7 extra planned (excluding the upgraded vessels) this results in 20 vessels able to install the 15MW turbines. Assuming the European market is able to charter half of these vessels each year, each vessel will need to install an average of 94 turbines per year (<4 vessel days per WTG) to reach this target (without mentioning the required balance of plant for all these wind farms). This is an optimistic number looking

at the current industry practice of an average of 5 vessel days required per Wind Turbine Generator (WTG) installation ¹ when not taking into account seasonal changes in installation rate [90]. Looking at the total installed capacity over the last years in Northern Europe, a similar trend can be discovered (see Fig. 1.2). The total installed capacity between 2016 and 2024 varies between 2 and 4 GW/year, without showing any clear increasing trend. This hindcast data is far from the desired 14 GW/year on average until 2031.

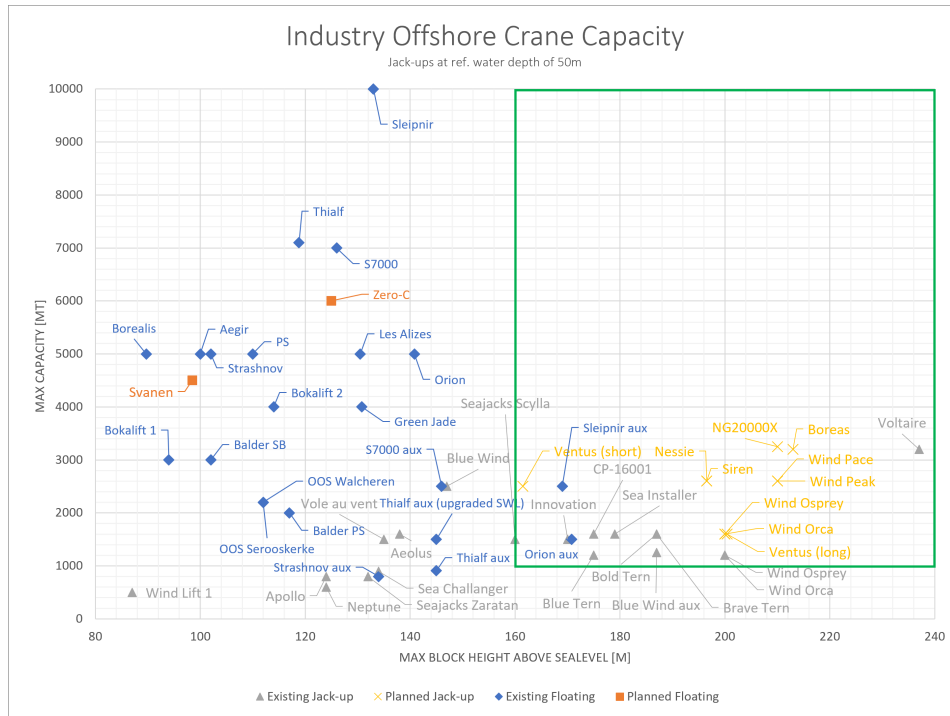


Figure 1.1: Selection of the offshore wind industry heavy lift crane vessel capacity. The vessels in the green area are estimated to be able to install 15MW turbines.

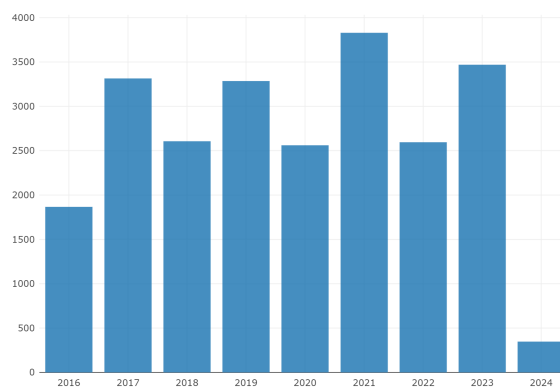


Figure 1.2: Total installed WTG capacity, in megawatts, in Northern Europe between 2016 and 2024. Note that the 2024 data are not complete, since not all 2024 data is available [90].

To achieve the ambitious goals of the EU, it is imperative to create an attractive market that reduces the investment risk in the offshore wind sector and its supply chain. The past few years this desired effect has not been achieved, resulting in lower amounts of newly installed MWs for the upcoming years (see figure 1.3). Whether the predicted increase after 2025 will become reality will depend on the feasibility of future wind farms. This depends on factors such as Levelized Cost Of Electricity (LCOE),

¹including transit and loadout

auction design, increase in WTG scale, design optimisation and developments in the floating wind sector.

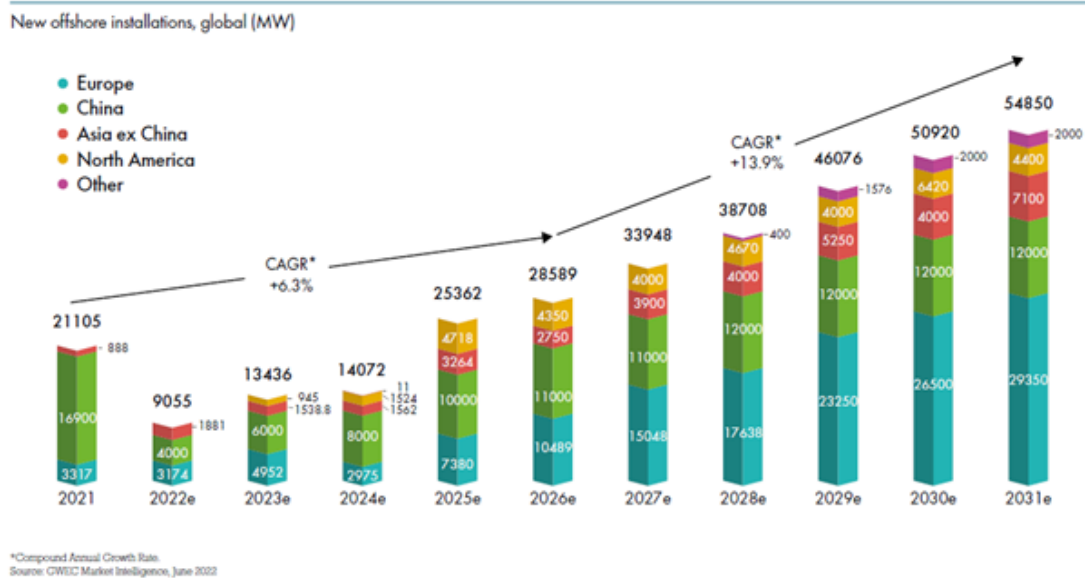


Figure 1.3: New offshore installations, global, in megawatts [108].

Especially scale increase of WTGs was a driver in reducing the investment cost (and thus LCOE) over the last decade. With sizes growing to the limits of equipment and installation vessel size, huge investments are required to install bigger turbines. Besides, the benefit of scale increase levels off when the scale increases: i.e. if you want to build a 500MW wind farm, a turbine scale increase from 1 MW to 2 MW reduces the number of turbines needed by 50%. If the turbine scale is increased from 14 MW to 15 MW, the number of turbines is only decreased by about 7%. These decreasing cost savings are accompanied by increasing structural costs to accommodate larger bending loads on larger rotors. This can be explained by the fact that the induced bending loads increase cubically with increasing rotor diameter, while the WTG's rated capacity only increases quadratically with rotor diameter. Overall, this results in the WTG cost per MW to increase for future (bigger) WTGs [68]. Even when taking into account the cost reduction because of fewer turbines required, the LCOE increases for WTGs with a greater rated capacity [68].

In the same report, DNV states that there are no technical barriers to limit further growth of turbine rating, but that numerical analysis shows there is no LCOE decrease with increasing turbine capacity rating. Therefore, it expects the growth in turbine size to slow down over the coming years. Original Equipment Manufacturers (OEMs) are calling for a standardised turbine size and to optimize this design [49]. DNV expects the largest cost reduction can be achieved by industry learning and standardisation in the fabrication process [68]. Also, the focus should shift from an eternal search of reducing LCOE to circularity of the offshore wind industry and nature inclusiveness, according to the ex-CEO of Siemens Gamesa David Molenaar [49]. Nevertheless, WTG size is still increasing, as turbine size increase is associated with technical development.

The market has improved over the first half of 2023. Six projects have reached FID totalling 5 GW of extra capacity [110]. One of the rapidly growing new sectors is the floating wind industry, exemplified by the completion of the Hywind Tampen wind farm, which nearly doubled Europe's installed floating wind energy capacity from 113 to 208 MW [110]. Although this is negligible to the bottom-fixed market, this is just the beginning of floating wind. Several GWs are under development in the UK and France is auctioning a 250 MW wind farm off the coast of Brittany. It is expected that Europe will have 3-4 GW of floating wind energy in operation in 2030 [110]. Although this capacity is still marginal compared to the bottom-fixed capacity planned until 2030, it is a big ramp up from its current size. Therefore, the

industry urges the EU to invest in up-scaling of the supply chain instead of only funding innovation. A part of the supply chain is the fleet of installation vessels, capable of installing the WTGs offshore. As shown in Figure 1.1, only a small portion of the current fleet is expected to be able to install large WTGs (>15 MW). Next to investments in larger installation vessels, options should be explored to repurpose other installation vessels to be able to install (part of) these larger WTGs.

1.2. Problem Statement

The development of bigger Offshore Wind Turbines (OWTs) is estimated to reach the historical turbine size value of 25 MW [68, 97]. This scale increase will have numerous effects on the design, manufacturing, and installation processes. As outlined in the previous paragraph, a shortage of installation vessels capable of installing the next generation turbines is one of the challenges. As swift installation of these huge turbines is required (see Section 1.1) to keep cost down and reach the set capacity targets for 2030 and 2050, fast and large installation equipment is required. Re-purposing floating Heavy lifting vessels (HLVs) now mainly used in the Oil & Gas industry to the Offshore Wind industry is a solution for the vessel shortage. These vessels already have the required lifting capacity to install enormous turbines. The weight of towers and Nacelle Hub Assemblies (NHAs) is expected to pass 1000 mT and therefore become a challenge to install for most conventional jack-up installation vessels. Faster installations can be achieved by floating HLVs as the time-consuming operation of jacking up and down is not required for floating vessels. A limitation of some floating HLVs is the maximal crane lifting height, although dual crane lifting configurations could surpass this problem.

A consequence of installing WTGs from a floating vessel is that relative motions will occur between the vessel and the intended load set down area (support structure). WTG installations with floating vessels are quite rare and thus little experience has been gathered. Especially when lifting heavy loads with a high Centre of Gravity (CoG), which is the case for single-lift WTG installations, relative motions can become critical to the stability of the load and vessel. To account for this, technologies have been developed such as ballasting systems, Dynamic Positioning (DP) systems, Heave Compensation (HC) systems in cranes and Guide & Bumper (G&B) systems. Their mutual goal is to gain control of the motions related to the vessel and load during installations. The challenge in using these systems to install complete WTGs lie in the relative high CoG combined with a small set-down base. Therefore, the stability region during the load transfer from vessel to support structure should be investigated.

One of the effects of larger WTGs is the enormous overturning moment and axial loads they will generate. These are applied throughout the tower and its support structure. To couple the turbine and support structures, a connection with a high ULS and FLS capacity is required. The C1 Wedge Connection is a newly developed connection that claims to be able to handle these larger loads, in addition to being safe, fast and maintenance free. Since the connection allows larger installation tolerances², it might be a suitable connection for floating offshore installation operations. The C1 Wedge Connection, in combination with the use of HLVs may be a very promising set-up to install WTGs with a single-lift in a fast and safe manner with an acceptable operability.

This thesis is about the installation of whole WTGs from a floating vessel. More specifically, the thesis will investigate the stability region during the load transfer from vessel to support structure. To assess this, an installation scenario will be examined. Heerema has developed a single-lift WTG installation configuration, making use of a dual crane lift, see Figure 1.4. Making use of two cranes instead of one, it is possible to lift the turbine with lifting points at the bottom and halfway up the turbine tower. This reduces the required lifting height of the cranes, making the installation of bigger WTGs possible, but decreases the stability. A stabilising frame alongside the tower is positioned only just above the vertical CoG of the WTG. During installation, the load is transferred from the cranes to the support structure. External loading from wind and waves induce forces on the turbine and on the crane. During lifting, the tension in the crane wires is holding the turbine upright, preventing it from toppling over. However, when the tower is being lowered onto the support structure, the tension in the crane

²installation tolerances here refer to the tolerances allowed when aligning the upper and lower section during the installation. They can refer to tolerances in radial, circumferential and/or longitudinal direction. For the C1 Wedge Connection, this applies for all of these, as described in section 2.5.3



Figure 1.4: Render of dual crane whole WTG installation with SSCV Sleipnir

wires, and thus the up-righting moment, decreases. The base of the tower should now provide this up-righting moment, but with a relatively small base without any connection to the support structure it is not realistic to assume the tower base can do this (see Section 6.2). Therefore, C1 Connections developed the Quick Connection System (QCS, see Chapter 2.5.3). This system extends remotely activated hydraulic cylinders to create a temporary connection between the WTG and the support structure. With this temporary connection, the base is expected to be able to provide sufficient up-righting moment to prevent the WTG from falling over. Then, outside of the critical time path, the permanent connection can be made manually. However, the conditions under which the QCS can be activated are unknown. This thesis therefore examines the installation conditions under which the QCS can be activated.

This thesis is written in collaboration with C1 Connections and Heerema Marine Contractors. Additional information about C1 Connections can be found at c1connections.com and additional information about Heerema is available in Appendix A.

1.3. Research objective

In this paragraph the research goal and scope are presented. This paragraph explains the main objective of the thesis and the questions used to break it down into research steps. Furthermore, the scope is presented, as well as the main assumptions.

1.3.1. Research Goal

The goal of this thesis is to determine the conditions under which the QCS can be activated, as explained in Section 1.2. In the offshore industry this is done by assessing the operability and/or workability of an installation activity. To keep the results generic, it is decided to assess the operability in this thesis. Furthermore, the stability during the load transfer phase is calculated and discussed. Finally, the operability is optimised, as this is desirable for the feasibility of the installation method. Are design alternations required? What implications do these have on cost, procedures, and safety?

From the problem statement and the research objective, the main research goal is formulated:

'How to optimise the operability of a floating single-lift installation of a Wind Turbine Generator (WTG) with a quick connection system (QCS)?'

The main research goal is divided into the following questions:

1. What effect do wind and waves have on the dynamics of a WTG after the alignment phase of the installation?
2. Is a QCS required to keep the WTG stable during the load transfer phase?
3. What is the operability of the activation of the QCS during a single-lift WTG installation?
4. Is the stabbing window a limiting factor for the application of the QCS?
5. How do the support structure, WTG, rigging, and crane interact after the QCS is deployed?
6. How does the C1 QCS perform compared to alternative connections during installation?
7. What design improvements are required, if any, to make the C1 Wedge Connection suitable for a single-lift WTG installation?

These sub-questions will help guide the thesis in finding an answer to the main research question. The approach taken to answer the (sub-)questions is given below.

1.3.2. Scope

Due to limited resources a specific scope is selected to make the project manageable. First of all, a state-of-the-art scale WTG will be considered. The models created will be simplified to ensure manageable simulation durations. The models will simulate motions in the in-plane horizontal x , vertical z and rotational θ direction (around y), totalling 3 Degree Of Freedom (DOF) directions. With these directions, enough information is gathered to draw conclusions about stability in the main direction of interest. Models are built and expanded step-by-step to keep track of changes and the (lack of) influence they have on the results. Vessel hydromechanics are only touched upon superficially and the crane tip motion is used as the input to the model. The installation vessel used in this thesis is the floating HLV SSCV Sleipnir and the WTG is installed on a mono-pile support structure.

1.3.3. Main Assumptions

In the thesis, a lot of assumptions are made to create the models. A list of the main assumptions is given here. More specific assumptions are mentioned in the model descriptions.

- The support structure is rigid and fixed to the seabed.
- The WTG is modelled as a rigid body.
- No tuggers are added to the rigging arrangement. This can be done in future research to control the load motion even better. But since this is not the goal of this thesis, it is left out here.
- The C1 Wedge Connection is modelled as a number of spring/dampers equally spaced around the tower's circumference. Before the QCS is activated, they only work in compression (no tension), mimicking the flange contact force. After the QCS is activated, they work both in compression and tension.
- Bending forces in the C1 Wedge Connection are disregarded. To ensure the C1 Wedge Connection's structural integrity, deformation of the connections upper or lower flange is not allowed. Once the WTG is rotated beyond the rotational tolerance in the fork, the C1 is assumed to fail.
- Constant stiffness and damping values are assumed for all modelled objects, except for the C1 Wedge Connection as described above at the fourth point.

1.4. Research Methodology

This paragraph presents the approach taken in the thesis as a whole. This paragraph elaborates on the methodology and assessment criteria used to address the research question. Finally, the structure of the literature review is presented in the report outline.

1.4.1. Approach

The thesis is built up in several stages. First, literature research is conducted. Here, relevant sources from scientific papers, books, theses, patents, and other material are selected, evaluated, and synthesized to write a comprehensive and balanced literature review from several perspectives. Then conclusions and recommendations are drawn to incorporate during the thesis research. Input is gathered to build a model to replicate the motions present in the case study. A Python model, based on

analytically derived equations, is built up from scratch and is expanded step by step. This model is built to increase understanding of the fundamental physical phenomena present during the WTG installation. Once this model is sufficiently developed, it will be verified using a similar model built in the widely used industry software package OrcaFlex (Chapter 4). This model is then expanded with more complex features. The output of this model is analysed and a parameter sensitivity analysis is performed. Finally, the model is used to assess the stability during the load transfer for different load cases. By iterating over the input parameters and limiting parameters, the operability of the installation is optimised. The iteration loop of: model construction/adjustment → result generation → comparison/discussion → model construction/adjustment → etc. is ran several times to acquire the desired model and results.

1.4.2. Assessment Criteria

In this subsection, the main assessment criteria are mentioned on which the model results will be evaluated. First an assessment is made on whether the QCS insertion slots in the C1 Wedge Connection are overlapping for a long enough period of time to make a quick connection (T_{stab} criterion). A minimum period is needed to activate the QCS, to make sure a safe and proper connection can be made by completely inserting all pins. It would be dangerous if only a part of the pins is inserted. A second criterion on which the installation will be evaluated is the ability to keep the rotation of WTG under a certain threshold. This applies both before activation of the QCS (retain C1 structural integrity) and after activation of the QCS (during load transfer). The third criterion concerns snap loads in the rigging occurring during set-down of the WTG on the support structure. These result from impact of the WTG. Literature research will be used to assess whether a maximum snap load or a maximum impact velocity is preferable as a limiting criterion. Realistic values for all above mentioned criteria are taken from the literature research. A comprehensive description of all used limiting criteria can be found in Section 5.2.

1.4.3. Outline of Report

The literature review is divided up into two parts: First, in Chapter 2, a more general assessment is provided for all state-of-the-art structures and equipment involved in offshore WTG installations. The functionality, applications and limitations of structures and equipment such as turbine parts, vessels and connections are described. Then, in Chapter 3, the physics involved in the installation is described. The loading on WTG and vessel are assessed and the methodology of modelling these systems in software is explained. After these two chapters of theory, intermediate conclusions are drawn from several different perspectives and recommendations for the thesis are proposed. Chapter 4 then describes an overview of the first modelling phase. In this phase two models are built (one Python model and one OrcaFlex model). These models are compared and discussed, which leads to the development of the Enhanced OrcaFlex model, described in Chapter 5. For this model, the contents, assumptions, and methodology are presented. Chapter 6 then presents the results of the enhanced model, including the results of the sensitivity study and the optimisation. The results here are specified for two situations, where Situation 2 is the installation situation before activation of the QCS and Situation 3 is the installation situation after activation of the QCS (the load transfer phase). The Chapter finishes off with a discussion about the validity and reliability of the results. Chapter 7 finalises this thesis with the conclusions (per research question) and proposes recommendations for further research on this model or a way to use the conclusions from this thesis for further research on this topic.

2

State of the Art Offshore Structures and Equipment

This chapter provides a theoretical background of offshore structures and wind turbine installation equipment. Information is provided about equipment required to integrally install WTGs. This includes the installation vessels, lifting configurations, installation aids and the connections between these components.

2.1. Offshore Wind Turbines

Offshore Wind Turbines generally consist of two parts: the Wind Turbine Generator (WTG) and the substructure. The offshore WTG is relatively similar to the onshore WTG. It consists of a tower, nacelle hub and three blades. The offshore substructure differs from its onshore equivalent in most aspects (size, shape, and composition). There are many different offshore substructures possible, here divided into the two main categories bottom-founded and floating.

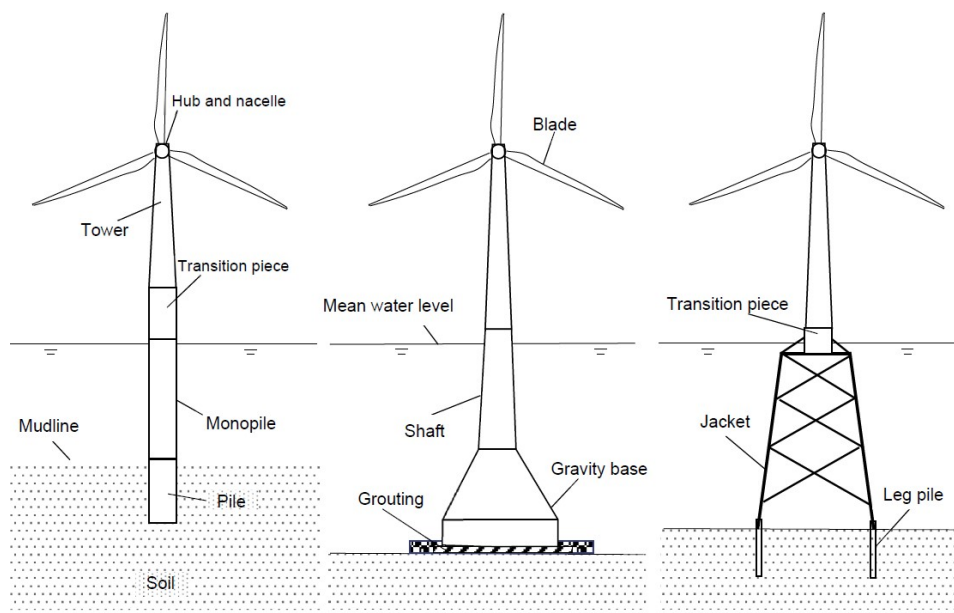


Figure 2.1: Schematic of the Mono-pile, gravity-based and jacket offshore wind turbine support structures [55].

2.1.1. Bottom-Founded Support Structures

Support structures are the basis of the wind turbine. They transfer the loads from the turbine to the earth and supply the turbine with the required connections. Most offshore support structures installed so far are bottom-founded. There are three common types, as shown in Fig. 2.1: Mono-piles, jackets and gravity-based [55]. The mono-pile (MP) is the simplest concept. A steel tubular is driven into the soil. MP diameters currently lie between 3 and 8 meters, but diameters are still increasing. SIF, for example, is building a new MP manufacturing plant to handle MPs up to 11 meters [88]. MPs are being applied up to water depths of around 60 meter (see Fig. 2.2). A transition piece (TP) is fitted on top of the MP to connect it to the turbine tower. Since the TP does not suffer piling impacts (as the MP does), it can accommodate complex welded secondary steel structures like the access platform to the WTG. TP-less support structures have been constructed for Hollandse Kust Zuid, among others [11]. Secondary steel items are hung-off the MP after its installation. Although this design reduces the weight of the total primary structure, concerns arise about the availability of crane vessels able to install these MPs, since they are longer and heavier. The gravity-based structure (GBS) is most comparable to an onshore substructure. A large concrete base resists the overturning moments. The GBS is mostly applied in shallow waters (<20 meter water depth) on clay, sandy soil and rock seabed conditions [55]. Jacket substructures are space frame structures made from steel tubulars that are welded together. Jackets are used for intermediate water depths (20 to 60 meters water depth). Their broad base resists the overturning moments, and the slender tubulars are loaded less by waves than the MP. The cross tubulars give the structure its shear strength.

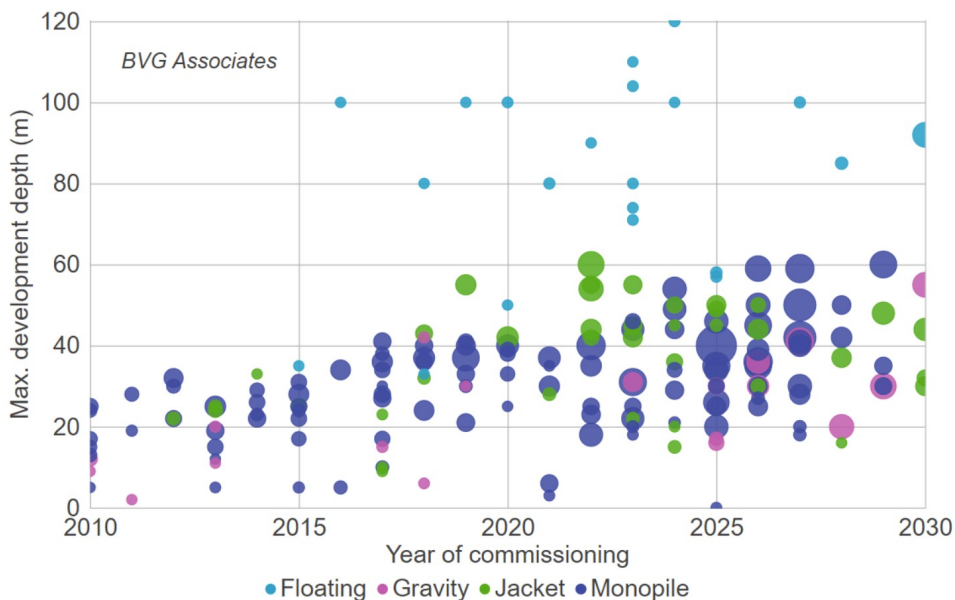


Figure 2.2: Support structure type versus maximum development water depth and installation date, for global projects excluding China. The bubble area is approximately proportional to installed capacity [11].

2.1.2. Floating Support Structures

Floating support structures consist of a body that displaces water to make the OWT buoyant and a mooring and anchoring system to prevent the OWTs from drifting off. Three examples of floating support structures are shown in Fig. 2.3. OWTs can be ballast-, buoyancy- or mooring-stabilised (or a combination of multiple). Since the commercial interest for floating support structures is relatively new, a wide range of concepts is still being considered, some with customized WTGs and/or installation methods [55].

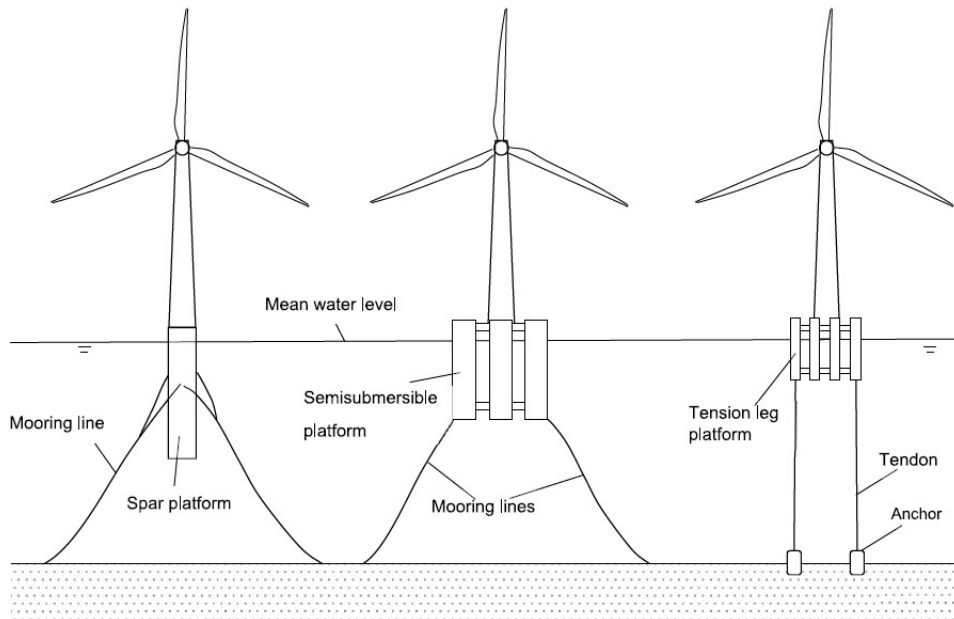


Figure 2.3: Schematic of spar, semi-submersible and tension leg platform floating wind turbines.[55].

2.2. Wind Turbine Installation Vessels

In turbine installation strategies there are two main approaches used: (1) assemble the turbine onshore and transport it to its location in one piece or (2) load the turbine in parts on a vessel and assemble the turbine at its location of operation. Most wind turbines are assembled offshore, with the help of a crane vessel. There are several distinct types of lifting vessels installing turbines which can be categorised in jack-up and floating crane vessels. One type of jack-up crane vessel and three types of floating crane vessels are discussed below. They are illustrated in Fig. 2.4.

2.2.1. Jack-up Installation Vessel

A Jack-up vessel is a vessel with retractable legs that can lift the vessel hull out of the water by extending its legs to the seabed. This makes lifts to bottom-founded support structures almost entirely unaffected by vessel motions due to waves, thereby simplifying alignment of WTG components. Soil conditions are particularly important for the applicability of a jack-up vessel as a punch-through can be catastrophic for the stability of the vessel. Jack-up legs are a threat to cables. Therefore, a safe distance should be maintained, limiting the options for jacking up positions [28]. This causes the process of jacking up to be time-consuming especially since lowering and lifting of the legs can only be done under calm sea conditions. Despite this, almost all OWTs are installed with jack-up vessels [90]. State of the art jack-up vessels can install up to water depths of around 70 m [15] taking 1 to 2 days per turbine (time at turbine).



(a) Cadeler's Jack-up vessel Scylla



(b) HMC's Semi-submersible vessel Thialf



(c) DEME's ship-shaped mono-hull vessel Orion



(d) Scaldis' sheer leg crane barge Gulliver

Figure 2.4: Four distinct types of offshore crane vessels [14, 44, 23, 105].

2.2.2. Floating Installation vessel

The floating crane vessel (or heavy lift crane vessel) is an upcoming type of installation vessel in the offshore wind market mostly driven by the enhancement of the dynamic positioning (DP) system and the need to install OWTs at locations where the soil is not suited for jack-up legs, or the water is too deep. New vessels like DEME's Orion or JdN's Les Alizés are designed for bottom-founded support structures installation [23]. The main benefits of floating installation vessels are its independence of water depth, soil conditions and its capability to weathervane; they choose the most optimal heading for installation whereby minimizing wave and/or wind interaction. Heavy lift crane vessels can be categorised as follows:

- Semi-submersible crane vessels (SSCVs) can lift great loads but generally come with high day rates.
- Ship-shaped mono-hull vessels can lift medium-sized loads but are sensitive to roll motions.
- Sheer leg crane barges can lift great loads but are limited in manoeuvrability and operability at sea.

The continuous development of equipment, such as DP, crane, and motion compensation systems (see section 2.6) enhance the operability of the floating vessel types. Also, the need to install OWTs in deeper water and in locations with less favourable soil conditions increases the demand for floating vessels.

2.3. Installation Methodology

By far most turbines are installed from jack-up vessels in five offshore lifts (tower, NHA and three blade lifts) [3]. To reduce this number of critical (weather dependent) lifts, innovative configurations have been thought of (see Fig. 2.5). Full rotor installation (3 lifts) and bunny ear installation strategies (3 lifts) are examples of this. Heerema recently developed and executed a double lift installation strategy (tower and RNA) in the Arcadis Ost 1 wind project [42]. In this strategy the RNA was preassembled on deck on a dummy tower and thereafter connected to the already installed tower. SAIPEM installed five turbines in a single-lift for the Hywind pilot project in sheltered waters [107]. This project was also ground-breaking as the turbines were installed on floating support structures with the use of a stability frame. SAIPEM designed and patented the clamping system used to lift the 6 MW turbines [87]. The lifting configuration is shown in Figure 2.6.

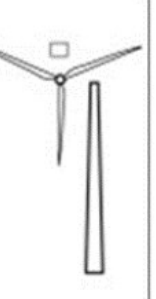
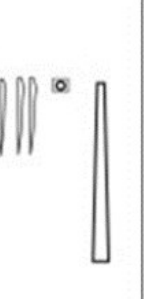
Installation method	Full OWT	RNA	Bunny ear	Rotor	Classic
Visual representation					
Number of lifts	1	2	3	3	5

Figure 2.5: Offshore Wind Turbine Installation Methodologies and the number of critical lifts associated with them [55].

Another project was executing in Europe involving a single-lift installation: the Beatrice Wind Farm Demonstrator Project. This installation involved the sheerleg heavy lift vessel Rambiz's two cranes, a 5 MW WTG and a jacket support structures (see Figure 2.7). Although the tower was relatively short, the turbine was stabilised with an Upper Stabilising Frame (USF) and a Lower Lifting Frame (LLF). The LLF was given a large diameter to give the WTG a large base to ensure sufficient stability during the load transfer phase of the installation. Although this type of LLF required a lot of additional steel, it did provide a stable landing of the WTG on the jacket. For the installation considered in this thesis, such a LLF is not considered, since minimal changes to the support structures are desired and the connection of such a frame to a TP or MP is considered too complex and expensive for the added benefit.

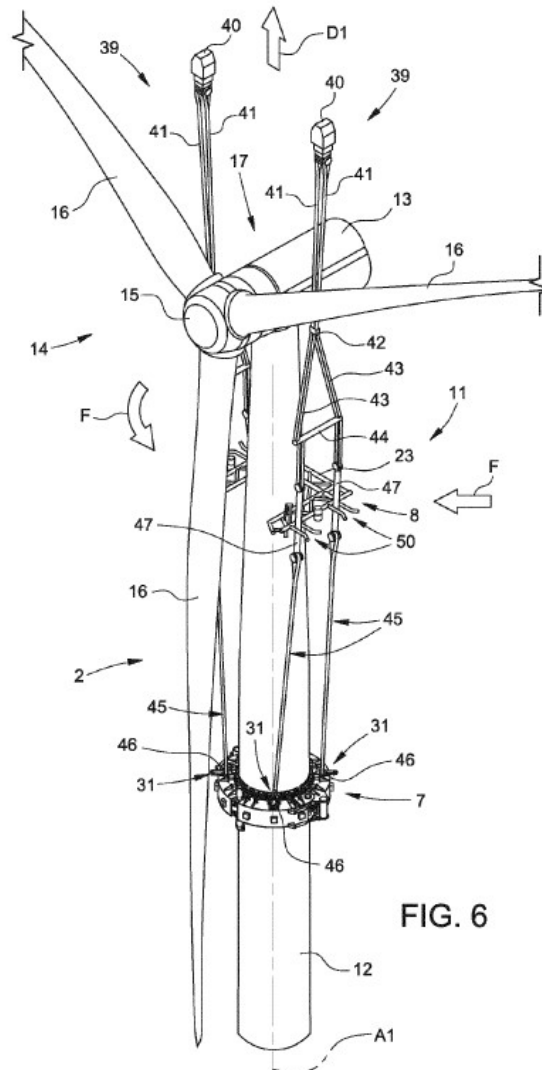


Figure 2.6: The lifting configuration used for the installation of the Hywind Pilot Project. The clamping device indicated by number 7 is patented by SAIPEM and is a type of Lower Lifting Frame (LLF). The numbers 40 represent the crane's blocks. Part 11 is the Upper Stabilising Frame (USF) [87].

The chosen installation method depends on numerous factors including the installation equipment, turbine size, wind farm location and supply chain specifics. Reducing the number of lifts can reduce the charter costs but may also increase the installation difficulty. The costs can be reduced by faster installation and doing commissioning actions onshore but can also be increased due to the need of developing (project specific) installation tools or because of a reduced operability. Since the installation of OWTs is a repetitive process, a project specific assessment should be made if faster installation methods outweigh the extra cost made.



Figure 2.7: The lifting configuration used for the installation of the Beatrice Wind Farm Demonstrator Project [84].

Next to the installation methodology, the transportation strategy also heavily influences the installation process. Logistical considerations should be incorporated to determine the best installation methodology. Three transportation strategies for the single-lift installation method are explained and illustrated below:

1. **Shuttling**; The installation vessel will sail back and forth from the marshalling port to the OWF with one OWT suspended in its cranes. A large, deep-water quay is required with cranes able to assemble the WTG on the quay and a support structures able to handle the WTG loads. The feasibility of this strategy depends heavily on the sailing distance and the port selected. The sailing distance is likely to be significant since floating vessel installations will mainly become relevant for deeper waters, which are usually further away from ports.
2. **Feeder barge**; In this strategy, the installation vessel will stay at the OWF and one or multiple barges will shuttle between the port and OWF. A prerequisite here is that a barge can sail with a completely assembled WTG on its deck. If this is technically unfeasible, a transport similar to a semi-submersible floating support structure tow-out could be used, although this could be quite cumbersome.
3. **Sheltered waters**; The installation vessel will pick up pre-assembled WTGs from the quay (like in the shuttling strategy) and install them on floating support structures in sheltered waters, as with the Hywind Pilot Project. Here, a major cost saving is the sailing time. Since the installation vessel can stay in the sheltered waters, short cycle times can be achieved. The floating OWTs can be towed out to the site after mating of the support structure and WTG. Limiting factors here are the onshore supply chain mobilisation speed and long-distance tows.



(a) Shuttling transport strategy example of HMC's Aegir lifting the DOT SJOR Turbine before sailing to the OWF [94].



(b) Feeder transport strategy example of Boskalis' Manta towing a pre-assembled WTG on a semi-submersible floating support structures [98]. Note that this is a possible example of how a feeder strategy could be executed. In the project related to this figure, the transport was not for feeder purposes.



(c) Sheltered water strategy example of SAIPEM's S7000 lifting a WTG from the quayside to later install it on a floating support structure in the sheltered waters [95]. Multiple turbines are built up on the quayside awaiting their turn for the mating operation.

Figure 2.8: Examples of the three considered transport strategies.

A final, pioneering concept to be discussed in this paragraph is Huisman's concept of a Windfarm Installation Vessel (WIV), as shown in Figure 2.9. Huisman claims to reach a workability of 85% on the North Sea resulting in a twenty to forty per cent reduction on installation costs per turbine [9]. The semi-submersible vessel can carry and install 10 TPs and MPs or 8 WTGs [50]. Tridirectional motion compensation and a DP-3 system enable the WIV to reach an extremely high workability. A large installation tower at the bow of the vessel can rotate its dual hoisting systems, enabling parallel activities. A scala of grippers, railings and beams enable the installation tower to lift hammers and assemble WTGs onboard the vessel. The lack of crane booms and freely hanging crane blocks enables this vessel to operate under severe weather conditions. Although this concept looks very promising for the wind market, no detailed engineering or fabrication has commenced since its presentation in 2020. Reasons for this lack of progress could be the high investment cost, low Technology Readiness Level (TRL) of tridirectional motion compensated grippers or the insecure wind market circumstances.



Figure 2.9: Windfarm Installation Vessel (WIV) concept by Huisman [9].

2.4. Steel Rigging Wires

Steel wires are used in many areas of engineering: from onshore applications in bridges or elevators to offshore application in mooring lines or drilling lines. In crane vessels they are used to suspend the crane boom and in winches to hoist loads for example. There are several types of wire configurations used, see Figure 2.10 for some examples. To model the hoisting and rigging wires, representative values for the stiffness and damping values need to be determined. A wire can be modelled in two different ways: (1) as a tensile bar (see Fig. 2.11) or (2) as a combination of a spring and a damper. The main difference between these methods is that the wire mass is accounted for in the tensile bar method and not in the spring/damper combination. Both methods are applied when modelling crane wires and rigging wires [114, 38, 81]. In the lifting set-up used in this thesis, the spring-damper combination will be applied because the wire rope lengths are relatively small.

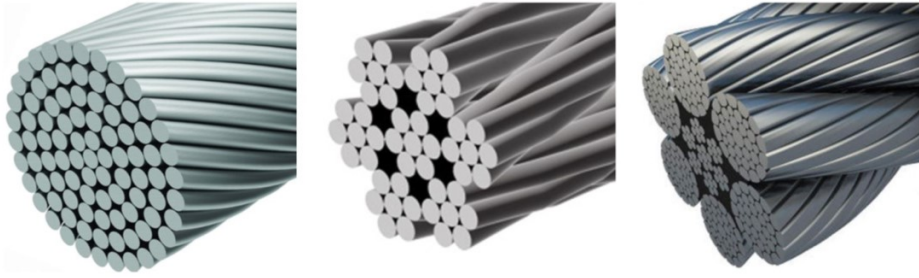


Figure 2.10: Spiral strand, wire rope, and 6xK36WS IWRC (used in HMC's SSCV Thialf) [101].¹

To determine the appropriate stiffness k and damping c equations 2.1 and 2.2 are used. Damping is caused by inner rope friction [35]. The damping is modelled as viscous damping and is calculated as a percentage of the stiffness². Literature papers use values between 1 and 10 % [114, 38, 81], while a value of 1% seems more realistic according to [35] and [70], who use values between 0.7 and 2%.

$$k = \frac{nEA_{eff}}{L} \quad (2.1)$$

$$\frac{c}{k} = \zeta \sqrt{\frac{m}{k}} \quad (2.2)$$

where n is the number of wires; E is the Young's Modulus of the wire; A_{eff} is the effective cross-sectional area of the wire; L is the wire length; ζ is the critical damping ratio (assumed to be 5%) and m is the load mass.

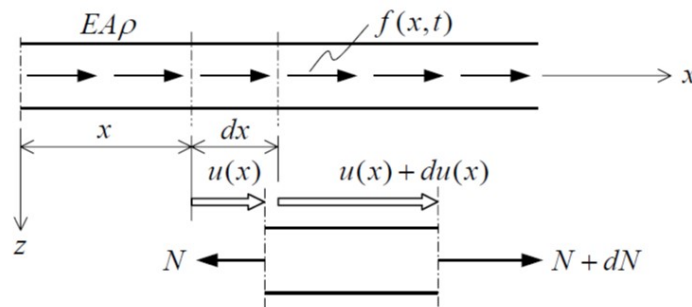


Figure 2.11: Tensile bar [89].

¹The difference between spiral strand wires and wire ropes is the way the single wires are laid in successive layers to provide flexibility and integrity. A spiral strand consists of a group of wires laid in helically layers around a central straight core wire. A wire rope has generally six strands laid helically over a central wire, called the king wire, which is consisting of minor separate wire ropes or twisted threads. Wire ropes are a lot more flexible in bending than spiral strands, which is why wire ropes are used in pulleys and winch drums in cranes. Wire ropes are compacted, resulting in a larger effective area. While the wire stretches it automatically starts to untwist. To minimise this twist, the cores are oppositely spiraled.

²notice the percentage has the unit seconds.

2.5. Structural Connections between Turbine Tower and Support Structure

The type and amount of connections present in an OWT is especially important for the design of the installation methodology. The tolerances can vary multiple orders between different connections and the speed of connecting and associated risks involved make connections an important part of the off-shore operations. In this paragraph, the bolted L-flange, Slip Joint and C1 Wedge Connection will be discussed, see figure 2.12.



Figure 2.12: Three connection types used in offshore wind turbines [31, 30, 12].

2.5.1. Bolted L-flange Connection

Currently, most connections between large OWT components are bolted connections. Bolts are fasteners that, in combination with a nut, apply an axial clamping force to two unthreaded components [65]. In OWTs, the bolt assembly is used to connect large components such as tower parts or tower and substructure. The bolts are arranged in a ring-flange connection, see Fig. 2.13. The L-shape of the flange displaces the bolt axis eccentrically to the line of force of the connection [65]. The bolts are pretensioned during installation to reduce the fatigue loads [106]. However, it is hard to achieve the desired bolt tightness. Torque tools can deviate up to 30% of the desired bolt tightness, while hydraulic tensioners can deviate up to 20% [6]. Furthermore, elastic interaction during installation could cause bolts to lose preload up to 98% after bolt tightening of adjacent bolts, although on average this is expected not to be this much [115].

This is not the only problem associated with the bolted L-flange connection. The clearance in bolt holes is only a couple of millimetres, making alignment of the bolt holes difficult during installation in the offshore environment [27]. Also, maintenance is required on the bolts since bolts are sensitive to the highly corrosive offshore environment and the loss of pretension over time [13]. DNV advises to inspect critical items at least each year [27].

Another risk associated with the bolted connection is the compliance to Health, Safety and Environment (HSE) limits. With increasing turbine size (and thus loads), exceptionally large bolt diameters such as M72 and M80 are required. These bolts can weigh up to 20 kg each, exceeding HSE man handling limits [22, 34]. Getting the bolts into their installation position can become a complex operation if they cannot be lifted in by hand and thus a crane is required. Also, the fatigue life assessment of these large scale bolts is very difficult due to the lack of experimental data points to derive the fatigue design curves [65]. A final downside of the bolted L-flange is the scalability of the connection. With growing turbine sizes, flange and bolt loads increase. According to SIF, the bolted connection is close to its

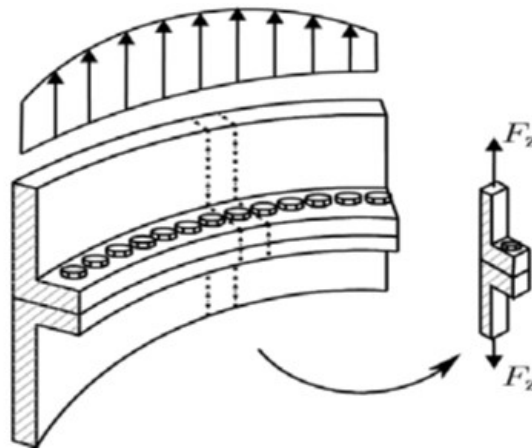


Figure 2.13: Bolted ring flange connection and equivalent single bolt segment [67].

maximum scalability [62]. This could be due to technical/economic factors or since these extremely large bolts and flanges are difficult to produce [12].

All risks mentioned above make bolted connections unfavourable for future offshore installations, where even larger turbines and relative motions pose great safety risks. The offshore wind industry is familiar with these risks. Therefore, a project was launched by the GROW consortium to develop a model for bolt and ring flange fatigue assessment for future large wind turbines [36]. The industry has a strong need to improve the ring flange connections, as the current design procedures are insufficient [52].

IQIP developed the Flange Clamp Tool (FCT) to facilitate a temporary axial connection between two flange structures (see Fig.2.14). This can help with the installation of large turbine components since it removes the need for personnel to stand under a suspended load. The tool is remotely operated and has a fail-safe system arrangement. The system consists of two cylinders and a shaft that can clamp inside a bolt hole with capacities up to 60 mT. [54].

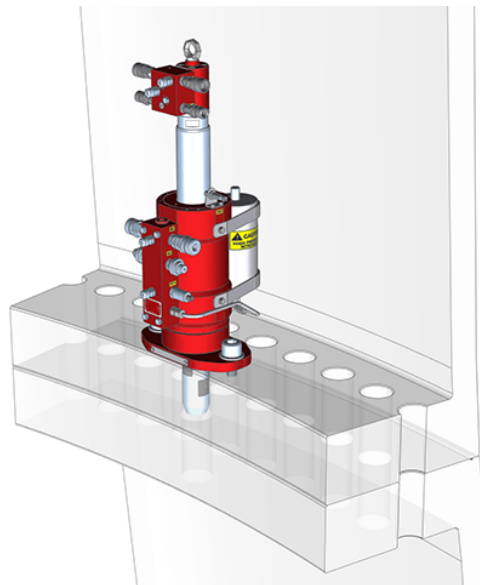


Figure 2.14: Flange Clamp Tool (FCT) from IQIP

2.5.2. Slip Joint Connection

An alternative to the bolted L-flange Connection is the Slip Joint. In the Slip Joint connection two conical pieces are slid over each other to create a friction-based connection, as shown in Fig.2.15. The connection does not need any moving parts or tools to secure or finalize the connection. This lack of components also results in no need for maintenance. The difference in diameter between the lower part of the upper cone and the upper part of the lower cone allows a large positioning tolerance during installation, reducing the installation time substantially [93]. The Slip Joint can be applied between MP and TP, TP and tower, and even between tower and RNA [30, 33]. So far, the Slip Joint has been tested in numerous offshore projects but has not been commercially applied to a complete Offshore Wind Farm (OWF).

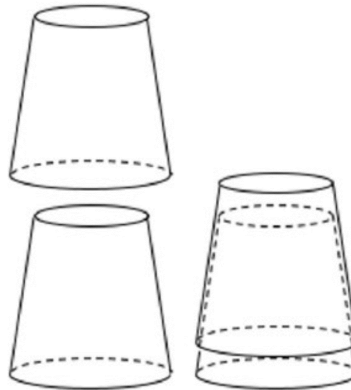


Figure 2.15: The Slip Joint working principle of a friction-based connection.

Possible drawbacks of the Slip Joint are the extra material being used in the connection: it is double walled over an overlap length of around 10 meters (for large OWTs). The overlap length also causes the need for extra lifting height of the crane installing the Slip Joint. Although the installation is simplified, the Slip Joint settles over its lifetime. In the Borssele V project, the Slip Joint settled over its entire lifetime, with peaks during its installation and the installation of the WTG components [93]. The reported overall settlement during WTG installation is in the order of centimetres. Over the entire lifetime of the turbine a maximum settlement of around five times this settlement is expected, all very gradually. The fact that settlement occurs in this connection, requires an adapted design for components such as cable and hose connections.

2.5.3. C1 Wedge Connection

The last connection discussed in this paragraph is the C1 Wedge Connection. Here, a straight and a fork-shape flange are pushed towards each other by wedges inserted in slots in radial direction. The wedge is extended by tightening a nut on a horizontally oriented stud, which push the two inclined surfaces closer to each other creating a vertical force about 5 times the horizontally applied stud force. This vertical clamping force is applied between the top surface of the lower flange and the centre surface of the upper flange. The novelty compared to the bolted L-flange connection is that the load is transferred direct and concentric between the segments and that bolt failure is avoided under static and cyclic loads [17]. The required bolt size for this connection is much smaller than for the bolted L-flange connection. The force variation in the bolt is almost negligible under service loads due to the hysteresis effect in the fastener [18]. This makes the fastener insensitive to fatigue loading, increasing the Fatigue Limit State (FLS) capacity of the connection.

The Ultimate Limit State (ULS) capacity can also easily be increased by using a larger wall thickness of the lower flange. The use of a higher strength grade steel can also increase the ULS of the C1 Wedge connection, in contrast to the bolted L-flange [17]. The wedge assemblies are too heavy to lift by hand but can be prepositioned on the upper flange. During installation, the assemblies are slid through the slots and thereafter are tightened by a hand tool. A portable pretension tool is used to achieve the final desired tension in the fasteners. The flanges are designed such, that they allow

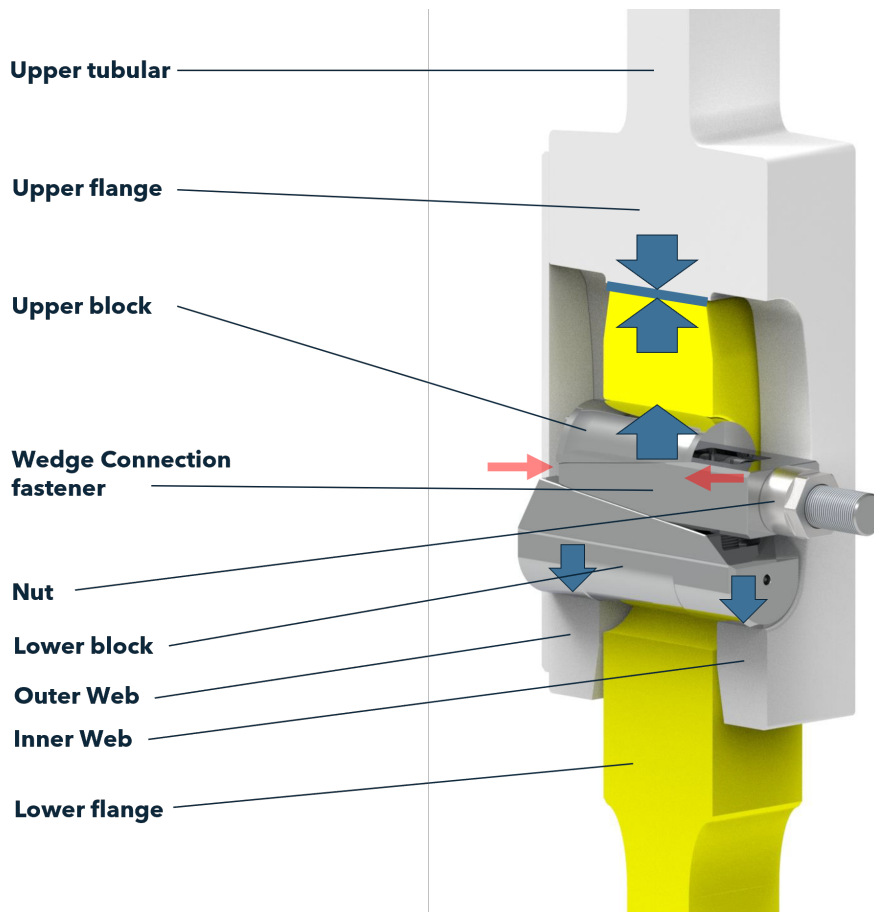


Figure 2.16: The C1 Wedge Connection working principle [12].

for radial and tangential misalignment. The connection is also less susceptible to waviness (flatness of the flange) than the bolted L-flange [22].

The C1 Wedge connection is also equipped with guiding plates and pins to avoid impact between the upper and lower flange and to ensure the correct orientation of the connection. Extra bumpers can be added to take out any ovality present in either one of the tubulars. After the alignment of the upper and lower flange and slots, a hydraulically activated Quick Connection System (QCS) is activated. The QCS automatically pushed out a number of pins to create a first locking mechanism in the connection. This is shown in Figure 2.17. C1 Wedge Connections claim to reduce fabrication, installation, and maintenance costs due to the use of a smaller flange & smaller diameter bolts compared to the L-flange [22].

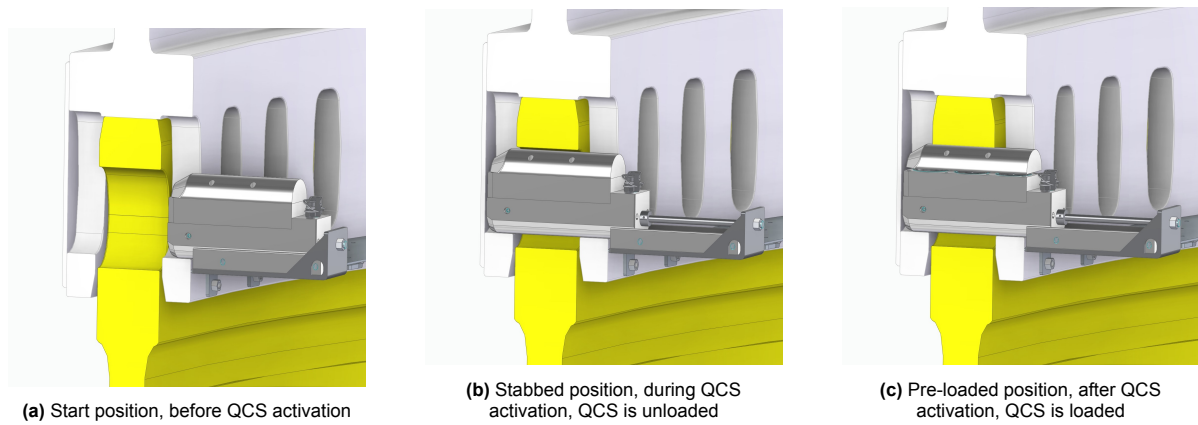


Figure 2.17: Quick Connection System (QCS) [12].

2.6. Heave Compensation for crane loads

In the offshore industry, the environmental conditions determine whether operations can be executed or not. Increasing the operability of an operation will lower waiting on weather (WoW) time and ultimately result in a faster and cheaper installation method. One technology used to increase operability is heave compensation. This technology aims at reducing load motions and/or impact forces by compensation of vessel motions in heave direction. In other words; the vessel motions are decoupled from the load motions. In general, there are two types of heave compensation: Active Heave Compensation and Passive Heave Compensation. This section elaborates on these types and assesses their performance.

2.6.1. Passive Heave Compensation (PHC)

The main principle of the PHC is to store energy from an external source and dissipate this later when required. The standard model does not require energy to operate. The PHC consists of a gas accumulator, coupled to a hydraulic cylinder with a nozzle (see Fig. 2.18) [16]. The nozzle ensures damping in the system by restricting the flow. The hydraulic fluid is present at the rod-side of the piston and is separated from the gas by a floating piston. The gas, usually Nitrogen, is compressed when the load on the cylinder rod is decreased. By setting the accumulator pressure and volume, the stiffness of the PHC can be determined. It therefore acts as the spring element in the system. A vacuum is present at the non-fluid side of the piston [16].

The spring force is non-linear, but is modelled here as a function of the stroke (s) and (constant) stiffness (k):

$$F_{spring} = ks \quad (2.3)$$

If non-linear effects are ignored, the stiffness can be obtained as a function of the gas pressure at equilibrium stroke (p_o), the area of the piston (A), the total stroke length (s_{total}), the compression ratio (C) and the adiabatic coefficient (a) [16].

$$k = \frac{p_o A}{s_{total}} (C^a - 1) \quad (2.4)$$

The dampening force is non-linear and dependent on the squared stroke velocity and the damping coefficient (c), which depends on the flow characteristics through the nozzle [16].

$$F_{damping} = c \left(\frac{ds}{dt} \right)^2 \quad (2.5)$$

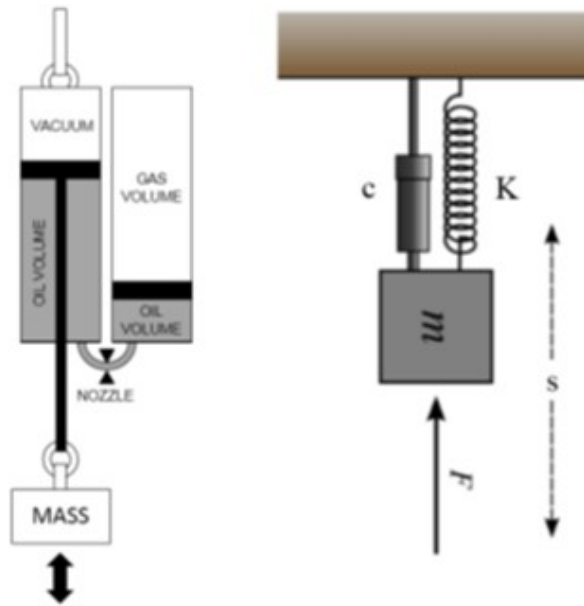


Figure 2.18: Standard PHC & equivalent Spring-Mass-Damper Model [16].

PHC is praised for its simplicity and robustness. In today's industry, higher safe working loads (SWLs) are available for PHC than for external AHC systems (not integrated in the crane) [86, 21]. A limitation of PHC is the added weight, around 10% of the SWL, which can be significant for lifts designed on the crane's lifting limits. The available stroke of the PHC limits the wave height it can compensate for, although PHCs can be put in series to increase the stroke (with all the corresponding consequences). The performance of PHC is dependent on the excitation frequency of the vessel and the PHC settings (stiffness and damping). Figure 2.19 shows how the relative load motion is dependent on the frequency, as in a low-pass filter. By compensating the system with a PHC, the natural frequency can be tweaked to assure the wave frequency spectrum is in the damping region of the system. Optimal tweaking of the PHC will, in general, result in heave decoupling efficiencies up to 80% [57].

Over the last years, extra features have been added to PHC. Where the widespread application is in subsea lifts, new features, like quick lift, make it also relevant for in-air lifts [16]. Quick lift enables a load to be lifted off the deck of a vessel or barge by retracting the cylinder simultaneously to lifting the load by the crane thereby reducing the chance of re-contact between load and deck. In the sub-sea application, it is important to determine the critical stages and tune the PHC to operate best in these phases. If desired, dual valve control settings can be added to the PHC, creating a step change in system stiffness.

2.6.2. Active Heave Compensation (AHC)

A unique way to reduce load motions and/or impact forces is to actively control the heave compensation. There are two types of AHC: tension control and motion control. Both systems operate similarly but require different inputs and controllers. AHC usually involves a closed-loop control system that requires energy input to operate as can be observed for a reference system in figure 2.20. The system consists of a Motion Reference Unit (MRU), a control system (often a PLC) and an actuator (hydraulic or electric). The input for the system usually consists of the heave motion of the vessel but can also use wave data and/or forecasting. The choice of control method (using delayed signals or preset values) can have a noteworthy influence on the performance of the AHC, especially with irregular waves [111]. Electric AC motors are preferable if high power efficiency is required [4]. Although a dynamo can regenerate energy during braking, it is difficult to store the energy on the vessel's electrical grid (creating the need for a battery). Hydraulic actuators provide the highest power to weight ratio of all actuator types currently on the market [73]. This allows hydraulic motors to reduce the footprint at the point of actuation which

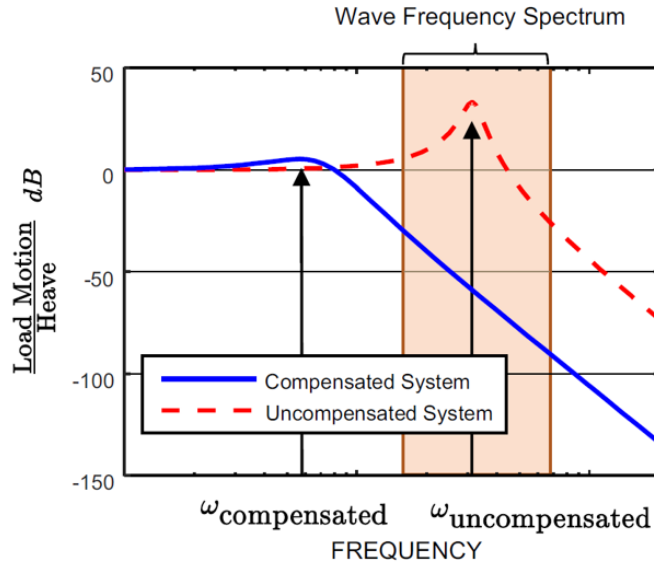


Figure 2.19: Bode diagrams showing an uncompensated (or poorly compensated) system operating within the wave spectrum and a compensated system with the damped natural frequency lower than the wave frequency spectrum [111].

can be beneficial. System performance can be limited by the available vessel power, motor speed and torque, measurement accuracy and delay, or computing algorithms. Besides, the wear of sheaves and wire rope on the winches is increased by AHC. For sub-sea lifts, resonance of the wires should also be investigated.

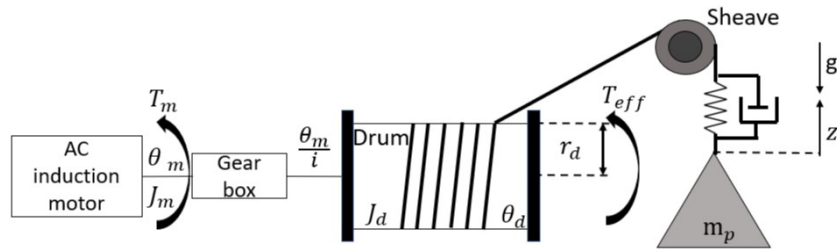


Figure 2.20: AHC Electro-mechanical system [32].

State of the art AHC systems are real time systems that can calculate and compensate any displacement almost instantaneously. Accuracy then depends on the control model used and phase lag in the controller. A way to correct for large phase lag is to make use of Model Predictive Control (MPC). A MPC solves a quadratic optimization problem by minimizing a cost function (as depicted in equation 2.6 [111]) to determine the optimal controller output.

$$J = \sum_{i=0}^{N_p} x_i^T Q x_i + \sum_{i=0}^{N_c} u_i^T P u_i + \sum_{i=0}^{N_c} \Delta u_i^T P \Delta u_i \quad (2.6)$$

Here, x is the model state, u is the controller. Q , P , and R are weighing factors and N_p and N_c are the predictive and control horizon, respectively. The choice of the horizons and weighing factors will determine computational time and therewith the error. Figure 2.21 shows a visualisation of the MPC behaviour.

The addition of predictive modelling on the motion decoupling is significant. Kuchler et al. [61] showed that adding prediction to a controller can reduce the peak value with over 50%. In general, AHC can have efficiencies up to 95% [2, 37]. However, DNV GL [28] states that for AHC, the stated

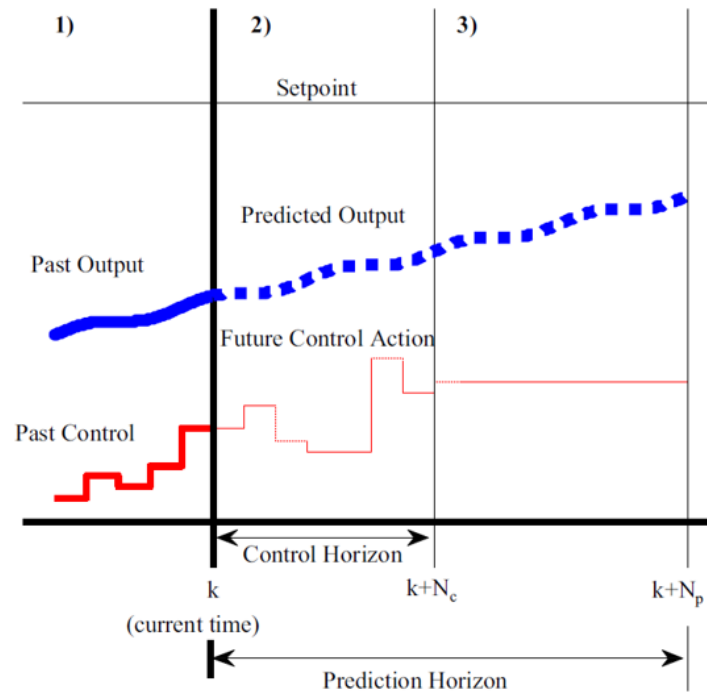


Figure 2.21: An example of the behaviour of a MPC system [111].

documented efficiency shall be multiplied with a safety factor of 0.9 with a maximum theoretical operational efficiency of 0.8. Therefore, designing an AHC with an efficiency above 90% is not feasible for engineered lifts at this moment.

2.6.3. Comparison and variations of Heave Compensation

In this section PHC and AHC are compared, and alternatives are presented.

Comparison

To determine what type of heave compensation is required for a project, it is convenient to understand the benefits and drawbacks of heave compensation. By identifying the differences and similarities of PHC and AHC, a judgement can be made whether it is an added benefit for an offshore lift. Table 2.1 shows the main benefits of the AHC & PHC functionalities.

Description	Applicable Type
Decrease of heave motions	AHC
Decrease of impact loads	AHC & PHC
No re-impact possible after set-down	AHC & PHC
Tension slings after landing	PHC
Requires no power to operate	PHC

Table 2.1: Comparison of PHC and AHC. The type(s) mentioned possess the described positive functionality.

Besides the differences of PHC and AHC, it is also good to look at the weaknesses of heave compensation in general. An obvious downside is the added cost of renting or buying the equipment. AHC is more expensive than PHC, in general, but price ranges within AHC suppliers can vary, mostly due to the power consumption and efficiency [111]. A second disadvantage of heave compensation is the required additional lifting height. For AHC, it is easier to integrate the system in the crane, although this should be done during the design phase of the crane. For PHC, solutions are presented such as 'lock & release' - where the piston can be locked during lifting from the deck (when lifting height is usually more critical) - and 'same side pad-eyes' - where the lifting points of the PHC are attached to the same side of the piston, reducing the effective equipment height (although it can induce bending loads on

pistons) [16, 20]. Another limitation is the maximum SWL of heave compensation. Especially in AHC, the applicability of the technology is currently determined by its lift capacity. Some AHC systems can reach a SWL of 1100 mT, while PHC is now in the design phase for 2700 mT [86, 21].

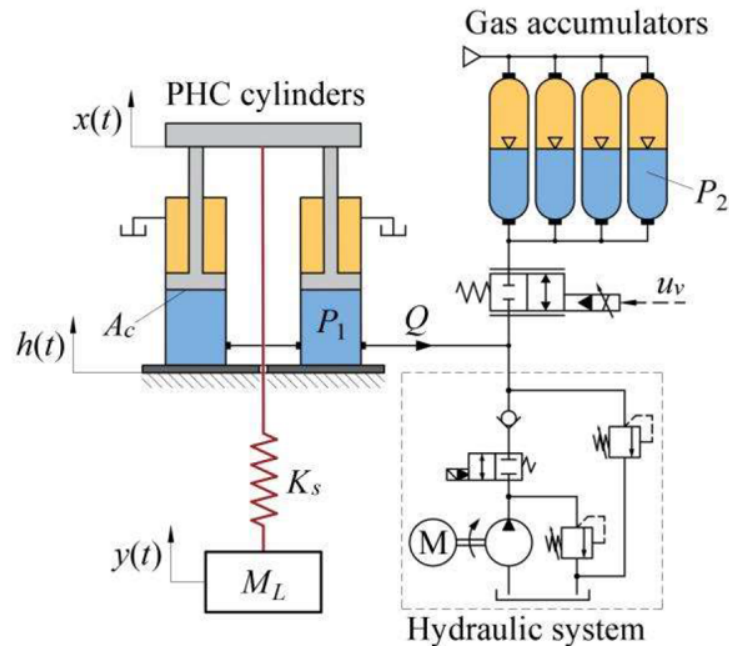


Figure 2.22: An example of an APHC model. Here, controlling the valve opening determines the stiffness parameter [47].

Alternatives

To mitigate the weaknesses of HC, manufacturers have combined PHC and AHC and created a hybrid form of HC. This form is known under multiple names, but here we will use Adaptive Passive Heave Compensation (APHC). APHC can adjust its stiffness and damping parameters with prescribed values specified on the equipment. Then, during the lift, certain modes can be activated for corrections such as crossing the splash zone (dry weight to submerged weight), depth compensation (continuous adjustment for hydro-static pressure increase over the depth) and landing compensation (adjustments made to lower landing velocity) [16].

Overall, PHC will achieve sufficient motion decoupling at lower costs for lifts where complete decoupling is not essential. When higher motion decoupling is required, active or a combined form of heave compensation can be used. However, system complexity is increased, and the current industry is limited in SWL and allowable efficiency limits prescribed in DNV standards. For the offshore wind industry, heave compensation can play a role in component transfers from barges to installation vessels and in installations from floaters. Currently, by reducing impact loads with PHC, and in the future possibly with AHC if it has become more energy efficient, as the hybrid form APHC has.

2.7. Intermediate Findings Offshore Structures and Equipment

The goal of the broad analysis of installation elements was to get a general understanding of how OWT installations take place nowadays, to identify possible knowledge gaps and discover where improvements can be made. WTG installations with floating vessels are quite rare and thus little experience is gathered. If large WTGs are installed, the lifting height of current floating HLVs will become a problem. The single-lift installation method, making use of a dual lift, is the only way these turbines can be installed without the need to modify the crane vessel. As the lifting height is limited, the lifting points are situated at the bottom and halfway up the turbine tower. The nacelle is then positioned in between the two cranes, higher than normally would be possible when lifting with one crane. Mating the WTG to its support structures is expected to be an unstable operation, although this should be confirmed with simulations. A Bolted L-flange connection with a FCT, a C1 Wedge Connection with a QCS or a Slip Joint connection are all connections that can potentially provide a safe restoring moment to assure stability during the load transfer phase of the installation. However, scalability of the bolted L-flange connection, lifting height reduction of the Slip Joint and strength of the QCS and FCT form risks to the implementation of these techniques. Excessive motions of the WTG can be damped in some direction by using heave compensation, guides and bumpers, and/or tuggers.

Now that a general understanding of the current state of WTG installations is gained, it is possible to try to combine this knowledge and develop a theoretical framework able to represent all these effects. This framework, and the implementation of this to model the system behaviour, is described in Chapter 3.

State of the Art Modelling of Dynamics of WTG during Installation

This chapter provides a theoretical background on installation dynamics. This includes the loading on the installation equipment (vessel, crane, load, etc.) ; operational limits and modelling of the system. For this thesis, wind and wave loading are considered. The potential presence of ambient current is neglected because it is assumed that the vessel DP system will counteract most of the effect of such an ambient current.

3.1. Wind Loading

The force acting on a body due to wind is called wind loading. The wind speed U is an important parameter in the assessment of wind loading. Wind loading can also be critical during the alignment phase of wind turbine components, especially when the mean wind speed and turbulence are high [56]. The mean wind speed can be given for different time periods, i.e. 10 minutes, 1 hour or 10 years. DNV-RP-C205 states that short-term wind conditions (relevant for installations) typically refer to 10-minute average wind speeds at 10 m height above the still water level, denoted as U_{10} [25]. The standard deviation σ_U is a measure used to describe the wind variability.

3.1.1. Variations in Time

Wind speed has a wide frequency range, see Figure 3.1. Long term effects are created by seasonal changes in temperature, passages of high- and low-pressure zones and daily changes in temperature. Short term effects are due to turbulence, created by terrain, obstacles, and local temperature differences. For this thesis, a long term mean wind speed is considered as constant wind loading on the WTG. Furthermore, the short-term effects are interesting since the time required to install a whole WTG is expected to be in the order of minutes. Therefore, the next part will elaborate on the modelling short-term effects.

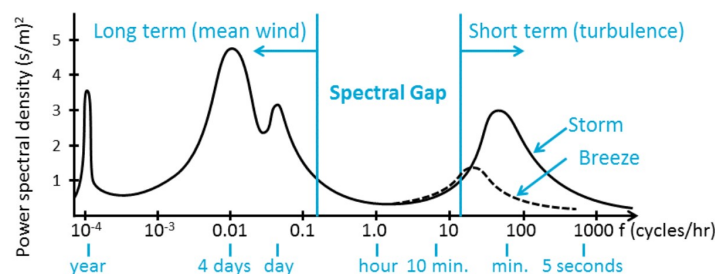


Figure 3.1: Wind speed energy per frequency. The 'Spectral Gap' represents the relatively low spectral density around a frequency of 1.0 cycle/hr [112]. The short-term effects are relevant for this thesis and a mean wind speed is incorporated to capture the long-term effects.

3.1.2. Short-term Variations

The short-term variation in wind speed is called turbulence. It is often parameterized by the turbulence intensity I (see Eq.3.1). Typical intensity values range from 5 to 30% [112]. There are different definitions of turbulence spectra. The three most commonly used spectra are the Kaimal, the Von Karman and the Mann turbulence spectrum. Of these, the Kaimal spectrum is best used for modelling empirical observations of atmospheric turbulence [79]. Therefore, the Kaimal turbulence spectrum (Eq. 3.2 [25]) will be used in this thesis.

$$I = \frac{\sigma_U}{U_{10}} \quad (3.1)$$

$$S_U(f) = \frac{6.868\sigma_U^2 L_{1U}/U_{10}}{(1 + 10.32fL_{1U}/U_{10})^{5/3}} \quad (3.2)$$

$$\begin{aligned} \Lambda_1 &= 42m \text{ for } z > 60 m \\ L_{1U} &= 8.1\Lambda = 340.2 m \\ L_{1V} &= 2.7\Lambda = 0.3333L_{1U} \\ L_{1W} &= 0.66\Lambda = 0.08148L_{1U} \end{aligned} \quad (3.3)$$

Here, z is the height above sea water level and subscripts U, V and W indicate the turbulence directions (longitudinal¹, lateral and upward resp.) [25]. According to IEC 61400-1 the design load case for transport and assembly should follow the normal turbulence model, giving a representative value of the turbulence standard deviation as the 90% quantile for the given hub height wind speed (Eq. 3.4 [60]).

$$\sigma_{U1} = I_{ref}(0.75U_{hub} + 5.6) \quad (3.4)$$

here I_{ref} is a reference value of the turbulence intensity ranging from 0.12 to 0.18 for different turbulence categories. U_{hub} is the wind speed at hub height.

3.1.3. Variations in Space

The wind speed varies not only in time, but also in space. There is a large variation of wind speed in altitude, because of surface roughness. This can be taken into account in wind speed predictions by applying a wind profile. Two common wind profiles used are the logarithmic and the power law wind profile. Since the power law wind profile is better suited for large altitudes (above 100 m), this wind profile will be used in this thesis [112]. The wind speed profile $U(z)$ can be calculated with Equation 3.5 if the wind speed at reference height U_{ref} is known [60].

$$U(z) = U_{ref} \left(\frac{z}{z_{ref}} \right)^\alpha \quad (3.5)$$

here, the power law exponent α is determined by the surface roughness, which can be assumed as 0.12 for open seas with waves [25]. z is the height above sea water level and z_{ref} is the reference height.

Another space-dependent influence affecting the wind velocity is wake generation due to upwind objects such as operational OWTs or the crane of an installation vessel. Also upstream of the object, stagnation causes wind variations. The proposed installation method modelling does not include these effects as no nearby operational turbines are expected during installation and the influence of the crane is assumed to be minimal. Turbulence is a large local variation of wind speeds. Turbulence appears in patterns, which are called eddies. Eddies move along the main flow and cause local variations in wind speed and direction when passing objects. This ultimately causes local force variations on the turbine's blades and tower surface. Eddies can be caused by local rising hot air, reflections and other random, small-scale effects. Turbulence is incorporated in the Kaimal spectrum that is used in this thesis.

¹in the direction of the mean wind speed

3.1.4. Lift and Drag

Lift and drag are the two loading components of wind on an object. Lift is the component perpendicular to the relative incoming wind direction and drag is the component parallel to the incoming wind (see Equations. 3.6 and 3.7 [113]). Wind loading occurs on all modelled objects and will be discussed for the most important modelling object here: turbine rotor and tower, and the vessel.

$$F_{lift} = C_L \frac{1}{2} \rho_{air} U_{air}^2 A \quad (3.6)$$

$$F_{drag} = C_D \frac{1}{2} \rho_{air} U_{air}^2 A \quad (3.7)$$

here ρ_{air} is the air density; U_{air} is the relative incoming wind speed; A is the surface in which the wind is acting; and C_L and C_D are the lift and drag coefficients, respectively. They depend on the shape of the object.

Rotor loading

The rotor of a WTG is designed to extract as much wind energy from the wind as possible. Therefore, the lift forces are maximised to obtain maximal loading in the tangential direction of the rotor (lift). This is done by creating curved surfaces on the blade. The wind needs to 'travel' a longer distance going around the upper curved side than around the lower side, as shown in Figure 3.2. This creates a low air pressure on the upper surface side and a high pressure on the lower surface side, thereby 'pushing' the blade upwards. The angle of attack α determines the ratio between lift and drag forces and can be adjusted by pitching the blade. This is done to optimise the wind power output for different wind speeds. Note here that a too large α will cause the wind flow to separate from the upper surface and the lift will decrease (stall) [112].

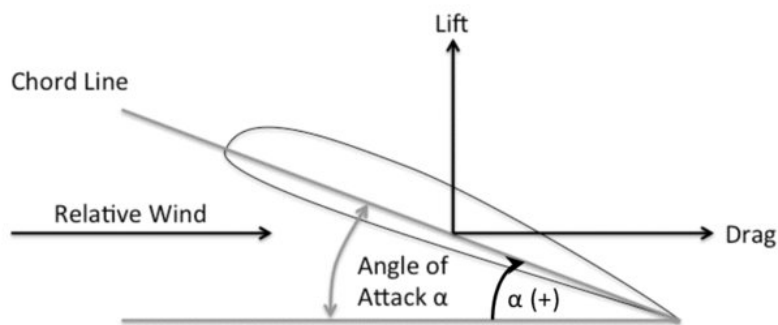


Figure 3.2: Lift and drag forces on a wind turbine air foil (blade cross-section) [99].

An principal factor that determines the direction of the relative wind is the rotational velocity of the main shaft. The absolute velocity of a blade element due to the rotation of the blades increases towards the tip of the blade. Since the incoming wind velocity is about the same everywhere in the rotor surface, the total resultant wind speed direction varies in the radial direction of the blade. To extract maximum energy from the complete swept rotor surface, blades are designed in such a way that the blade is thinner and curved towards the tip of the blade, see Figure 3.3.

During the installation of the WTG, rotation of the rotor is constrained by a locking pin or brake. The blades should be pitched such, to minimize the forces on the blades. But still, considerable wind loading will occur because of the curvature of the blades. The installation orientation of the WTG is pre-determined and therefore, the incoming wind direction cannot be chosen once the WTG is assembled on the quay.

Tower loading

The wind loading on the tower is drag-dominated, and proportional to the tower diameter [112]. The

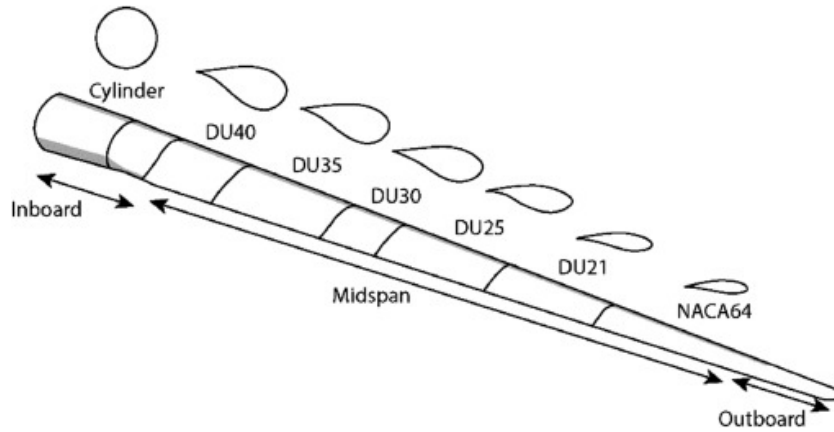


Figure 3.3: Schematic representation of a 5MW blade, showing air foils and their changing chord lengths and orientation [59].

wind speed is non-constant over the tower height (as explained in Subsection 3.1.3 and the drag coefficient is dependent on the Reynold’s number and thus the surface roughness. Another effect of wind loading on the tower is Vortex Induced Vibration (VIV). Relevant consequences of VIV on slender elements are the possible increase of fatigue damage and the increase of the mean drag coefficient [25]. The effect of VIV is neglected in the modelling of wind loading in this thesis, since the effect is assumed to be minimal due to the relative short installation period and distortion of the wind flow around the tower by the rigging, lifting frames and cranes. Whether this assumption is valid, should be further researched.

Vessel loading

In addition to the WTG, also the vessel experiences aerodynamic loads [5]. Similar to the tower, these are drag dominated and only loading in surge, sway and yaw direction of the vessel will be incorporated according to Equation 3.7.

3.2. Wave Loading

3.2.1. Description of Waves

Wave loading is the main additional loading for offshore installations with respect to onshore installations. To quantify the wave loading on vessels and offshore structures it is required to understand the theory behind ocean waves. Figure 3.4a shows the terminology used in this thesis to express the wave loading. η is the surface elevation: the distance between the still water level and the wave surface. H is the wave height: the maximum difference in elevation within one period (trough to crest). λ is the wavelength: this is the distance between successive crests. d is the water depth and T is the wave period: this is the time interval between successive crests passing a particular location.

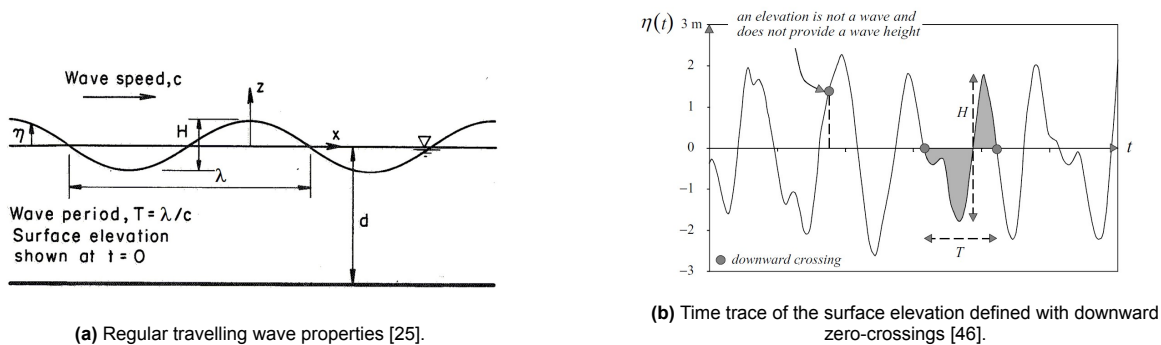


Figure 3.4

These parameters are used to describe regular waves. These are harmonic waves with a constant wave height and length. In irregular waves, the wave height and length are not constant. The local

wave period can then be determined by measuring the time between two consecutive zero downward crossings (see Fig. 3.4b). Almost all real ocean waves are irregular waves. In ocean engineering, these are approximated as a summation of harmonic components. To do this, the wave elevation can be expressed as a Fourier series (see Eq. 3.8 [46]).

$$\eta(t) = \sum_{i=1}^N \frac{H_i}{2} \cos(2\pi f_i t + \phi_i) \quad (3.8)$$

Here, N is a great number (of frequencies), $H_i/2$ is the amplitude, f_i the wave frequency, and ϕ_i the phase for each component i . In a random-phase/amplitude model the wave height and phase are random variables. They are randomly chosen for each realisation of the time record and are characterised with their respective probability density functions (PDFs). The phase at each frequency is uniformly distributed between 0 and 2π in a random-phase/amplitude model. The amplitude is Rayleigh distributed at each frequency (only parameter μ_i is varying over the frequencies) [46]:

$$p(a) = \frac{\pi}{2} \frac{\phi_i}{\mu_i^2} \exp\left(-\frac{\pi\phi_i^2}{4\mu_i^2}\right) \quad \text{for } \phi_i \geq 0 \quad (3.9)$$

Here, a is the amplitude, μ_i is the expected value of the amplitude $E\{a_i\}$. If the amplitude spectrum $E\{a_i\}$ is known, a realisation of $\phi(t)$ can be created by drawing samples for the amplitudes and phases from their PDFs. It should be noted that the random-phase/amplitude model generates a stationary process. It is common to assume the sea is stationary for a duration of 20 minutes to 3 hours [25]. Additionally, wave components are not really independent from another. However, if waves are not too steep and not in very shallow water, these interactions can be ignored.

The amplitude spectrum is usually presented in a different form: as the variance density spectrum $E(f)$. This is done because of three reasons [46]. First, the variance is a more relevant statistical quantity: the sum of the variances is also the variance of the sum. Second, the energy of the waves is proportional to the variance. This enables a link to be made to physical properties such as wave energy. Third, the amplitude spectrum is based on discrete frequencies. Since nature has all frequencies, the spectrum should be a continuously defined. This is done in Equation 3.10 [46].

$$E(f) = \lim_{\Delta f \rightarrow 0} \frac{1}{\Delta f} E\left\{\frac{1}{2}a^2\right\} \quad (3.10)$$

The variance density spectrum gives a complete description of the surface elevation of a sea state in a statistical way, assuming the surface elevation is a stationary, Gaussian process. An example of a variance density spectrum is shown in Figure 3.5.

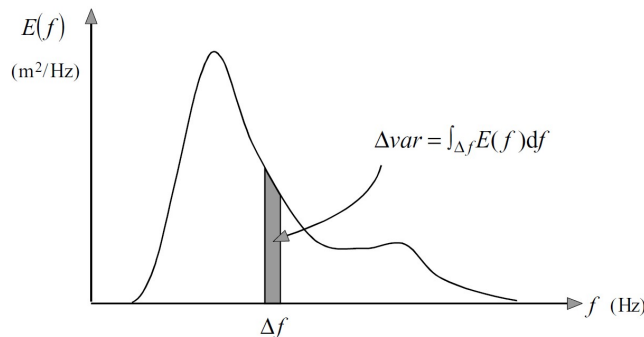


Figure 3.5: Variance density spectrum showing the variance of (a part of) the spectrum can be obtained with integration [46].

In this thesis, second order wave loading effects such as Stokes drift is neglected.

3.2.2. Wave Spectra

A stationary sea state can be characterised by parameters such as the peak period T_p and the significant wave height H_s . The peak period T_p is the wave period at which a wave energy spectrum has its maximum value. The significant wave height H_s is defined as the average height of the highest one-third waves in a determined time-period (also written as $H_{1/3}$ or H_{m0}^2). Wave spectra show the distribution of energy for different frequencies. There are two often applied wave spectra for wind seas: the Pierson-Moskowitz (PM) spectrum and the Joint North Sea Wave Project (JONSWAP) spectrum (see Fig. 3.6) [40, 80]. The PM-spectrum (Fig. 3.11) is created for fully developed wind-generated seas.

$$S_{PM}(\omega) = \frac{5}{16} H_s^2 \omega_p^4 \omega^{-5} \exp\left(-\frac{5}{4} \left(\frac{\omega}{\omega_p}\right)^{-4}\right) \quad (3.11)$$

with $\omega_p = 2\pi/T_p$.

The JONSWAP spectrum (Eq. 3.12) is based on extensive wave spectra measurements taken in the North Sea. It is formulated as an adaptation of the PM-spectrum with a peak enhancement function $G(f)$ and a normalizing factor A_γ for a developing wind generated sea state in a fetch limited situation, although it can be used for arbitrary wind conditions in deep water. Deep water is defined as: $d/\lambda > \frac{1}{2}$.

$$S_J(\omega) = A_\gamma(\gamma) S_{PM}(\omega) G(f) \quad (3.12)$$

with

$$A_\gamma(\gamma) = \frac{0.2}{0.065\gamma^{0.803} + 0.135} \quad (3.13)$$

$$G(f) = \gamma \exp\left(-\frac{1}{2} \left(\frac{\omega - \omega_p}{\sigma \omega_p}\right)^2\right) \quad (3.14)$$

$$\sigma = \begin{cases} 0.07 & \text{for } \omega \leq \omega_p \\ 0.09 & \text{for } \omega > \omega_p \end{cases} \quad (3.15)$$

Here, γ is the peak-enhancement factor. For $\gamma = 1$ the JONSWAP-spectrum reduces to the PM-spectrum. The average value for the JONSWAP experimental data is $\gamma = 3.3$. DNV states that the following value for γ may be used, if no particular value is given [25]:

$$\gamma = \begin{cases} 5 & \text{for } T_p/\sqrt{H_s} \leq 3.6 \\ \exp\left(5.75 - 1.15 \frac{T_p}{\sqrt{H_s}}\right) & \text{for } 3.6 < T_p/\sqrt{H_s} < 5 \\ 1 & \text{for } 5 \leq T_p/\sqrt{H_s} \end{cases} \quad (3.16)$$

In this thesis, Equation 3.16 will be used to find the appropriate value for γ , as no particular value is given.

²Note that $H_{1/3}$ is the measured characteristic wave height and H_{m0} is estimated from the wave spectrum.

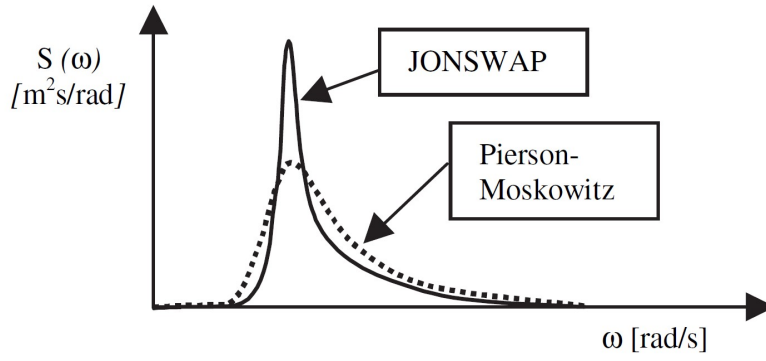


Figure 3.6: PM and JONSWAP spectral shapes [102].

3.3. Vessel Motions

To understand which motions may affect the operational limits of the installation it is required to understand the basics of hydromechanics. Since the vessel is excluded in the used models in this thesis, only the relevant knowledge will be treated. For a complete overview of hydromechanics, please consult *Offshore Hydromechanics* [58].

3.3.1. Hydromechanics

The motion of rigid bodies, such as vessels, can be split up into 6 directions: Three translations (surge η_1 , sway η_2 , and heave η_3) and three rotations (yaw η_4 , pitch η_5 , and roll η_6), see Figure 3.7. These motions are called Degrees of Freedom (DOFs). The vessel position and orientation at any given time can be expressed by a combination of these 6 DOFs, given the corresponding coordinate system. To express the time dependency of a DOF, the Equation of Motion (EOM) can be used using Equation 3.17.

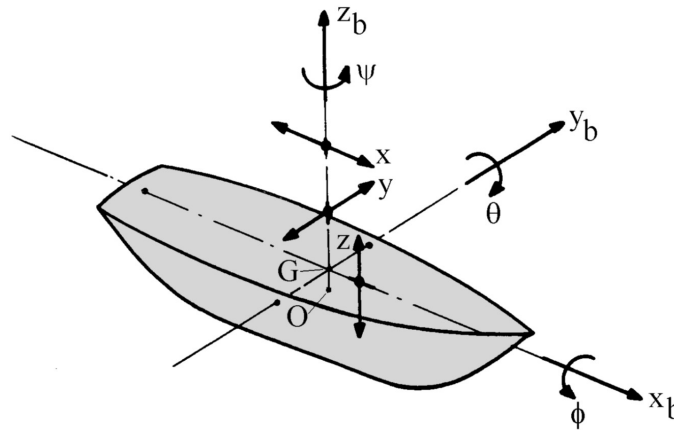


Figure 3.7: Definition of vessel motions in 6 DOF's [58].

$$\overline{\overline{M}}\ddot{\eta} + \overline{\overline{C}}\dot{\eta} + \overline{\overline{K}}\eta = \overline{F} \quad (3.17)$$

Here, M , C , and K contain the $(n \times n)$ mass³, damping- and stiffness coefficients. n is the DOF direction (1-6). F is the sum of all external forces⁴ working on the system per direction n . The double

³including added mass for (partially) submerged bodies.

⁴For the translations F_n is a force. For the rotations F_n is a moment

lines above the letters indicate matrices, the single lines vectors, and $\dot{\eta}$ and $\ddot{\eta}$ are the first and second time derivative of η , respectively. For a body like a vessel, F contains the Froude-Krilov forces and the diffraction forces.

3.3.2. Response for Regular Waves

The vessels heave response due to regular waves is given by Equation 3.18. In Eq. 3.18, $\hat{\eta}_3$ is the vessels heave amplitude, f is the wave frequency and ϕ_{η_3, η_a} is the phase difference between the wave and vessel. The ratio between the amplitude of the vessel motion and the incoming wave motion, $\frac{\hat{\eta}_3}{\eta_a}$, is called the Response Amplitude Operator (RAO). The RAO can be computed for all DOFs and represents the bodies motion as a function of the wave frequency (and direction). The RAO and phase as a function of the frequency are usually shown in a figure when vessel behaviour is described.

$$\eta_3(t) = \hat{\eta}_3 \cos(\omega t + \phi_{\eta_3, \eta_a}) \quad (3.18)$$

with the vessel motion amplitude $\hat{\eta}_3$, the wave frequency $\omega = 2\pi f$, and ϕ_{η_3, η_a} the phase difference between the vessel and wave motion. Figure 3.8 shows an example of a heave RAO. The figure distinguishes three different areas in the RAO [58]:

1. In the low frequency range ($\omega^2 < k/m$), the motions are dominated by the spring terms. This can be physically interpreted as the body following the water surface elevation. The RAO converges to 1.0 and the phase lag to 0.0.
2. In the mid frequency range ($\omega^2 \approx k/m$), the motion is dominated by the damping term. The higher the damping, the lower the amplitude in this region. A phase shift of $-\pi$ occurs at about the natural frequency.
3. In the high frequency range ($\omega^2 > k/m$), the motions are dominated by the mass terms. This can be interpreted as the waves "losing" influence on the bodies behaviour.

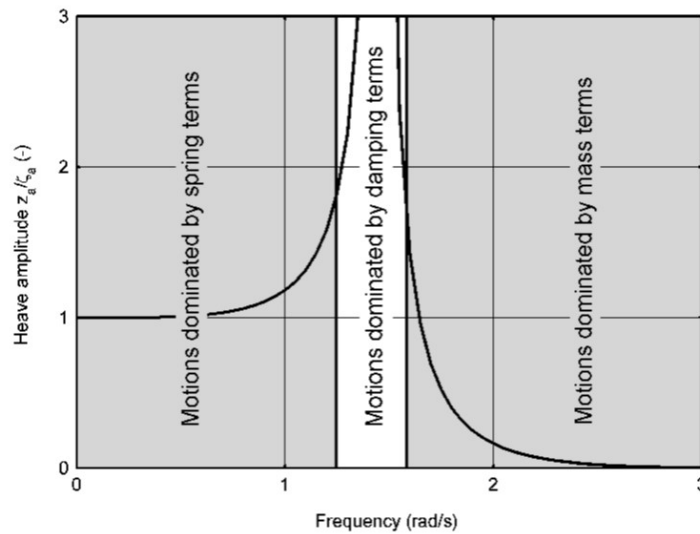


Figure 3.8: RAO with frequency areas [58].

Similar to the transition of amplitude spectrum to variance density spectrum, the response spectrum $S_R(\omega)$ of a motion can be found with the transfer function of the motion and the wave spectrum (see Eq. 3.19).

$$S_R(\omega) = |RAO(\omega)|^2 \dot{S}_I(\omega) \quad (3.19)$$

Here, $RAO(\omega)$ is the RAO of the motion and $S_I(\omega)$ is the input spectrum, i.e. the wave spectrum.

3.4. Operational Limits for Installations

The operability is an important measure for an operation as it states under which environmental conditions (usually H_s and T_p) an operation can still be executed [1]. These are usually presented as a graph for each limiting parameter showing for which H_s and T_p a limiting criterion is still met. To obtain the operability of an operation, first, the critical events and corresponding limiting parameters should be identified based on numerical analysis. Then, the allowable sea states can be established methodically. Figure 3.9 describes these steps in more detail. Note that safety factors need to be applied to take uncertainties for the allowable limits (of limiting parameters) into account.

The limiting parameters can be obvious for some allowable limits (e.g. wire rope Working Load Limit (WLL), crane capacity, off-/side-lead angle or clearance between load and crane vessel). For other limiting parameters structural damage criteria are required, which need to be assessed from Finite Element Method (FEM) modelling. FEM modelling is not included in the scope of this thesis. Instead, the initial impact velocity is used as the limiting parameter for structural damage.

3.5. Stability of the WTG

As mentioned in the Chapter 1, the stability of the WTG will be assessed during the set-down phase of installation. It is important to define what is meant with the term 'stability', as it is used differently in different engineering fields. Some examples are given below:

1. In floating structure terms stability means the capability of a floating structure to resist an inclining moment [85].
2. In terms of lifting operations, stability means to be able to resist overturning forces (i.e. not fall over) ; to be supported adequately; to not rotate of their own accord during lifting [78].
3. In engineering stability is defined such that upon releasing a structure from a virtually displaced state the structure returns to its previous configuration, where the structure is in stable equilibrium [78].
4. In numerical mathematics a physical phenomenon is called stable if a small perturbation of the parameters (including initial conditions) lead to a small difference in the solution [104]. A numerical scheme is stable if and only if:

$$|Q(\lambda\Delta t)| \leq 1 \quad (3.20)$$

with $|Q(\lambda\Delta t)|$ the amplification factor depending on the eigenvalues λ and the chosen time step Δt [104].

In this thesis, when stability is mentioned, the engineering definition is meant (see Fig. 3.10). To quantify this in the model as a limiting parameter, a maximum rotational angle for the WTG will be set in Chapter 4. This assumes that if this angle is reached, the WTG angle will be such that, components in the C1-Connection will fail or the WTG will topple over due to the lack of restoring moment. Apart from this, the numerical mathematical definition will be used to assure computational stability of the models. This is done through the design of the simulations.

Some examples of unstable behaviour are buckling of an axially loaded bar or resonance of a bridge under wind loading (flutter). Here, energy is extracted from the wind to amplify its own motion. This is called 'negative' damping. Vortices also impose dynamic loads on tall slender structures. Periodically released 'Von Karman' vortices behind the structure impose an alternating load perpendicular to the wind direction. Systems can become dynamically unstable if the excitation frequency is equal or close to the eigenfrequency of the system. Then the system is excited, and motions increase until a certain component fails. According to DNV-ST-0054 adequate stability of loads should be ensured during lifting by considering all possible unfavourable combinations of sling loads, wave, wind, and current loads, lift dynamics and manufacturing tolerances [24].

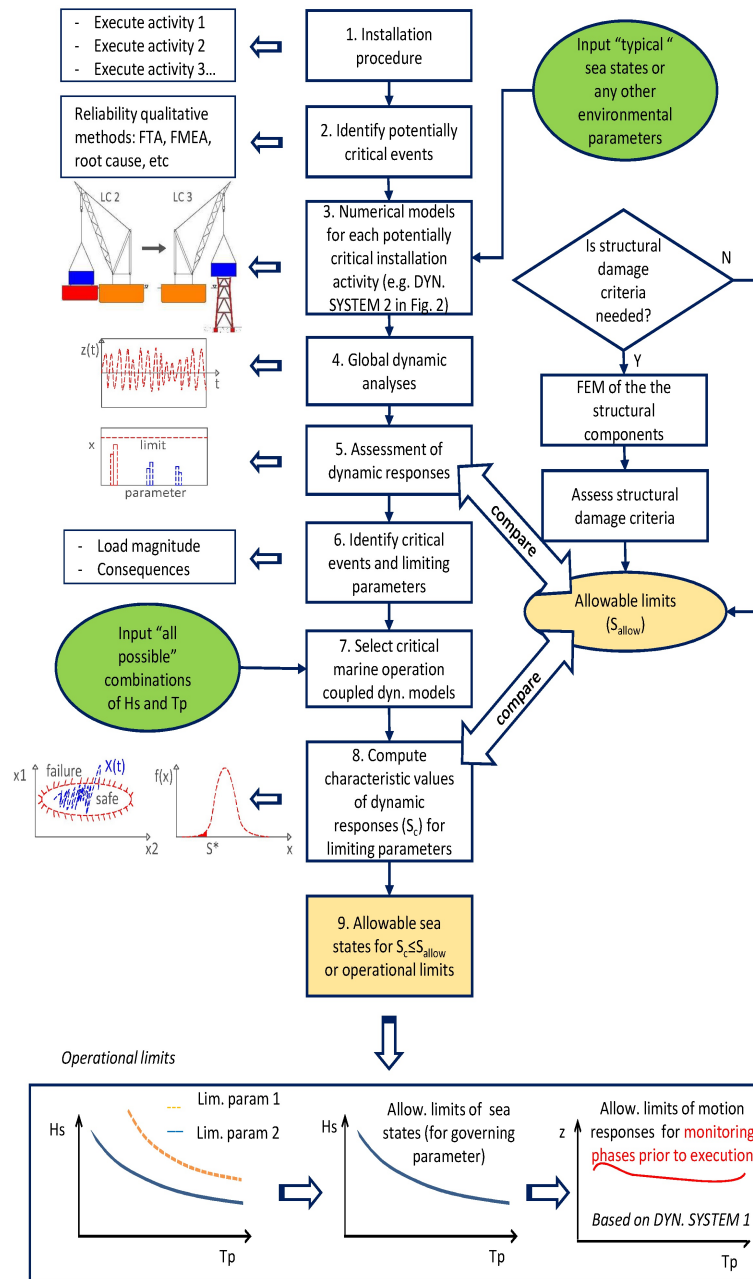


Figure 3.9: General methodology to establish allowable operational limits [39].

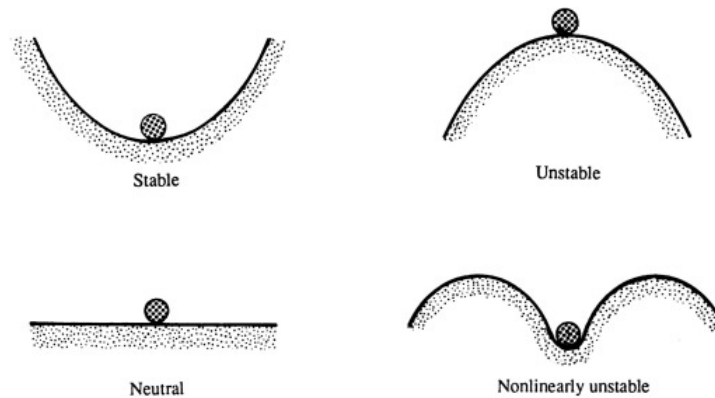


Figure 3.10: Stable and unstable mechanical systems (gravity is presumed to act downward here). A small displacement of the ball away from its equilibrium position will (a) be opposed by the action of gravity and the object will move back toward its equilibrium location (top-left) ; (b) be enhanced by the action of gravity and the object will move away from its equilibrium location (top-right) ; (c) not produce a new force (bottom-left) ; or (d) possibly place the ball beyond its region of stability, depending on the displacement (bottom-right) [63].

3.6. Modelling Software

In this subsection, the used software is described.

LiftDyn

LiftDyn is a Heerema in-house developed, validated software program that can solve frequency domain linear hydrodynamic models [43, 45]. The program solves the equations of motions (EOMs) for user defined objects such as rigid bodies, connectors, and hinges, see Appendix B for more information. LiftDyn can solve system motions in 6 DOF directions and generate results in the form of object RAOs; responses for the given input wave spectrum and direction; and operability curves. The results can easily be exported to be used in other software. Limitations of the software are the restriction to frequency domain and therefore no wind field loading can be incorporated.

OrcaFlex

OrcaFlex is also a program used to simulate hydrodynamic models but can do this also in the time domain (apart from the frequency domain) [76, 75]. OrcaFlex time domain models are nonlinear and are therefore solved in an iterative way using the multi-dimensional form of Newton's method. The mass, damping, stiffness, and external loading are calculated for every time interval and the EOMs are integrated either implicit or explicit. The user can define the wind and wave spectra for the simulations. Limitations of OrcaFlex are the large simulation time required in case of time domain simulations.

Spyder (Python)

Spyder is an open-source scientific environment written in Python (programming language) [91]. It is designed by and for scientists and features a combination of editing, analysis and developing functionalities. Python was the most popular programming language in March 2024 and was selected Programming Language of the Year in 2007, 2010, 2018, 2020 and 2021 [96].

3.7. Intermediate Findings Literature Research

This literature review outlines the relevant theory necessary to execute the thesis plan and construct the models for assessing the research questions. Chapter 2 described the installation elements present in the adopted case study and the newly developed technology relevant to this subject. Chapter 3 explains what should be taken into account when building a model to describe the installation dynamics involved in the case study. These chapters combined form the basis upon which the thesis is built and present the argumentation why certain modelling choices are made. Although the focus of the thesis is on the technical feasibility of the installation, numerous different perspectives on the installation are relevant for the feasibility of the single-lift installation methodology. The main discussion topics and conclusions from this literature research are shown here, presented from these different viewpoints.

For a more detailed analysis of the used sources, see Appendix C.

IP Perspective

With regards to Intellectual Property (IP), attention should be paid to patented lifting configurations or lifting tools. As described in Chapter 2.3, SAIPEM patented a clamping tool used for single-lift installations of WTGs. They heavily invested in this innovative tool, aiming to ensure a return on their investment. Patents protect such investments but can also drive-up costs, as competitors cannot utilize the technology without paying a high fee. This could lead them to develop their own tooling, resulting in many different tools, with distinct parts and different capabilities, resulting in higher costs than standardisation would do. On the contrary, innovation could lead to overall lower cost eventually. Given the volatility of the offshore wind market, contractors aim to achieve a return on their investments in newly developed equipment within the first few projects due to relatively short payback windows. This also drives up the costs, which is tried to be compensated for by increasing the WTG size. This has created a vicious circle over the last 20 years, of which it is unknown when it will stop.

Environmental Perspective

The environment is especially important for the offshore industry. It is the reason the renewable sector exists and therefore the caused harm to the environment should be minimised. This means that the seabed should be unharmed, which gives floating vessels an advantage over jack-up vessels (if no anchors are used). Also, the emissions of fuel combustion and spilling of chemicals should be minimised. Large HLV's are almost all diesel fuelled. Diesel has a high energy density, which is required to operate for prolonged periods without needing to refuel frequently. However, there are developments to switch to bio-fuels for large vessels such as HLV's. Besides fuel emissions, noise emissions are also truly relevant in the offshore industry. The noise emissions depend on many factors, among other things, support structure type, installation strategy and noise mitigating measures. The environment also determines the weather under which operations have to be executed. A WTG's function is to extract energy from the wind, hence high wind speeds are common at offshore wind farm locations. Reducing the required installation window to one critical lift may therefore increase the installation rate significantly. However, the installation vessel will have longer Waiting on Weather (WoW) windows, since the operation is expected to require calmer sea conditions. Retouching upon the emission subject, a reduced installation time will also reduce the fuel emissions. Here, it must be noted that a shuttling installation strategy will require the installation vessel to commute back and forth to port for every OWT, increasing the fuel emissions significantly. Furthermore, operations on DP consume more fuel than operations while jacked-up.

Economical Perspective

From an economic perspective it is difficult to determine the consequences of the operation, since it is really dependent on the logistics whether the business case is good or bad. In general, WTG installation with floating assets will increase the range of options for the offshore wind industry. It will become possible to install OWT's on muddy soils and in deeper waters. Furthermore, it will be possible to install larger turbines, since the weight of the turbine is, in general, not a limiting factor for floating HLV's. Other consequences are really dependent on the installation strategy. Therefore, three strategies are presented in section 2.3. Although installation in sheltered waters seems most promising from a technical point of view, the floating wind market is not mature enough to compete with the bottom-founded market and create work for a floating HLV single-lift WTG installation fleet. The fastest option is not necessarily the cheapest. Although the single-lift WTG installation does seem really fast (only one critical lift), cost of engineering, lifting tools and loss of time due to WoW and shuttling may increase the cost. Furthermore, it is unknown if the supply-chain can keep up with this high offshore installation pace. In current offshore wind projects, there are already many supply chain issues. General conclusions are that installation cost is mainly driven by the offshore duration and day-rate of the installation vessel/methodology. Here, the day-rate is relatively high for floating HLVs, while the offshore duration can be shorter for floating HLVs compared to jack-up vessels.

Safety Perspective

The number one priority in the offshore industry is safety. With many fatal incidents in its history, the industry is very aware of the hazards that come along with working offshore. One of the main take-

aways of using the C1 QCS is to reduce the number of people present under suspended loads and in and around the connection during lifting. By automating the connecting and disconnecting phase of the installation, the safety is expected to increase significantly. Also, the abundance of large and heavy bolts increases the safety since manual handling of bolts is no more. The number of critical (offshore) lifts is decreased by a factor of three to five when the classical method is replaced by the single-lift method (see Figure 2.5). This is all greatly beneficial since 67% of lost working day incidents were caused offshore in the offshore wind industry in 2018 (see Figure 3.11 [34]). Thus, altering the installation strategy to a single-lift methodology is greatly beneficial from a safety perspective.

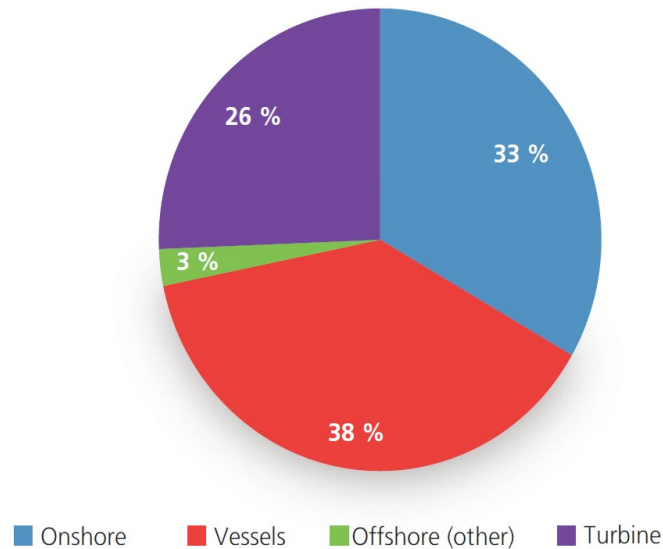


Figure 3.11: Lost working day incidents in 2018 [34].

Technical Perspective

The literature review mentions many technical aspects involved in the single-lift installation methodology. Concluding this, the single-lift installation methodology is beneficial because it reduces the number of critical lifts. It is more efficient, allows for shorter installation windows, and multiple trials show the methodology of single-lift WTG installations work (see Chapter 2.3). Nevertheless, the turbine still has to be assembled (onshore ⁵), which requires a large onshore crane and the one lift that remains offshore is quite complex (sailing with load in the crane, installing on DP, ballasting). To draw conclusions regarding the technical feasibility of the single-lift installation, model simulations are required to quantitatively assess the operability of the installation given a set of limiting criteria.

Concluding

Overall, the single-lift installation methodology seems ready for state-of-the-art scale application. The combination with the C1 Wedge Connection can increase the safety of the remaining critical lift and also offer redundancy for minor misalignments. The QCS can potentially offer the stiffness and damping required to transfer the load from the crane to the support structure in a stable manner. Time domain simulations will show if this potential is justified, or if the operability of the installation is too low to create a good business case. While major safety risks of installing a WTG using the single-lift method are mitigated by using C1's QCS, its adoption will depend on the method's economic viability.

Based upon the literature research, the following main recommendations are given about offshore installations of WTG's:

- It is advisable to further research and develop the single-lift installation method due to the (governmental) urge to install larger offshore WTGs faster and/or cheaper.

⁵an operation that is still sensitive to wind loading, although wind speeds are on average lower onshore than offshore.

- It is recommendable to extensively research if a larger annually installed capacity can be accomplished with many installation lifts that have a relative high operability or few critical lifts with a low operability from a governmental point of view, or what other factors are the main influences on the annually installed capacity.
- Market research should be performed to assess the market potential of the single-lift installation method. How many potential wind farms require floating installation vessels due to deep waters or unstable soils? What cycle time is required to make the single-lift installation method competitive with other methods?

These recommendations will be considered during the rest of the thesis project.

4

Fundamental Models for WTG installation

In this chapter, a summary is given of the building and verification process of the models. Two models are built; a Python model based on analytically derived Equations Of Motion (EOMs) and an OrcaFlex model (industry standard simulation software). The Python model is built to verify the initial OrcaFlex findings and increase understanding of the general model behaviour. This chapter starts with a description of the general model development, valid throughout the thesis. Then, the model-specific characteristics for the analytical Python model and the OrcaFlex model are detailed in Sections 4.2 and 4.4. Finally, the initial results of these models are presented and compared. Based on this, it was decided to expand the OrcaFlex model. The model description of this Enhanced OrcaFlex model is given in Chapter 5.

4.1. Model Development

In this section, an overview is given of the evaluated model contents; the environmental loading incorporated, the installation procedure adopted, the lifting configuration used, and the general simulation settings applied.

4.1.1. Installation Procedure

This thesis is limited to the docking operation of a WTG onto a support structure with a C1 Wedge Connection. The preceding operations are not examined extensively. In other words, it assumes that the actions of rigging connection; WTG lift-off from the quay; transport barge or support structure; transport to the monitoring position (tower bottom above support structure) are possible. Furthermore, no distinction is made whether the support structures' connecting part is the TP or a TP-less MP. Although in this thesis a bottom-founded substructure is used, it is also an option to install the WTG on a floating substructure [92].

The WTG single-lift installation procedure adopted in this research is briefly described below:

1. **Align the tower and support structure vertically with a small deviation away from the guides present on the support structure and monitor tower bottom motion responses.**
2. **Start lowering the WTG until guides/bumpers overlap:** The tower has moved below the top of the guides on the support structure.
3. **Start moving the WTG horizontally to initiate contact between tower bumpers and support structure's guides;** the WTG and support structure are now aligned in the horizontal plane.
4. **Lower WTG vertically until the tower's lower double-walled 'fork-shaped' C1 flange and the support structures' upper cylindrical shaped C1 flange overlap:** rotational outlining of the C1 Wedge slots is accounted for by rotational guides inside the tower. Any horizontal motion of the tower is now restricted to the C1 Wedge Connections radial clearance. Lateral contact

between the structures will occur frequently, but this is not critical because contact surfaces are conformal, and the motions are restricted.

5. **Monitoring of the tower bottom motion responses:** Assess if the motions of the tower are sufficiently small to activate the C1 QCS in the next phase. Ideally this phase is incorporated into the first monitoring phase, but this can only be done if sufficiently accurate tower response approximations can be made during that phase for the activation of the QCS.
6. **Initial landing of tower on support structure:** First contact is made between the C1 Wedge Connection flanges in vertical direction. A small portion of the WTG's weight is transferred from the rigging to the support structure to prevent re-impact. Sling peak loads or large accelerations due to substantial impact velocity are potential critical events of this operation. This activity takes up to a couple of minutes.
7. **Activation of the QCS:** Once the green light has been given, an operator remotely activates the QCS. Hydraulically activated cylinders push a number of C1 Wedges into the Connection slots. The wedges are automatically pretensioned to take out any freedom of movement between the WTG and support structure. This activity is expected to take around 5 seconds. Failure to insert all wedges is a possible critical event of this operation.
8. **Total landing of WTG on support structure:** Main load transfer phase where all weight of the WTG is transferred to the support structure until the rigging is slack. Structural failure of the C1 Wedges is a possible critical event of this operation. This activity lasts up to 2 minutes.
9. **Full Connection capacity and rigging decoupling:** personnel is transferred to the WTG to complete the installation of the C1 Wedge Connection. This consists of inserting all C1 Wedge Connectors, tightening of the wedges and deactivation of the QCS. The rigging is disconnected from the WTG and retrieved to the installation vessel.

This thesis addresses the installation phases items 5 through 8 (2nd monitoring phase through the total landing phase). All activities considered are relatively short (a couple of minutes). Relatively here means short with respect to the entire operation, but still long enough to include a few wave cycles.

4.1.2. Lifting Configuration

In the modelling of the single-lift WTG installation, a certain general lifting configuration is adopted to accommodate the lifting of a complete WTG with a dual crane setup. Here, all (rigging) elements, from crane tip until WTG are described. The lifting configuration was not designed for this thesis, as it was previously designed for a case study by Heerema. Therefore, the design of individual parts of the lifting equipment is not elaborated. The models are evaluated in 2D (in plane) view; therefore the rigging configuration is also simplified to 2D. To take some dual crane effects into account, some stiffness values and weights are doubled, since these items are used in parallel. Table 4.1 shows the considered elements. The upper stabiliser frame (USF) is not designed to transfer any shear forces from the WTG to the rigging and is only used to transfer normal forces to the WTG, keeping it upright. The Lower Lifting Tool (LLT) hangs off on the C1 Wedge Connection's upper flange (see Figure 4.1). This is favourable since it does not require any alterations on the WTG tower design.

Table 4.1: Lifting configuration overview. Both the situation without as the situation with Heave Compensation is addressed. Visualisations of the rigging arrangement with and without HC are given in Figure 5.1 and 4.10.

Component	Mass [mT]	Unstretched Length [m]	Stiffness [kN]	Damping [kNs]
Lifted object (assumed rigid to WTG)				
WTG	2074	100	inf.	0
Lower Lifting Tool (LLT)	200	1	inf.	0
Upper Spreader Frame (USF)	200	1	inf.	0
Slings between LLT & USF (4 pcs.)	26	99.5	2.84E+07	0
Total Lifted object	2500	100	inf.	0
Rigging no HC (assumed hinged to WTG)				
Slings from front of USF to shackle (2pcs)	8	4	1.42E+06	0
Slings from back of USF to shackle (2 pcs.)	8	4	1.42E+06	0
Shackle (2 pcs.)	21.6	1	inf.	0
Slings from shackle to block (2 pcs.)	20	10	1.42E+06	0
Blocks (2 pcs.)	262	8.5	inf.	0
Hoisting Wires (20 pcs.)	0	variable	4.0E+06	5.88E+04
Rigging with HC (assumed hinged to WTG)				
Slings from front of USF to HC (2pcs)	8	4	1.42E+06	0
Slings from back of USF to HC (2 pcs.)	8	4	1.42E+06	0
Heave compensators (2 pcs.)	152	8.57	2.62E+04	6.37E+03
Slings from HC to hook (2 pcs.)	20	10	1.42E+06	0
Block	262	8.5	inf.	0
Hoisting Wires (20 pcs.)	0	variable	4.0E+06	5.88E+04
Total Crane load	2819.6	175.2	-	-

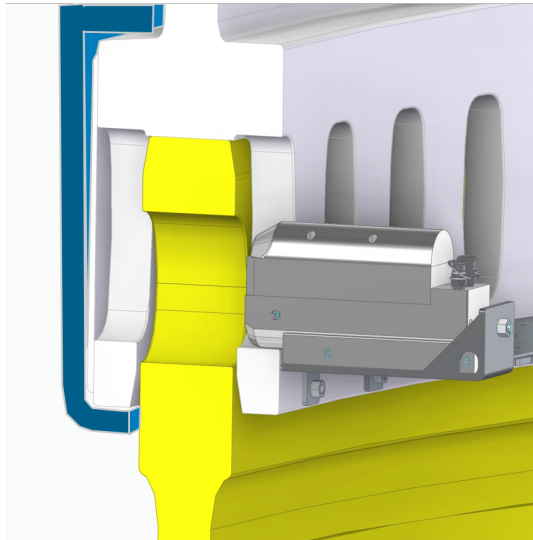


Figure 4.1: Visualization of the clamping of the Lower Lifting Tool (blue part) on the C1 Wedge Connection upper flange.

Turbine

For the turbine, a general reference turbine of 18 MW, developed by HMC, is used. This turbine has the following properties:

Table 4.2: Wind Turbine Generator (WTG) Parameters

Parameter	Value	Unit	Comment
Rated power	18	MW	Approximate
Rotor diameter	250	m	
Hub height	142	m	w.r.t. Tower bottom flange
RNA mass	1037	mT	
Tower height	134	m	
Tower bottom diameter	8	m	
Tower mass	1037	mT	
Support structure height	23	m	above MWL
WTG CoG-X	1.9	m	w.r.t. Tower centre
WTG CoG-Z	92.45	m	w.r.t. Tower bottom flange
USF height	100	m	w.r.t. Tower bottom flange

Vessel

The vessel used in the model is the SSCV Sleipnir. More information about the Sleipnir can be found in Appendix A. To obtain sufficient lifting height and lifting capacity both auxiliary (Aux) hoists will be used. Each aux hoist has a WLL of 2500 mT. A visualization of the Sleipnir model is given in Figure 4.2. Definitions of the crane boom radius, slew angle, boom angle and coordinate system are provided in Figure 4.3. Figure 4.4 shows the definitions of the relative wind and wave directions used in this report.

The following vessel configuration is used:

Table 4.3: Additional Sleipnir Installation Parameters

Parameter	Value	Unit
Draft	27	m
Crane Aux radius	43.00	m
Mass	2.44E+05	mT
Slew angle PS	145.00	°
Slew angle SB	215.00	°

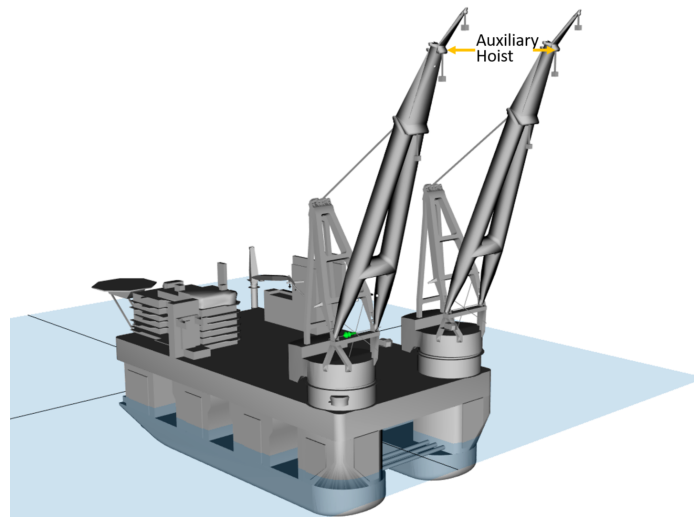


Figure 4.2: Visualization of the Sleipnir model [92].

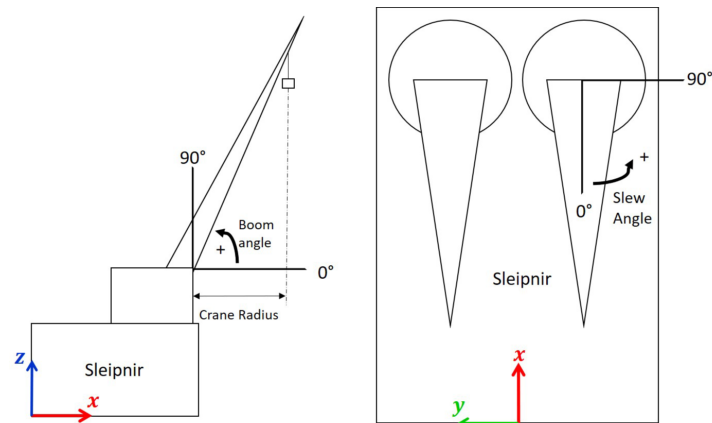


Figure 4.3: Vessel definitions [92].

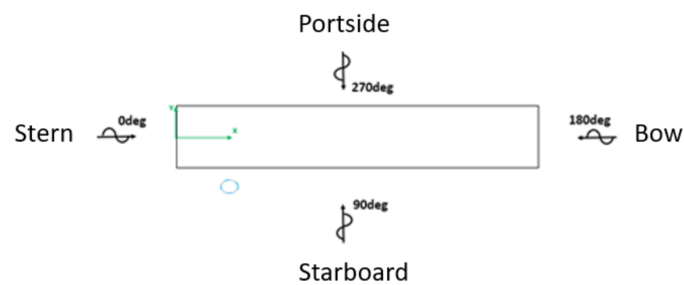


Figure 4.4: Wind and wave headings definition.

4.1.3. Environmental Loading Incorporated

The environmental loads considered in this thesis are wind and first-order wave loads. Second-order wave loads, and current loads are low-frequency and therefore can induce slow varying motions on the vessel. Given their low frequency, these are not expected to significantly influence the WTG excitation. Therefore, in this thesis, these low-frequency effects are not incorporated. In other words: the DP system is assumed to fully compensate for the effects, with zero DP drift. This is a progressive assumption, and therefore the results should be interpreted with care. In the Python model and fundamental OrcaFlex model, only wave loads are incorporated. For the Enhanced OrcaFlex model, wind loads are

also added, as the overturning moment it creates at the tower base is essential to assess the stability during the load-transfer phase.

A JONSWAP spectrum is used to model first-order wave loads. A range of H_s and T_p values is used to capture different sea states: [0 - 4] metres and [6 - 15] seconds, respectively. These ranges cover the most important sea state ranges relevant for this installation; see Section 4.3. To model the wind loading, a Norwegian Petroleum Directorate (NPD) spectrum is used. This spectrum is based on a Kaimal spectrum, which was proposed in Chapter 3.1. A mean wind speed of 10m/s is used at a height of 10m above the mean sea level. The power law wind profile is used to implement an altitude-dependent wind speed. No spatial variation in longitudinal direction is incorporated.

4.1.4. Dynamic Simulations

To assess the operability, time domain dynamic simulations are conducted. Time Domain (TD) simulations are required, with respect to frequency domain (FD) simulations, to take non-linear effects into account. To obtain stationarity, 3h time domain simulations are advised for stochastic modelling [26]. However, 20 min simulations are carried out because these are more representative for the duration of the critical part of the installation operation. As the TD simulations are computationally intensive, model simplicity is desirable. Therefore, the vessel model is simplified to a crane tip input signal. It is justified to make this simplification if the global vessel response is not affected by the set down of the WTG. This is valid for loads around 1-2% of vessel displaced volume according to DNV [26]. For the scenario considered, this ratio is 1.2%. Therefore, this assumption is deemed valid. The crane tip input signal is derived from the crane tip RAOs, calculated in a separate LiftDyn model. More information about the LiftDyn model can be found in Appendix E. Furthermore, modelling an exceptionally enormous number of elements can increase the computational time of a model significantly. Therefore, the rigging of the Lifted Object is combined into one modelling element, see Table 4.1.

The installation procedure steps (Section 4.1.1) 5 through 8 are projected onto three installation 'Situations'. These are defined as:

1. **Situation 1:** The WTG is hanging freely in the rigging, connected to the crane. No interaction between tower bottom and support structure is present. This situation is only used for verification during development of the model. No results are presented for this Situation.
2. **Situation 2:** The WTG is engaging the support structure. Most static weight is still supported by the rigging. Contact between the tower bottom and support structure is present. A secure time window to activate the QCS is looked for. A set of limiting criteria is used to assess this period T_{stab} .
3. **Situation 3:** The QCS is activated. A temporary connection between the tower bottom and the support structure is made. In this situation the rigging load is reduced until the rigging is slack and all WTG loads are accounted for by the support structure. Stability during this 'load transfer period' is assessed by the heeling angle of the turbine and the loads in the QCS.

These Situations are the main terms used in this thesis to indicate the specific installation steps.

Another aspect to pay attention to with regards to modelling is the comparison of results for different connector types, as this is one of the focal points of the research. In this research, it is chosen to model the C1 Wedge Connection because least is known about the behaviour of this connection in an offshore environment. But to compare the results with the Bolted L-flange and the Slip Joint, the modelling differences should be highlighted.

First, the shape of the flanges of the C1 Wedge Connection ensures that, once the webs of the upper flange overlap with the lower flange, the WTG is restricted to move horizontally (only the radial clearance gap is allowed). As this overlap is present in all Situations considered, a constraint of horizontal motion of the bottom flange of the WTG is introduced to the model. This affects the pendulum motion of the WTG as the moment of inertia for a bar around its tip is $\frac{1}{3}mL^2$, with respect to $\frac{1}{12}mL^2$ around its centre (assuming a homogeneous mass distribution). Furthermore, the constraint restricts the first (low-frequent) pendulum mode from occurring, leaving only one pendulum mode for the WTG. For the Slip Joint, a similar constraint could be applied, although the allowed motion of the Slip Joint cones

depends on the overlap of the cones. For the Bolted L-flange, no such constraint is applicable, unless a G&B system is added. Secondly, a certain overlap of the C1 Wedge Connection flanges is required to activate the QCS system. This is not the case for the Slip Joint or Bolted L-flange connection, although alignment of the flanges is required for the FCT to operate. Third, the QCS provides a restoring moment after its activation, to ensure stability during Situation 3 of the installation. The L-Flange in combination with an FCT could obtain a pretension force of 600 kN per FCT, which will be used to compare it to the QCS. For the Slip Joint, no such system is required, as the cone overlap will provide enough restoring moment to accommodate the load transfer phase. The only downside for the Slip Joint from an installation point of view is the extra required lifting height to position the WTG above the support structure.

4.2. Python Model Setup

The Python model is built to verify the main general OrcaFlex findings and to increase understanding of the general model behaviour. The Python model is based on analytically derived Equations Of Motion (EOMs), computed from the Lagrangian formalism.

To approximate the physical behaviour of a whole WTG installation, an equivalent dynamic model can be designed. Since the dynamic behaviour of such a system can be overly complex, choices are made about relevant elements to model and the DOFs of the system. All bodies with a finite number of DOFs are modelled as lumped elements, whose motion (displacement, velocity, and acceleration) are only dependent on time and are independent of spatial coordinates [71]. Such models are governed by (a system of) Ordinary Differential Equations (ODEs). A system of ODEs is presented in Eq. 3.17. Setting up the EOMs for a n -DOF dynamic system in the bi- or tri-directional plane can be quite challenging, labour intensive and sensitive to human-made errors [71]. Therefore, the Lagrangian formalism is often used for complex systems. The Lagrangian formalism is based on the Lagrange equations, see Equation 4.1:

$$\frac{d}{dt} \frac{\partial \mathbf{L}}{\partial \dot{q}_s} - \frac{\partial \mathbf{L}}{\partial q_s} = Q_s \quad (4.1)$$

$$\mathbf{L} = \mathbf{K} - \mathbf{P} \quad (4.2)$$

Equation 4.2 is the Lagrange function; q_s is the DOF coordinate¹ with $s = 1, 2, \dots, n$; Q_s is the external forcing acting on the system; and K and P are the kinetic and potential energy, respectively. The mathematical derivations to obtain the EOM from the Lagrangian equations are not included here to keep this part concise but can be found in any textbook on theoretical mechanics.

To include spring elements in a system of EOMs, as required to model the C1 Wedge Connection for example, and express them in ODEs in planar view, the elongations of the spring elements must be linearised [48]. Since the begin and end point of the spring element move relative to each other, the length l and angle α of the spring element change continuously. In the Python model, the linearisation for small elongations is adopted, as shown in Equation 4.3. This means that the elongation between time step 1 and 2 can be derived from α at $t = 1$ and the displacements u_x and u_z of the begin point (a) and end point (b) of the spring. Figure 4.5 presents a visualisation of an in-plane spring elongation and the coordinates used in Equation 4.4.

$$e_{1,2} = (u_{x,b} - u_{x,a}) \cos \alpha_1 - (u_{z,b} - u_{z,a}) \sin \alpha_1 \quad (4.3)$$

$$u_{i,j} = i_{j,2} - i_{j,1} \quad \text{for } i = x, z \text{ and } j = a, b \quad (4.4)$$

The full system of EOMs can be found in Appendix D. The lumped element model for which the equations are derived is presented in Figure 4.6. Here, three masses are considered: M_1 represents the WTG (only the tower is depicted), M_2 represents the connecting shackle in the rigging, and M_3 is the crane block and $u(t)$ is the crane tip, which is the input signal to the model. All string elements represent rigging spring/damper elements except for the green string, which represents the crane wires,

¹this can either be a displacement or an angle.

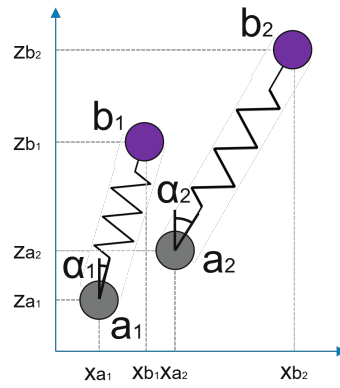


Figure 4.5: Parameters used to describe the elongation of a spring element between particles a and b for small elongations.

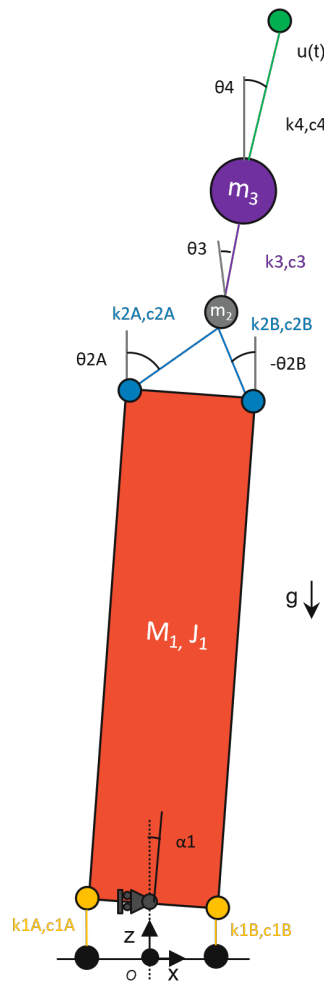


Figure 4.6: Lumped element model used to develop the Python model. The masses M_1 , M_2 and M_3 represent the WTG, Rigging Shackle and Crane Block, respectively. The green element is the Crane Tip, and its motion is considered an input signal to the model.

and the yellow wires, which represent the C1 QCS and/or support structure contact. These C1 QCS spring/dampers are position dependent because they mimic the contact between WTG and support structure. In other words; their stiffness and damping changes with respect to the position of the WTG. When the WTG's bottom flange is touching the support structure's flange, the stiffness is the contact stiffness. When the parts are not touching the stiffness is negligible (stiffness of air). The grey roller

support at the bottom of the WTG is the WTG's constraint in X-direction. This roller support includes the constraint during the installation of the C1 fork-shaped flange overlapping with the support structure's flange, thereby restricting horizontal movement. Gravity acts downwards and only the moment of inertia of the WTG is considered. The other masses are considered to be point-masses.

Statics are solved in an iterative way and the models eigenfrequencies and eigenvectors are obtained through modal analysis. Time Domain (TD) dynamic simulations are computed, where the EOMs are expressed in State Space form to reduce the second order differential equations to a system of first order differential equations. These are solved with forward Euler (explicit) integration for each time step because implementation of an explicit solver is much simpler than an implicit solver. Here, a sufficiently small time step is taken to ensure stability. Since this model is built from scratch, important numerical modelling choices need to be made. As this model is used to verify the main results of the OrcaFlex model and not used to generate the final results for the operability, the functionality of the model is prioritised and limited effort is put into the efficiency and elegance of the model. Filtering of artificial, non-physical, high-frequency noise on the input signal is done to increase computational simulation stability. The results of the simulations include all mass motions, rigging element tension, elongation and orientation and the crane tip motion and forcing.

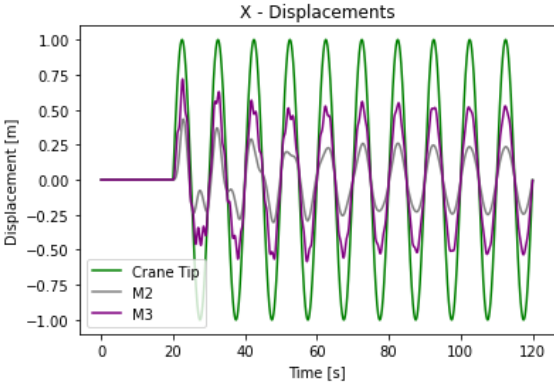
4.3. Python Model Results

The results of the Python Model consist of two parts: the modal analysis results and the dynamic simulations. The modal analysis results are presented in Figure 4.7.

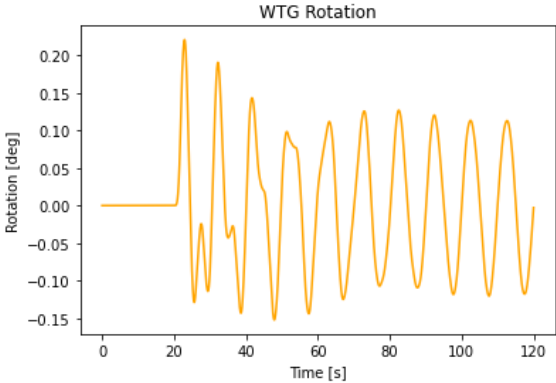
Mode number	1	2	3	4	5	6
Period (s)	10,90	2,32	1,41	0,32	0,32	0,13
Frequency (Hz)	0,09	0,43	0,71	3,13	3,16	7,53
Alpha1 [rad]	0,0064	0,0000	-0,0005	0,0000	-0,0002	0,0000
Z1 [m]	0,0000	1,0000	0,0000	-0,0391	0,0000	-0,0138
X2 [m]	1,0000	0,0000	-0,0516	0,0000	1,0000	0,0000
Z2 [m]	0,0000	0,7584	0,0000	0,4576	0,0000	1,0000
X3 [m]	0,6925	0,0000	1,0000	0,0000	0,0000	0,0000
Z3 [m]	0,0000	0,3848	0,0000	1,0000	0,0000	-0,1440

Figure 4.7: Eigen periods and eigenmodes of Python Model. The modes are ranked from low to high eigenfrequencies. Each row represents a single DOF of the system, with the letters referring to the direction of the DOF and the numbers referring to the body of the DOF. Z2, for example, is the vertical motion of the Shackle (Mass 2). Alpha is the rotation of the WTG. The mode shapes (eigenvectors) are scaled such, that the largest contributing DOF has a value of 1.0.

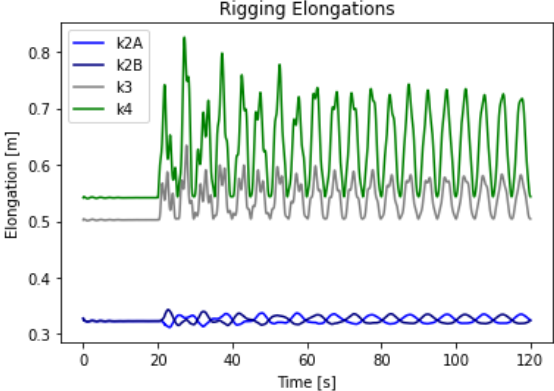
The dynamic simulations are split up into two different simulations. First, the results are shown for a horizontal sinusoidal crane tip input motion. Then, the results are shown for a vertical sinusoidal crane tip input motion. Both have a Crane Tip motion amplitude of 1 meter and a period of 10 seconds. The most relevant results are shown below in Figure 4.8 and Figure 4.9. The simulations start with a 20 second static period, where the static state can converge. Then, the crane tip input signal is added to the simulation. The results are discussed in Section 4.6.



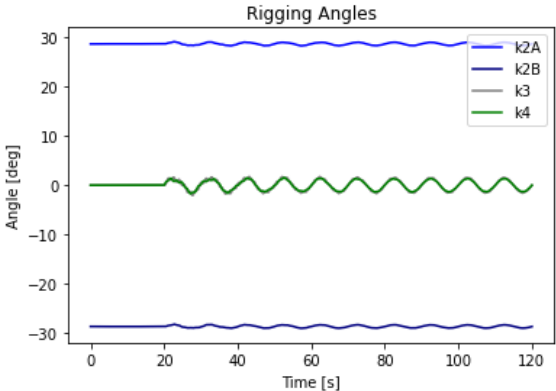
(a) Horizontal motions of Crane Tip, M2 and M3



(b) WTG rotation

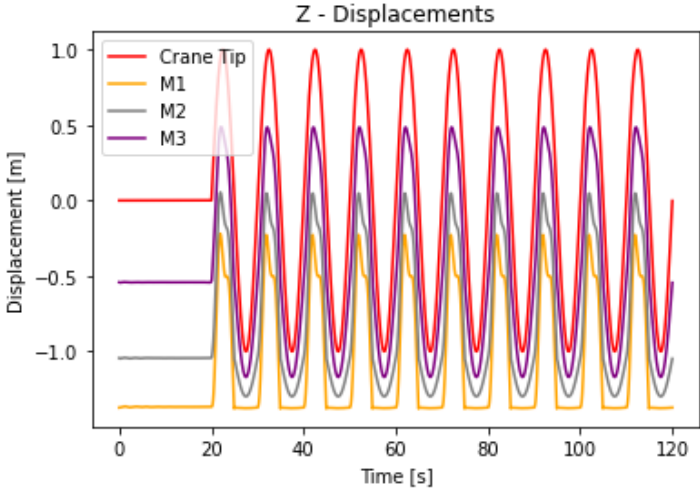


(c) Elongations of rigging elements

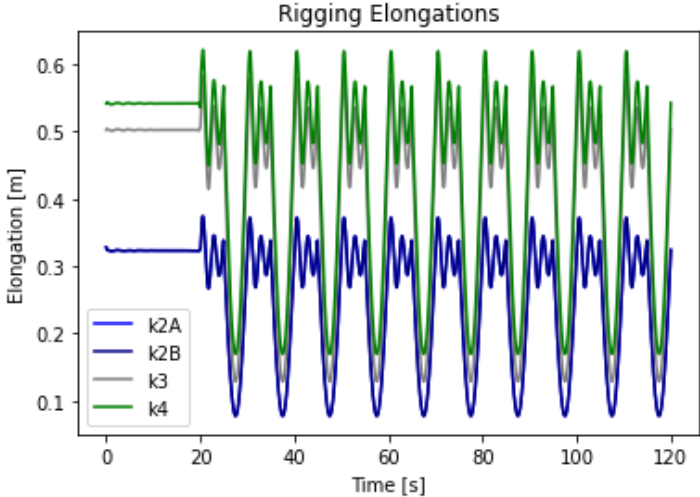


(d) Angle with respect to vertical of rigging elements.

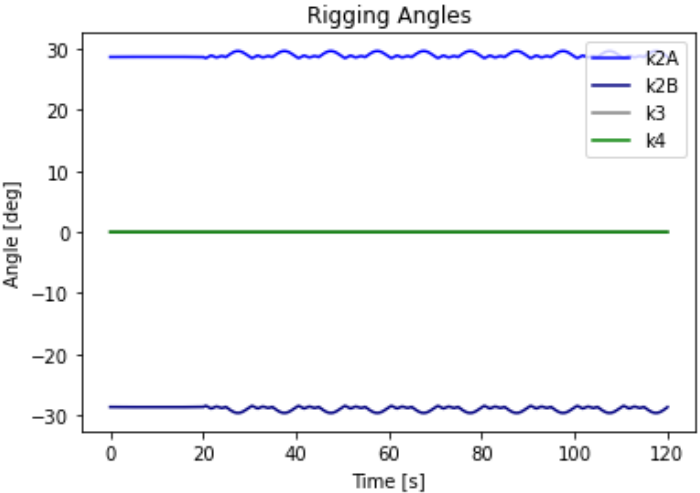
Figure 4.8: Main dynamic simulation results of Python model for horizontal motion of Crane Tip sinusoidal input signal.



(a) Vertical motions of Crane Tip, M1, M2 and M3



(b) Elongations of rigging elements



(c) Angle with respect to vertical of rigging elements

Figure 4.9: Main dynamic simulation results of Python model for vertical motion of Crane Tip sinusoidal input signal.

4.4. Fundamental OrcaFlex Model Setup

The goal of this model is to show the WTG motions for first-order wave loading, thereby mimicking the Python model as precise as possible. To do this, a model similar to Figure 4.6 is constructed. A visualisation of this model is shown in Figure 4.10. The model is almost an exact replica of the Python model, except for the following points:

- The damping of the spring/damper between the WTG and support structure is not position dependent (contact/no contact), but velocity dependent. This was the only spring/damper modelling option in the OrcaFlex software. As the upper limit was chosen, this resulted in extra damping in the system.
- The software solves the EOM with the generalised- α implicit integration scheme as described by Chung and Hulbert [75, 19]. The system of EOMs is solved at the end of the time step. Because the motions are unknown at the end of the time step an iterative solution method is required. Consequently, each implicit time step takes significantly more time to compute than an explicit time step. However, the implicit scheme is typically stable for much larger time steps than the explicit scheme and therefore the implicit scheme is often much faster. This results in obtaining results faster, while maintaining the quality.

The generalised- α integration scheme has controllable numerical damping, which is desirable since it removes artificial, non-physical high frequency noise. Numerical damping also leads to much more stable convergence and thus allows for longer time steps and much faster simulations. Caution must be taken to avoid damping response at lower frequencies. The generalised- α integration scheme is designed such by Orcina to minimise low frequency damping while completing simulations fast and maintaining accuracy [75].

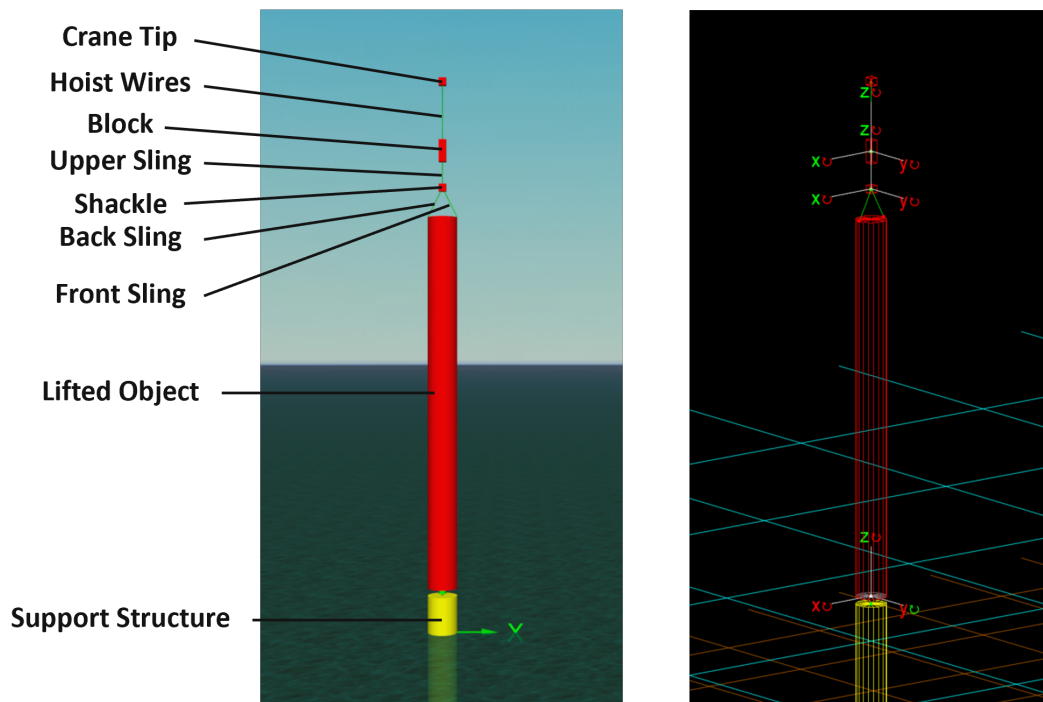


Figure 4.10: Visualisation of the Fundamental OrcaFlex model. The left figure shows a general model view with the components labelled. The right figure shows the shaded graphics view including the DOFs of the modelled masses (green DOFs are enabled, red DOFs are disabled).

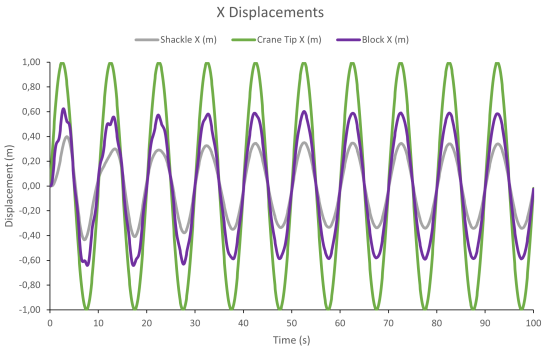
4.5. Fundamental OrcaFlex Model Results

The results of the Fundamental OrcaFlex Model are structured in the same way as the results of the Python model: first the eigenmodes are presented, and then the dynamic simulation results are shown. The eigenmodes are shown in Figure 4.11.

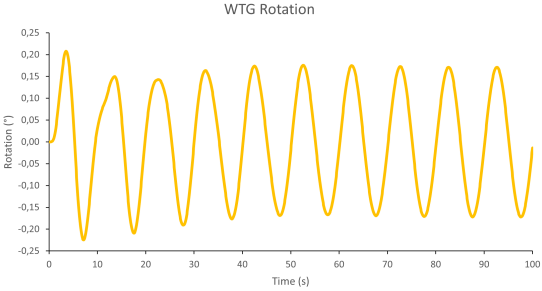
Mode number	1	2	3	4	5	6
Period (s)	11,02	2,31	1,48	0,32	0,29	0,13
Frequency (Hz)	0,09	0,43	0,68	3,13	3,50	7,57
Alpha1 [rad]	0,0097	0,0000	-0,0005	0,0000	-0,0002	0,0000
Z1 [m]	0,0000	1,0000	0,0000	-0,0392	0,0000	-0,0139
X2 [m]	1,0000	0,0000	0,0383	0,0000	1,0000	0,0000
Z2 [m]	0,0000	0,7621	0,0000	0,4507	0,0000	1,0000
X3 [m]	0,6562	0,0000	1,0000	0,0000	-0,0258	0,0000
Z3 [m]	0,0000	0,3867	0,0000	1,0000	0,0000	-0,1420

Figure 4.11: Eigen periods and eigenmodes of Fundamental OrcaFlex Model. The modes are ranked from low to high eigenfrequencies. Each row represents a single DOF of the system, with the letters referring to the direction of the DOF and the numbers referring to the body of the DOF. Z2, for example, is the vertical motion of the Shackle (Mass 2). Alpha is the rotation of the WTG. The mode shapes (eigenvectors) are scaled such, that the largest contributing DOF has a value of 1.0.

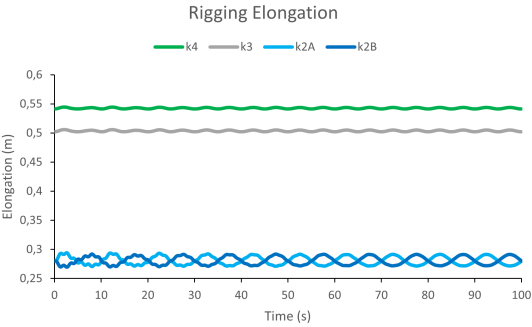
The dynamic results are presented below in an equivalent way to the results of Section 4.3. These are shown in Figure 4.12 and Figure 4.13. The only difference is the time trace of the results. In OrcaFlex, the statics are treated in a separate phase prior to the dynamic simulations. Furthermore, an 8 second ramp-up period is added before the dynamic simulations start at $t=0$.



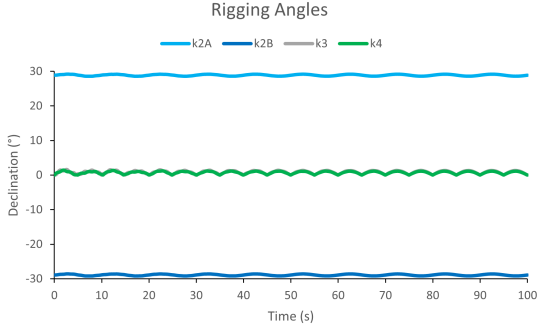
(a) Horizontal motions of Crane Tip, M2 and M3



(b) WTG rotation

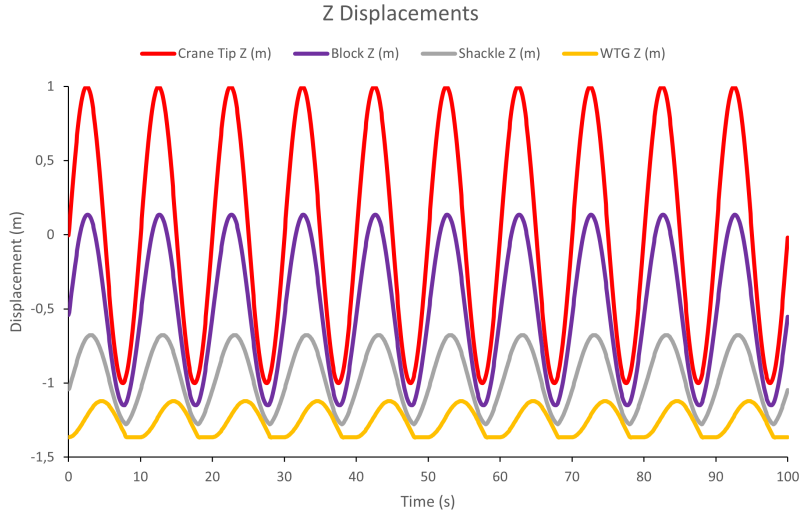


(c) Elongations of rigging elements.

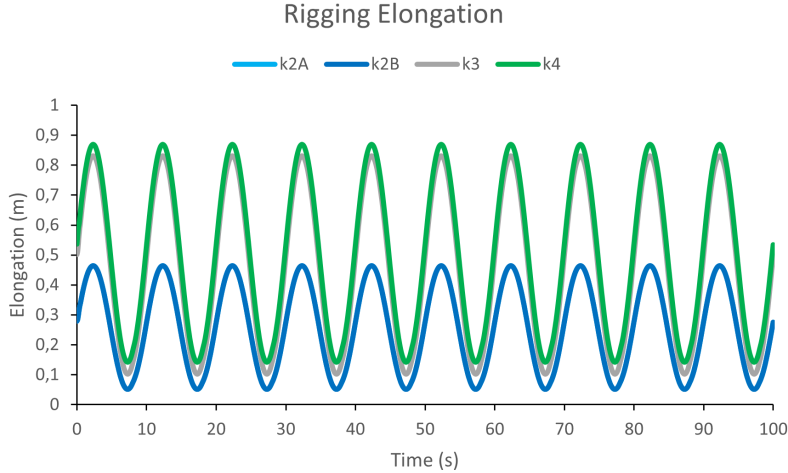


(d) Angle with respect to vertical of rigging elements.

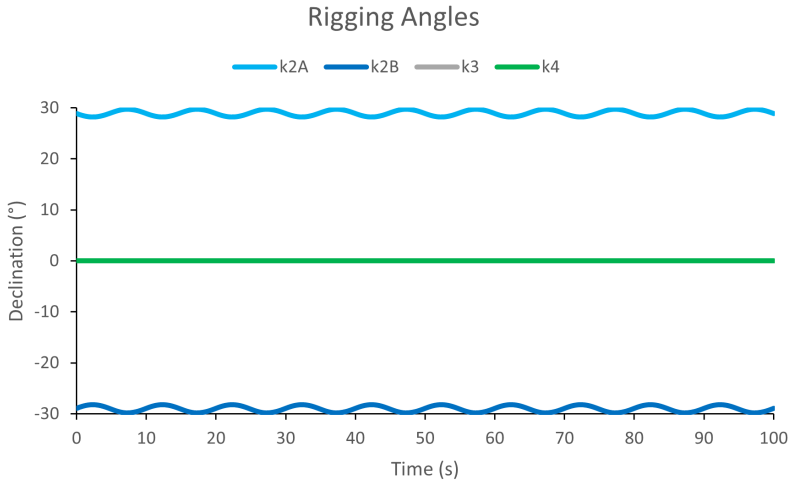
Figure 4.12: Main dynamic simulation results of Fundamental OrcaFlex model for horizontal motion of Crane Tip sinusoidal input signal.



(a) Vertical motions of Crane Tip, M1, M2 and M3



(b) Elongations of rigging elements



(c) Angle with respect to vertical of rigging elements

Figure 4.13: Main dynamic simulation results of Fundamental OrcaFlex model for vertical motion of Crane Tip sinusoidal input signal.

4.6. Comparison and Verification of Fundamental Models

The results of the Python Model and Fundamental OrcaFlex Model are presented in a way that allows comparison of the results. The modal analysis of the results is discussed first, after which the dynamic simulations are addressed.

The mode tables (shown in Figure 4.7 and 4.11) both show six eigenmodes for the model. The eigenfrequencies of the modes are mostly aligned, but some of the frequencies vary up to a maximum of 10%. The mode shapes are also mostly in accordance with each other, with the largest deviation below 10% of the main DOF component. A relatively major difference is the total absence of a contribution of X3 to Mode number 5 in the Python model. Here, a contribution of X3 can be expected as the masses of M2 and M3 and the stiffnesses of k2A, k2B, k3 and k4 are around the same order. The shape difference probably is a result of the eigenfrequency difference of Mode 5. As M2 has a larger stiffness in X-direction than M3, a higher frequency would excite M2 more. This is also seen for Mode 3, where the eigenfrequencies vary the most, causing the mode shapes to vary as well.

Although there are some variations of the eigenfrequencies and mode shapes (mostly in Mode 3 and 5), these are not expected to influence the model behaviour a lot. As most of the excitation due to (mean) wind and waves is on the low frequency side of the eigenfrequency spectrum; below 0.5 Hz, only Mode number 1 and 2 are expected to influence the model's behaviour significantly. The high frequent turbulent component of the wind excites structures usually above 10 Hz, which is also outside of the eigenfrequency range. Therefore, the modal analyses of the models do not show any significant difference between the models in the relevant frequency range.

The dynamic simulations show results for pure horizontal (X) sinusoidal motion of the Crane Tip and for pure vertical (Z) sinusoidal motion of the Crane Tip. This is done to make the time traces of the simulation comparable. If a random phase JONSWAP spectrum was used as input to the Crane Tip motion, no direct comparison of time traces would be possible and statistical quantities should be used to compare the results. As the comparison of these models is done for the initial model, no effort is put into obtaining statistical results for this model and the Python model and only the general dynamic behaviour is compared. Thereafter the best model is chosen to further develop and calculate the operability of the installation Situations.

As for the statics of both models, the models are in full agreement. This can be seen as all initial values of the graphs are similar (at $t=0$). The only deviation is in the rigging elongations of k2A and k2B, which are 0.28 m for the OrcaFlex model and 0.32 m for the Python model. Deriving statics analytically shows the OrcaFlex model gives the correct static elongation for k2A and k2B. The general dynamic behaviour for displacements, WTG rotation and rigging angles is similar for both models after the startup phase. The frequencies of the signals all follow the excitation frequency of 0.1 Hz. The amplitudes vary in general up to around 10%. The relative outliers here are the WTG rotation (0.06 ° absolute difference) and the rigging elongations. The rigging elongations by far show the largest behaviour differences, large peak loads can be seen in k3 and k4 in the Python model.

The WTG is lifted up further in the Python simulations (vertical Crane Tip motions). The rigging is storing less energy during the uplift of the WTG, while in the OrcaFlex model most of the energy is taken by the rigging. The OrcaFlex model shows mainly harmonic characteristics for the rigging elongations and angles, while the Python model shows rougher behaviour, more associated with impact modelling. However, the high frequent variations in the rigging tension of Python results occur during the lift-off phase of the WTG. This could suggest high-frequent motion of the modelled objects, but Figure 4.9a refutes this. Another possible explanation is that the high-frequent behaviour is numerical noise in the model. The OrcaFlex model does not have this because the OrcaFlex model has more damping, including high frequency response damping (see Subsection 4.4).

By quantifying the peak loads in the rigging for the horizontal crane tip motions, we might be able to say which model reports these loads more accurately. The dynamic rigging elongations in k4 in the Fundamental OrcaFlex model are 1.78mm, this equals to 9 mT of dynamic pulling force in the rigging. In the Python model the dynamic rigging elongations in k4 are 186mm, this equals to 947 mT of dy-

dynamic pulling force in the rigging. This is almost half of the WTG weight. This does not seem plausible for 1m of horizontal Crane Tip displacement. The OrcaFlex results therefore seem more realistic as the rigging tension slowly varies along with the Crane Tip motion. As the elongation never reaches zero during the set-down phase of the WTG (flat part of yellow line in Figure 4.13a), there is no need to expect any flat parts in the rigging elongation graphs (Figure 4.13b), as part of the WTG weight is still supported by the crane. The OrcaFlex model also shows a phase shift in the Z displacements for the different modelling bodies. This effect of inertia is not seen in the Python results. Both models seem to stabilise at the end of the simulation period. No large behaviour differences occur here in consequent Crane Tip periods.

What can these models say about the effect of waves on the motion of the WTG during installation? In general, the motion induced on the WTG are limited. The model results show general comparable results. For the deviations, the correct solution can be derived from logical reasoning. Although the horizontal motions seem insignificant due to wave loading, this might alter when the horizontal CoG offset, and wind loading are incorporated. The vertical impact of the WTG seems more relevant to the installation's operability. This could be managed by adding heave compensation to the rigging system. Furthermore, the WTG rotation motion is sensitive to excitation frequencies around 0.09 Hz. The vertical WTG motion is sensitive to excitation frequencies around 0.43 Hz.

After verifying the Fundamental OrcaFlex model and the analytically derived Python model, the verification implications are discussed. The first thing that should be mentioned is that the OrcaFlex model simulates the rigging elements much better. The rigging loads are more stable and show the correct static and dynamic behaviour expected from the model. Furthermore, the OrcaFlex model over-dampens the current contact modelling. Therefore, a new method to model contact between the support structure and WTG is implemented in the Enhanced OrcaFlex Model. Furthermore, it is hard to compare Python models for irregular input signals. OrcaFlex includes a functionality, in which a specific 'seed' can be selected for the applied wave and/or wind loads. This seed determines the uniformly distributed pseudo-random generated wind/wave component phases and thus the applied wind/wave train. This makes the simulations repeatable, which is an important principle in scientific experiments. Furthermore, OrcaFlex is much more user-friendly than Python, which increases the productivity of generating results. Taking all of the above into consideration, it is decided to further expand the OrcaFlex model.

5

Enhanced OrcaFlex Model

The Enhanced OrcaFlex model was built to include extra, relevant factors in the model that affect the installation. This includes wind loading, CoG-offset of the WTG in X-direction, contact modelling between WTG and support structure, bending of the tower and the option to add heave compensation (HC). In this chapter, the integration of these expansions into the Fundamental OrcaFlex model will be detailed. The latter part of this chapter explains how the data were collected for the limiting parameters, validation techniques, assumptions, and limitations. A summary concludes this chapter, presenting the main modelling choices and main model properties.

5.1. Expansions in Enhanced OrcaFlex Model

The Enhanced OrcaFlex model includes additional features with respect to the Fundamental OrcaFlex Model. These are described below. A visualisation of the Enhanced OrcaFlex model is given in Figure 5.1.

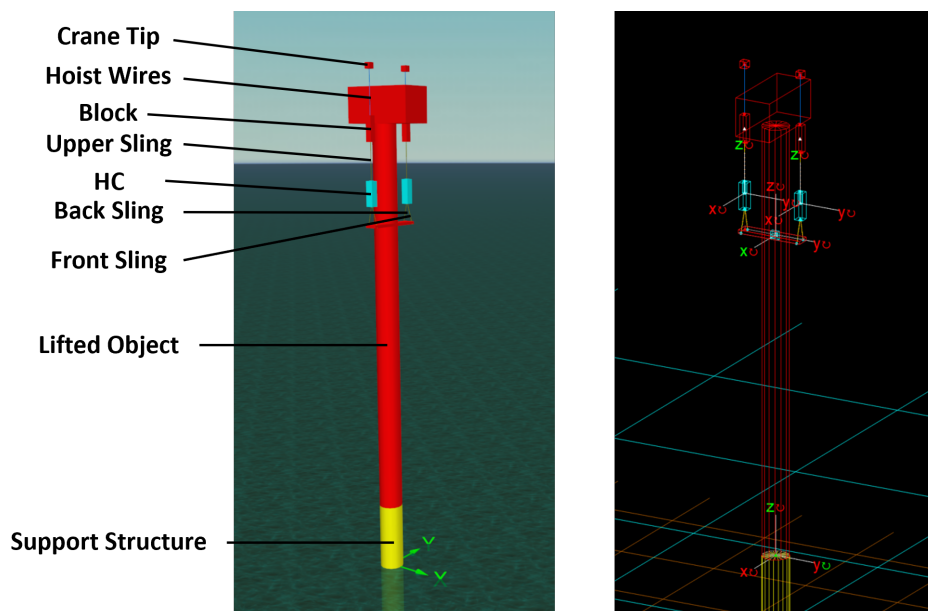


Figure 5.1: Visualisation of the Enhanced OrcaFlex model. The left figure shows a general model view with the components labelled. The right figure shows the shaded graphics view including the DOFs of the modelled masses (green DOFs are enabled, red DOFs are disabled).

Wind loading

As mentioned before, an NPD spectrum with a mean wind speed of 10m/s (at 10m height) is used in OrcaFlex to model wind loading. Wind loading is assessed on all WTG components (tower, nacelle, hub, and blades). As the rotor is not turning during installation and the blades can be pitched to an optimal heading prior to hooking on, the wind loading on the blades is found to be low with respect to the tower and NHA. Table 5.1 shows the static wind loading for the three cases assessed. As can be seen from the table, addition of pitched blades only leads to a 7% increase of wind loads. To reduce computational time, the blades are not incorporated in the model, but a high drag coefficient for the NHA is incorporated. Wind loading on the tower and NHA is incorporated in the model. Drag coefficients of 1 are used for both tower and NHA.

Case	Horizontal Wind Force (kN)
Whole WTG with blades unpitched	179.6
Whole WTG with blades pitched 90°	82.6
Tower and NHA	77.1

Table 5.1: Static Wind Load in global X-direction with a mean wind speed of 10m/s . Here, the unpitched blades are loaded with maximal drag forces while the pitched blades are loaded with minimal drag forces.

Contact modelling and initial static weight percentage

For the contact modelling between WTG and support structure the approach suggested by Orcina for modelling contact in OrcaFlex was followed [77]. This document advises to model the contact as contact between a buoy and an elastic solid shape. The stiffness and damping values can be specified for each object and the interaction is limited to the vertices of the objects, which can be specified. A stiffness value of 4.0GN/m is used for the contact modelling and no damping is incorporated here. This approach makes the contact position dependent, in which it deviated from the Fundamental OrcaFlex model, where the contact was modelled with the use of spring/dampers. Furthermore, the initial part of the load that is transferred to the support structure is varied to find the optimal operability for Situation 2. This part is defined as a percentage of the static WTG weight that is supported by the rigging (F_c). The remaining part is supported by the support structure as a constant contact force at the start of the simulations. By varying the hoist wire length, this initial percentage can be varied, and an optimal percentage is derived for which the operability has a maximum.

Tower Bending

As more weight is supported by the foundation, the function of the crane tip alters. Where the crane tip at first was carrying the WTG and thereby holding it upright, it now starts to destabilise the WTG. Large crane tip deflections in horizontal direction induce horizontal load on the WTG. As the WTG is modelled as a rigid body, these loads are directly transferred to the C1 Wedge Connection. By incorporating tower bending into the model, some of this energy is temporarily stored in the deflection of the tower. Incorporation of tower bending into the model is done by adding an equivalent tower bending stiffness between the WTG and the rigging connection points. The equivalent tower bending stiffness is derived from a separate model, in which a 15 MW Reference Wind Turbine model (developed by Orcina [75]) is scaled up to the 18 MW HMC model, and is equal to 5MN/m .

Revised modelling choices

Some other model attributes were changed. The rigging elements, which were modelled as spring/damper elements in the Fundamental OrcaFlex model, are exchanged for line elements. These are limited to tension only (no compression), which is a better representation of real slings. Another added benefit of this change is that OrcaFlex calculates statics in different steps. Line statics are calculated in a separate step, increasing the statics convergence of the model. The modelling of the crane wires has also been altered. These are now modelled as a winch element, making them easier to adapt pretension, length, and switch these in distinct phases of the simulation, which is especially useful for Situation 3. To achieve static convergence a small rotational stiffness was added to the rigging bodies (block, shackle, PHC).

Passive Heave Compensation

After assessment of the first results (without PHC), the impact velocity and stabbing periods were limiting for the installation. Hereafter, PHC was added to the model to compare the installation with and without PHC, thereby showing the effect of PHC on this installation. Two CraneMaster units are added to the rigging configuration, replacing the shackle bodies. The input used to the model is shown in Table 5.2. Each unit exists of a main body and an upper body. The main body includes the inertia characteristics, while the upper body represents the cylinder stroke. The bodies are connected through a constraint with only a DOF in the stroke direction of the PHC, that is restrained by a constant stiffness of $400mT/m$.

Table 5.2: Passive Heave Compensation Parameters

Parameter	Value	Unit
Mass	76	mT
Stiffness	400	mT/m
Damping	956	kNs/m
	24%	1/s
Size [l, w, h]	[2.53, 2.53, 8.43]	m
CoG [l, w, h]	[0, 0, 4.22]	m

5.2. Limiting Parameters

Preliminary screening of critical events and limiting parameters is done with regards to the installation procedure stated in subsection 4.1.1. The critical installation activity assessed in this thesis is the set down of the WTG on the support structure. A number of critical events and limiting parameters are identified and denoted in Table 5.3. These limiting parameters are applied to Situation 2.

Note that T_{stab} and F_{stab} are limiting parameters to move from installation Situation 2 to installation Situation 3. After identification of the limiting parameters, the dynamic model is evaluated for all possible combinations of significant wave height H_s and peak period T_p . The outputs of the OrcaFlex simulation files are processed by a Python post-processing script in Jupyter Notebook. This script extracts the relevant data from the simulation files and calculates the statistical relevant parameters of the dynamic responses. For this thesis, the Single Most Probable Maximum (SMPM) value is used as the statistical parameter to present the relevant results, because it incorporates exposure time as well, with respect to Significant Double Amplitude (SDA). One can imagine that the longer the exposure time or number of cycles, the larger the probability that the operability limit will be exceeded. Because limiting criteria are usually expressed in single sided terms, the maximum values are also expressed single sided. The SMPM value is derived directly from the standard deviation σ_{STD} as shown in Equation 5.1 [8]. These are then plotted in tables/graphs and compared to the limiting parameters.

$$SMPM = \sqrt{\frac{\ln(N_z)}{2}} SSA = \frac{1}{2} \sqrt{\frac{\ln(N_z)}{2}} 4\sqrt{m_0} = 2\sqrt{\frac{\ln(N_z)}{2}} \sigma_{STD} \quad (5.1)$$

Here, N_z is the number of cycles during the exposure time which is assumed to be 100 cycles for a 20min sea-state (with a Rayleigh distributed crest height), SSA the Single Significant Amplitude and m_0 the zero-order spectral moment. This equation is valid for random processes with a Gaussian PDF, such as the used wave spectra.

Modelling of Situation 3 is also done in OrcaFlex. For this, different models are evaluated, where the crane wire tension is decreased and the C1 QCS stiffness is chosen. This simulates the transfer of the WTG load from the crane to the support structure. This operation can be tweaked to make sure Situation 2 is the limiting phase of the installation. However, some of the relevant limiting parameters to Situation 2 are still relevant to Situation 3. This concerns the limiting parameters 'WTG rotation' (a measure of its stability), 'rigging and hoist snap loads' and 'crane wire offlead'. Especially the WTG rotation is interesting here, since the motions of the WTG are a measure for the stability of the WTG. The crane tip input motions are similar to Situation 2. Therefore, large rigging and crane wire loads may occur. Here, large is with respect to the WTG response, not to the vessel response. This can be

Table 5.3: Critical Events and Limiting Parameters

Critical Event	Limiting Parameter	Value	Unit
A maximum inclination angle during lifting should be adopted to assure stability of the lift and prevent the turbine from falling over. Next to the structural requirement, it also feels unsafe to lift an object under an angle far from vertical.	WTG rotation	1	°
If the WTG is lifted far from the support structure's flange, the two C1 flanges are not overlapping any longer and the constraint in horizontal direction, which is assumed in the models, is no longer valid.	WTG uplift	0.3	m
A maximum crane wire offlead is required to assure crane lifting capacity. An offlead away from the crane effectively increases the moment arm the crane experiences. It must be noted here, that no pure offlead is assessed in the model. Due to the in-plane view of the installation operation, a combination of sidelead and offlead is measured.	Crane wire offlead	3	°
Rigging is designed for a certain WLL. Due to dynamic loads, the WLL can be reached, compromising the design limit of the rigging or hoist wires. Therefore, a certain DAF limit is selected for the rigging and hoist wire loads.	Rigging and hoist wires DAF	1.2	-
Maximum accelerations can be specified for certain WTG components by a client, as some equipment is sensitive to accelerations.	Acceleration in X-direction of WTG	1.8	m/s ²
Maximum accelerations can be specified for certain WTG components by a client, as some equipment is sensitive to accelerations.	Acceleration in Z-direction of WTG	2.6	m/s ²
Structural damage due to impact of WTG on the support structure. Structural damage criteria need to be assessed from FEM analysis. FEM modelling is not included in the scope of this thesis. Therefore, this criterion is assessed in terms of initial impact velocity.	Impact velocity in Z-direction of WTG	0.2	m/s
Incomplete QCS activation. A sufficiently large period is required to activate the C1 QCS (stab the wedges into the slots). ALARP risk can be taken with regards to stabbing of the wedges. To have a large enough part of the stabbing slots aligned, a maximum uplift due to a combination of pure uplift and rotation of the WTG of Z_{max} is allowed.	T_{stab} , with Z_{max}	5, with 0.01	s, with m
From an operations point of view, it is desirable to be able to activate the C1 QCS at any time. However, the above-mentioned limit for activation of the C1 QCS limits this activation. This limiting parameter is added to make the operation feasible from an operational point of view. It prescribes a percentage of the observation time, for which the activation of the C1 QCS should be possible.	F_{stab}	20	%

compared to mooring line loads for anchored vessels. Here, implementation of Heave Compensation may offer a solution to reduce these peak loads. A constant wave peak period of 10s is chosen in these simulations. Table 5.4 shows the hoist wire lengths chosen to ensure the pre-set crane loads. It should be noted that these crane loads are the achieved loads in static calculation. During the dynamic simulations, this percentage varies due to excitation due to wind and waves. The amplitude of this variance depends on the sea-state.

Table 5.4: Hoist wire lengths for Situation 3 simulations

Crane load (%)	Hoist wire length without HC (m)	Hoist wire length with HC (m)
100	28.858	18.017
80	28.900	18.672
60	28.941	19.328
40	28.983	19.983
20	29.024	20.639
0	29.100	21.300

5.3. Verification Techniques

The OrcaFlex model used to generate the operability results is verified in diverse ways. Throughout the building of the model, each expansion of the model is thoroughly tested on its own before adding it to the main model. Testing is done by visual analysis, comparison of the order of magnitude of parameters, consistency with quick hand calculations, comparison to other models/projects. The building of the model is split up into two phases. The first phase is described in Section 4.6. After the expansion of the model, the second way of verifying the models' results is done by carrying out sensitivity analyses. This is done for both the limiting parameters and the input parameters, such as mean wind speed, stiffness values, and some physical properties of the model such as rigging design.

These two verification steps, carried out after each modelling phase, are expected to build sufficient confidence in the models' performance. These two verification steps are selected as they are complementary in their approach and independent of each other. The final model is also compared to other models developed to simulate offshore installations of WTGs.

5.4. Assumptions and Limitations

In the development of the models, many assumptions are made to ensure that an in-depth technical assessment of (part of) the installation feasibility could be executed in the limited time and resource frame provided for the thesis. The main assumptions are already listed in Subsection 1.3.3. Here, a more in-depth list will follow, categorised by model process phase:

General/main

- The main stability issues can be captured in modelling the installation in the X-Z plane. This assumption is supported by conclusions in the Thesis of T. Lengkeek [64]

Input from Liftdyn

- Vessel motion is unaffected by WTG motion, which is valid for loads around 1-2% of vessel displaced volume according to DNV [26].
- Wind loading on the vessel is not incorporated [29].

Environmental loads

- Wind and waves are unidirectional.
- Wave loading is incorporated with a JONSWAP wave spectrum for deep water.
- The sea is a stationary Gaussian process for a duration of 20 minutes to 3 hours.
- Wind loading is unaffected by objects upstream of the WTG.
- Wind power law exponent for surface roughness is 0.12.
- The effect of VIV is neglected.
- The DP system perfectly cancels out current, second order drift forces and wind loading on the vessel and has zero DP footprint for short installation periods.

Modelled objects

- The turbine properties are as stated in Table 4.2, provided by HMC.
- The vessel properties are as stated in Table 4.3, provided by HMC.
- All bodies are rigid.
- No material damping.
- Uniform tower diameter throughout the tower length.
- The support structure is fixed to the seabed.
- The NHA is modelled as a box for wind loading assessment.
- No tuggers are modelled.
- All wires are spring/dampers or lines without bending stiffness but limited in compression.
- Constant stiffness and damping values are assumed for all modelled objects, except for the C1 Wedge Connection.

- Critical damping value of 5% for slings.
- Bending forces in the C1 Wedge Connection are neglected.

Post-processing statistics

- The response can be described as a random process with a Gaussian PDF and a standard deviation of 4 times the SDA.
- A fixed number of 100 cycles during the exposure time.

Additional assumptions for the analytical Python model

- Linearisation for small elongation.
- Small angle approach.
- Lumped element model.
- C1 QCS works as a spring/damper system.

5.5. Model Design Summary

To assess the dynamics involved in a single-lift WTG installation, a specific installation procedure and dual crane lifting configuration are adopted. Using non-linear TD dynamic simulations, the operability of the installation is assessed. Expanding the model with effects like wind loading and including the option to implement HC in the rigging setup, the Enhanced OrcaFlex model is set for more realistic modelling of the installation than to the Fundamental OrcaFlex model. Critical events during the mating phase of the installation (Situation 2) are identified and limiting parameters are selected. The sensitivity of these limiting parameters is evaluated, next to model input parameters. Hereafter, the load transfer phase of the installation (Situation 3) is designed, focusing on a minimal WTG declination angle and as low as possible wire snap loads. This is all done with the goal to determine the operability of the mating operation. A sensitivity analysis of the limiting parameters and input parameters is performed to optimise the operability. The main modelling choices made in this Chapter are mentioned in Table 5.5.

Table 5.5: Main modelling Choices and Argumentation

modelling Choice	Argumentation
Include only 1st order wave loads	First-order wave loads consist of wave frequencies around the same magnitude as the model's eigenfrequencies. Therefore, these are relevant frequencies to incorporate in the model. The second-order wave frequencies are much lower and therefore are not expected to significantly influence the model.
Include wind loads	For wind, direct loading on the WTG is incorporated because the mean wind component creates an overturning moment with respect to the tower base. This is relevant to the tower's stability during the load transfer phase. Turbulence loading on the WTG is not included but can potentially dampen the WTG motions induced by the wave loading.
Not include current loads	Current loads are low-frequency and therefore can induce slow-varying motions on the vessel. Given their low frequency, these are not expected to significantly influence the WTG excitation.
All bodies assumed rigid	This modelling choice is a simplification of reality; the extent of its validity should be further researched. It is made to keep the model simple. The largest error is expected with regards to tower bending. This effect is expected to reduce the WTG bottom rotation as the top of the WTG can flex along with the crane tip motions. Therefore, the effect of this on the operability is determined and presented in Chapter 6
Simplify Lifted objects to one model part	The 'Lifted Object' parts are combined into one modelling part to simplify the model and increase the simulation speed. As the stiffness of all lifted objects is relatively high, this assumption can be made.
Add roller support to WTG bottom flange	This assumption takes out one DOF of the WTG, which is beneficial to the simulation speed. This is a valid assumption because the overlap of the C1 Wedge Connection flanges is one of the limiting parameters. In other words; if the flanges do not overlap, the sea-state is marked as not operable.
Include HC as an option	When the governing operability limits were first assessed, direct coupling between crane tip motions and WTG motions was seen to cause a decrease in operability. Partially decoupling this with HC was followed through to assess its effect on operability.

6

Results and Discussion of Enhanced Model

The research goal of this thesis is to optimise the operability of the single-lift installation of a WTG. The sub questions are aimed at assessing the operability of the installation operation and sensitivity of this operation to changes in design. This chapter presents the most important results of the thesis and discusses them in a structured way. The results of the Enhanced OrcaFlex Model are presented and discussed for both Situation 2 (free hanging, before activation of the QCS) and Situation 3 (load transfer, after activation of the QCS). The results of the sensitivity study are presented hereafter. Here, only single-parameter variations are included (no cross variations). The validity and reliability of the results are discussed lastly. Results of Situation 1 are not presented as they were only used to verify the model development.

6.1. Results Situation 2 (before QCS activation)

Here, the main results are presented for Situation 2 (before QCS activation). This consists of the operability with and without Heave Compensation (HC), the raw data output from the post processing script and the operability without tower bending incorporated.

Figure 6.1 shows the Single Most Probable Maximum (SMPM) operability for the Enhanced OrcaFlex model under standard conditions, with the significant wave height H_s shown on the vertical axis and the wave peak period T_p shown on the horizontal axis. The operability is the area under a graph. For the total operability, the area should be taken of the most restricting (combination of) limiting parameter(s). As can be seen in the graph, the limiting value of the stabbing period fraction 20% (red line) is governing in this situation. The operability is extremely limited and almost nought. However, the fraction and stabbing period (green and red lines) are operational limits (coming from the operation design). The first structural limitation on the operability is the dynamic resonance tension. Although this gives already a much better operability, it is still very restrictive. Section 6.3 discusses the effect of varying the operational limits on the total operability.

Other worthy findings are the big operability 'gap' between the four most limiting parameters and the other parameters. The correlation between the WTG rotation and the stabbing period is quite logical; the larger the rotation, the shorter the stabbing slots of the C1 are aligned, thus the shorter the stabbing period. Another noticeable phenomenon is the dip in the WTG rotation around $T_p = 6.5s$. It must be noted here that all values in this part of the scatter table lie really close together. Small variations in SMPM data due to computational inaccuracies for example may lead to small errors in the limiting parameter plotting. In other words, the error bars in this part of the graphs are large. The dots in the operability curves are the measured data points, connected by straight lines. The evaluated model grid has a resolution of $0.1m$ in the H_s direction and $0.5s$ in the T_p direction. This results in 779 simulations required taking over 12 hours to obtain the data to make such an operability plot. As a finer resolution is possible, it is not advisable from a computational time point of view.

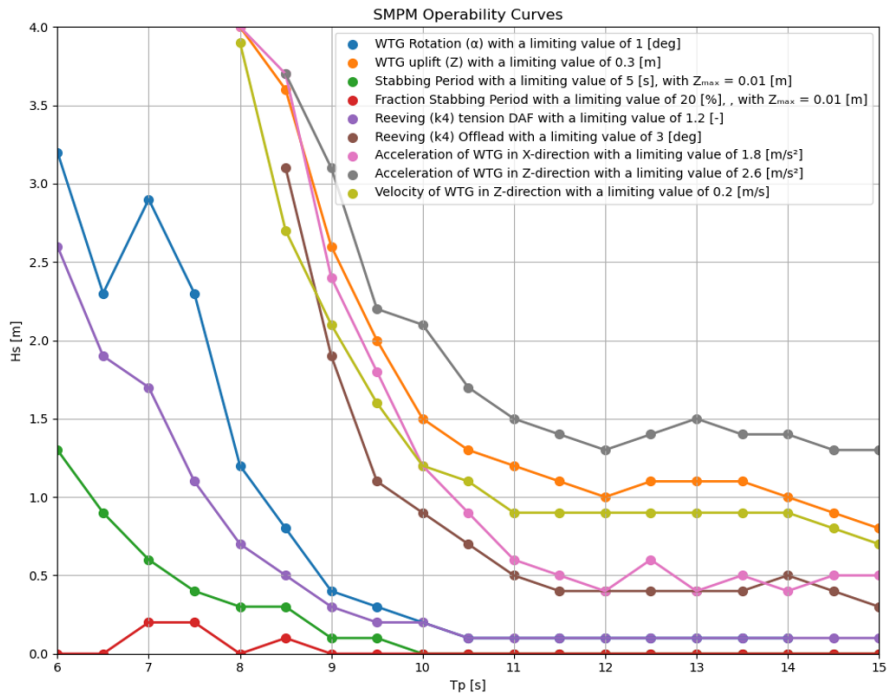


Figure 6.1: Operability for Situation 2 without Heave Compensation and $F_c = 100\%$.

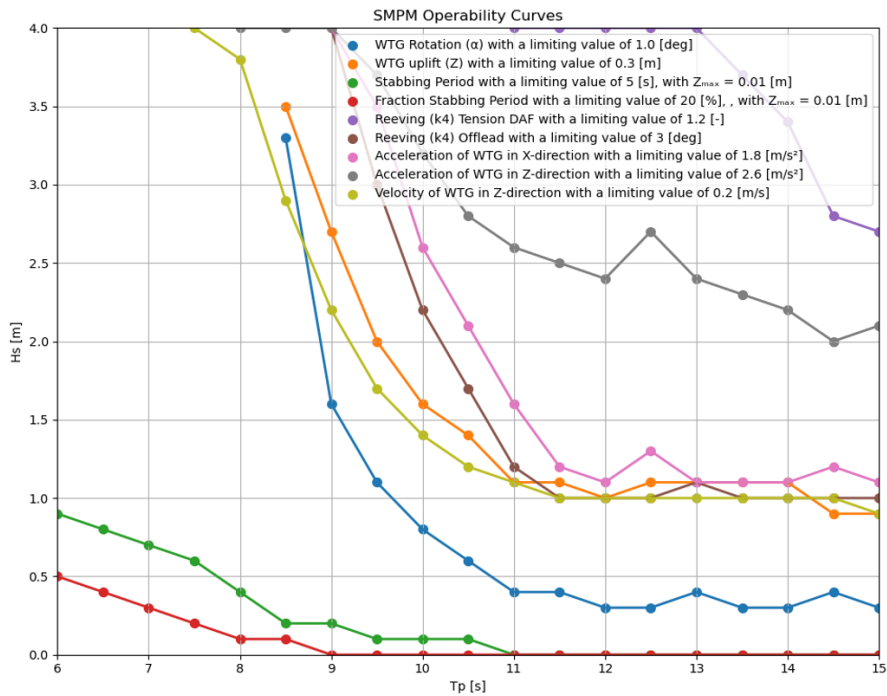


Figure 6.2: Operability for Situation 2 with Heave Compensation ($k_{HC} = 400mT/m$) and $F_c = 100\%$.

Figure 6.2 shows the operability for the Enhanced OrcaFlex model with heave compensation. The stabbing period and fraction are still the main limiting parameters, although the overall operability has increased slightly. Another distinction with regards to the case without HC is that the reaving tension graph has shifted towards the upper right corner of the plot. This also holds (partially) for the WTG rotation, acceleration, and reaving offlead. From this, it can be deduced that the motions of the WTG are reduced mainly in horizontal direction because of HC.

SMPM Velocity of WTG in Z-direction [m/s] for $T_{p,m} = 20.0$ [min]

T_p [s]	6.000000	6.500000	7.000000	7.500000	8.000000	8.500000	9.000000	9.500000	10.000000	10.500000	11.000000	11.500000	12.000000	12.500000	13.000000	13.500000	14.000000	14.500000	15.000000	
H_s [m]	4.0	0.106008	0.121033	0.131627	0.161902	0.209544	0.282938	0.371374	0.482946	0.604910	0.683944	0.790182	0.842156	0.903108	0.847782	0.873040	0.889155	0.880578	0.977309	0.981511
	3.9	0.103725	0.117291	0.128842	0.157810	0.203672	0.275930	0.361687	0.470336	0.589888	0.665962	0.768464	0.819078	0.877067	0.822917	0.846164	0.860100	0.853949	0.951283	0.955197
	3.8	0.101364	0.115492	0.125557	0.153989	0.198494	0.268521	0.351918	0.456028	0.571981	0.646716	0.746312	0.796161	0.851224	0.799862	0.823131	0.837164	0.828097	0.916501	0.925063
	3.7	0.098645	0.111680	0.121391	0.150165	0.193149	0.261396	0.342022	0.443591	0.555059	0.628862	0.725128	0.773199	0.827963	0.774068	0.798483	0.808848	0.803635	0.887251	0.899331
	3.6	0.096099	0.109389	0.118943	0.145719	0.187369	0.254258	0.332688	0.430279	0.539482	0.610833	0.704858	0.750026	0.801483	0.751889	0.775458	0.784112	0.778932	0.862593	0.870714
	3.5	0.092494	0.106085	0.115386	0.141489	0.182135	0.246640	0.322737	0.417576	0.523461	0.592626	0.683213	0.728317	0.777312	0.727591	0.750778	0.757999	0.755782	0.833734	0.843644
	3.4	0.090221	0.102998	0.112406	0.137819	0.177139	0.239267	0.314148	0.405332	0.507996	0.574686	0.662570	0.706148	0.751825	0.703896	0.727511	0.736771	0.731098	0.807785	0.815210
	3.3	0.087733	0.100633	0.108741	0.134084	0.171218	0.232070	0.304048	0.392183	0.492616	0.556874	0.641736	0.681718	0.727145	0.681724	0.703135	0.710280	0.706737	0.779389	0.787079
	3.2	0.085058	0.097212	0.105568	0.129377	0.166084	0.224523	0.294482	0.378957	0.476603	0.539620	0.620543	0.660267	0.701661	0.658995	0.680404	0.685522	0.683972	0.753465	0.760997
	3.1	0.081804	0.093721	0.102953	0.125721	0.161169	0.217647	0.285011	0.366437	0.459717	0.521975	0.598824	0.637303	0.677805	0.635557	0.655352	0.660875	0.661860	0.726711	0.734756
	3.0	0.079556	0.091020	0.099134	0.121635	0.155193	0.210263	0.275763	0.354388	0.444271	0.504190	0.579043	0.614051	0.654693	0.613230	0.632535	0.637811	0.639032	0.698718	0.706896
	2.9	0.077019	0.088344	0.095747	0.117318	0.150257	0.202997	0.265992	0.341431	0.423444	0.486078	0.557616	0.591269	0.628272	0.590910	0.608042	0.614045	0.617397	0.671686	0.681450
	2.8	0.074621	0.085429	0.092805	0.113351	0.145000	0.195381	0.256129	0.328203	0.413119	0.468250	0.537687	0.570364	0.603144	0.569553	0.586751	0.592052	0.593053	0.647602	0.657311
	2.7	0.072109	0.082396	0.089523	0.108972	0.139829	0.188200	0.246326	0.315556	0.397529	0.451186	0.517243	0.548757	0.579805	0.547760	0.561027	0.568803	0.572074	0.622219	0.629320
	2.6	0.069515	0.079889	0.086960	0.104921	0.134777	0.180971	0.238722	0.302653	0.382067	0.433168	0.496754	0.527469	0.556482	0.524957	0.538276	0.544339	0.548569	0.597205	0.601960
	2.5	0.067346	0.075998	0.083155	0.101158	0.129607	0.173617	0.227662	0.291161	0.368132	0.415599	0.474554	0.506518	0.532810	0.502868	0.516637	0.520417	0.525391	0.573581	0.578403
	2.4	0.064794	0.073268	0.079991	0.097049	0.124445	0.166411	0.218356	0.278883	0.352047	0.398491	0.454282	0.484404	0.510498	0.481034	0.495685	0.499035	0.503186	0.544016	0.553168
	2.3	0.061906	0.070142	0.076251	0.093728	0.118953	0.159323	0.209207	0.266649	0.336924	0.381196	0.433643	0.454153	0.487745	0.459276	0.472533	0.477090	0.480494	0.517707	0.526829
	2.2	0.059157	0.065982	0.071482	0.088481	0.113961	0.151207	0.199942	0.254899	0.321924	0.362577	0.413618	0.433288	0.464688	0.439277	0.450147	0.453331	0.456944	0.492212	0.502753
	2.1	0.056508	0.063664	0.068927	0.085541	0.108933	0.145029	0.190471	0.242263	0.308757	0.343665	0.392093	0.421959	0.441689	0.417347	0.428219	0.432894	0.436147	0.467972	0.478164
	2.0	0.053792	0.061113	0.066348	0.081308	0.103652	0.138155	0.181722	0.230979	0.291621	0.327345	0.374116	0.400225	0.419834	0.396808	0.405887	0.410804	0.414309	0.440815	0.453889
	1.9	0.051269	0.057922	0.063544	0.077355	0.098559	0.131016	0.172232	0.219312	0.276560	0.310126	0.354834	0.379181	0.396665	0.375482	0.383213	0.387775	0.390855	0.415983	0.429467
	1.8	0.049029	0.055093	0.059929	0.073036	0.093274	0.124230	0.163338	0.207776	0.261079	0.293371	0.335272	0.357726	0.374185	0.352952	0.361574	0.365515	0.368467	0.391013	0.405117
	1.7	0.046336	0.052196	0.056631	0.069371	0.088279	0.117122	0.153613	0.195836	0.246541	0.276036	0.316470	0.336436	0.352440	0.332392	0.340825	0.344326	0.348087	0.365514	0.381352
	1.6	0.043542	0.049087	0.053411	0.065284	0.082858	0.110373	0.144366	0.183854	0.230992	0.259296	0.298153	0.316439	0.329017	0.312102	0.318576	0.322061	0.324904	0.341212	0.357534
	1.5	0.040755	0.046201	0.050477	0.061641	0.077538	0.102325	0.134839	0.171669	0.215577	0.243406	0.278284	0.295687	0.307792	0.291928	0.297440	0.300458	0.303965	0.317849	0.333541
	1.4	0.038045	0.043446	0.047428	0.057456	0.072620	0.096277	0.126162	0.159604	0.201096	0.226453	0.258218	0.274633	0.285827	0.271892	0.276245	0.279090	0.281793	0.294808	0.309198
	1.3	0.035852	0.040327	0.043427	0.053318	0.067250	0.089453	0.116787	0.148516	0.186570	0.206263	0.239903	0.254369	0.265207	0.252116	0.254825	0.257533	0.259176	0.272016	0.287000
	1.2	0.032975	0.037150	0.040387	0.048985	0.061920	0.082591	0.107811	0.136951	0.171930	0.191189	0.220829	0.234355	0.244140	0.231678	0.233906	0.237223	0.239040	0.249932	0.262206
	1.1	0.030728	0.034342	0.036960	0.044891	0.057090	0.075797	0.099106	0.125475	0.157367	0.175268	0.200988	0.213101	0.223321	0.210488	0.213283	0.216917	0.218765	0.227485	0.239119
	1.0	0.028045	0.031551	0.034079	0.040975	0.052015	0.068946	0.089983	0.113715	0.143143	0.158892	0.182466	0.192770	0.201642	0.190135	0.192322	0.195139	0.195495	0.205234	0.216934
	0.9	0.025588	0.028553	0.030867	0.037015	0.046960	0.061823	0.080702	0.102463	0.128502	0.143154	0.164056	0.172984	0.181083	0.169807	0.172301	0.175570	0.176174	0.183406	0.194069
	0.8	0.023109	0.025748	0.027659	0.033110	0.041882	0.055188	0.071879	0.091028	0.113656	0.126622	0.145547	0.153018	0.159406	0.150763	0.151895	0.154499	0.155884	0.161738	0.172816
	0.7	0.020639	0.022993	0.024613	0.029139	0.036929	0.048240	0.063050	0.079177	0.099013	0.110480	0.126964	0.132965	0.138729	0.131865	0.132367	0.135139	0.135495	0.141495	0.151070
	0.6	0.018633	0.020224	0.021710	0.025339	0.032021	0.041679	0.054168	0.068285	0.084578	0.094435	0.108683	0.113389	0.119103	0.112976	0.112474	0.115311	0.115894	0.121159	0.129695
	0.5	0.016214	0.017577	0.018744	0.021573	0.027246	0.034935	0.045218	0.056960	0.070540	0.079035	0.090389	0.094337	0.099344	0.094643	0.095422	0.096522	0.096559	0.101267	0.107596
	0.4	0.014039	0.015080	0.015920	0.018039	0.022558	0.028312	0.036423	0.045551	0.056897	0.063420	0.072257	0.075055	0.079022	0.075865	0.074431	0.075353	0.076111	0.081441	0.086765
	0.3	0.012061	0.012700	0.013283	0.014693	0.017932	0.022167	0.028069	0.034624	0.042732	0.047609	0.054903	0.056539	0.059678	0.057553	0.056518	0.057564	0.058434	0.061379	0.065575
	0.2	0.010380	0.010694	0.011136	0.011768	0.013702	0.016174	0.019808	0.024375	0.029044	0.032084	0.036902	0.038514	0.040133	0.039597	0.037208	0.039016	0.039865	0.041804	0.044652
	0.1	0.008894	0.009120	0.009295	0.009923	0.010251	0.011195	0.012427	0.014902	0.016516	0.017551	0.020033	0.020895	0.021412	0.022187	0.019645	0.021230	0.022378	0.022619	0.024619
	0.0	0.008437	0.008437	0.008437	0.008437	0.008437	0.008437	0.008437	0.008437	0.008437	0.008437	0.008437	0.008437	0.008437	0.008437	0.008437	0.008437	0.008437	0.008437	0.008437

Figure 6.3: Scatter Table with SMPM Values for impact velocity in Situation 2 with HC (raw output). The darker the background colour, the larger the SMPM value.

To get a more general feeling for how the limiting parameters are distributed over the

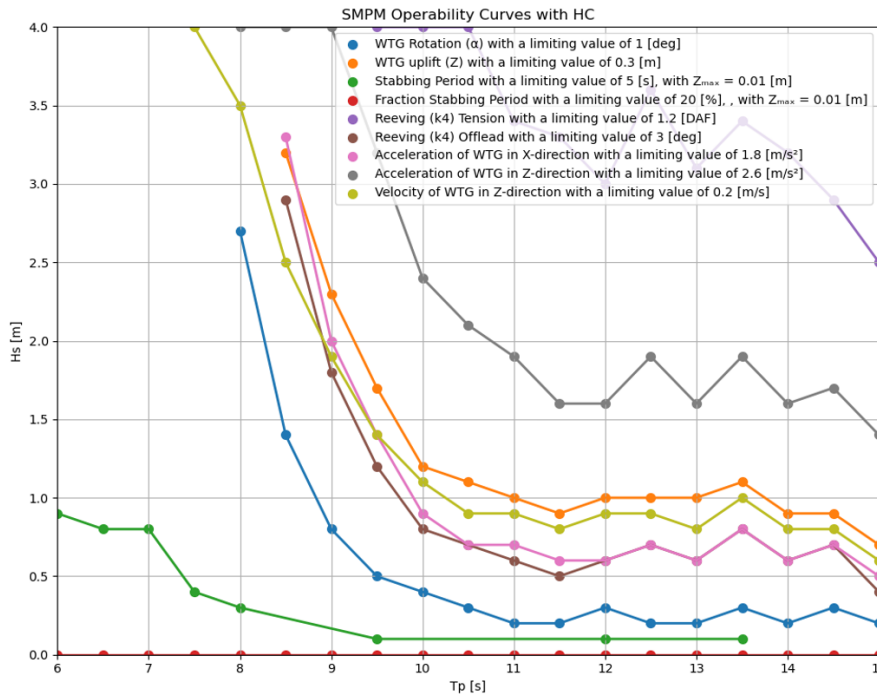


Figure 6.4: Operability without Tower Bending incorporated for Situation 2 with Heave Compensation.

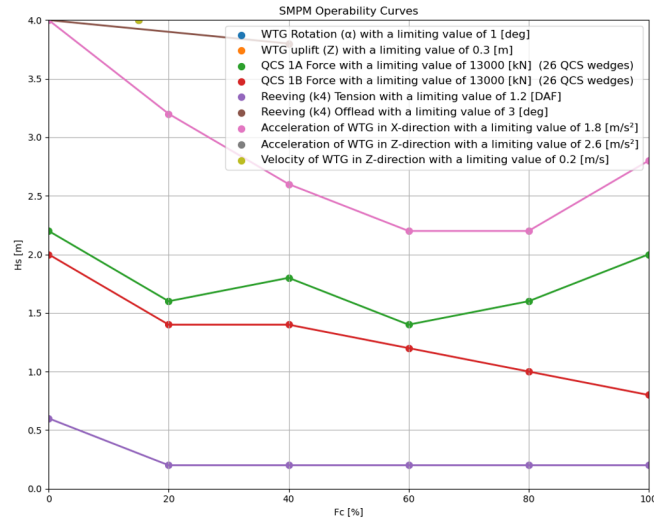
number of 26 QCS wedges is chosen (with respect to 100 wedges in total). This number is optimised in Section 6.3.

As can be seen in Figure 6.5a, the reaving tension is the limiting parameter in the case without HC (lowest limiting criterion). This makes sense as large crane tip motion will cause high tension in the rigging. Although this operability is still higher than Situation 2 without HC and therefore not governing, it is still poor. It is interesting to see that the operability is rather constant during the load transfer phase, with a slight increase for F_c of 0%. If the rigging is slack, the applicability of the limiting parameters is questionable as crane damage (offlead criterion) is not a realistic critical event any longer. However, impact of the block or HC on the WTG should be prevented. Assessment of this is left outside the scope of this research and should be checked when execution of this installation methodology is prepared.

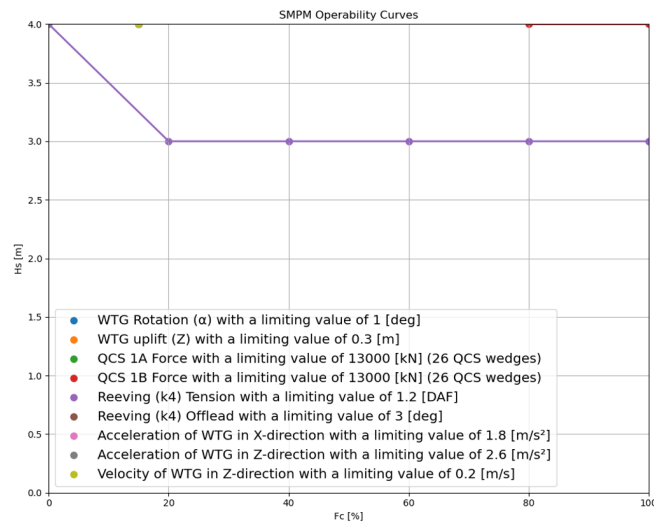
The operability for Situation 3 becomes much better if HC is included. The reaving tension is still governing, but for much larger values of H_s . Here it can be concluded that Situation 3 is not governing with respect to Situation 2 when HC is included and optimisation of the number of QCS wedges can be investigated. Figure 6.5c shows the operability for Situation 3 if tower bending is neglected. Comparison of the results with and without modelling TB reveal no increased operability by including TB into the model for Situation 3. The rigging tension is still the limiting parameter for both cases. The QCS loading is comparable in the case with TB, although it is slightly deviating for lower F_c values. What further stands out is the larger accelerations allowed for the cases with TB. This is expected as the TB acts as a spring in the horizontal direction at the rigging connection point of the WTG, thereby absorbing energy from the motion of the WTG.

In the early phase of the research, a preliminary assessment of the WTG stability was made. The WTG tilt was calculated, at which static equilibrium was found for a combination of a certain crane tip offset and a crane load F_c . This is shown in Figure 6.6a. Here, the crane load F_c is shown versus the WTG tilt. As can be seen in the graphs, the WTG tilt increases rapidly around 30-50% F_c for crane tip offsets larger than zero. This displays the instability of the WTG. The graphs return to zero below 30% F_c as the restoring moment due to the self-weight of the WTG becomes larger than the overturning moment induced by the crane tip at this point. Only lines that do not show a peak going to infinity have a stable load transfer phase. This is only the case for a crane tip offset of zero meters in Figure 6.6b. During the optimisation process of the operability, it was found that transferring a larger portion of the WTG load to the foundation prior to activation of the QCS was beneficial to the operability of Situation

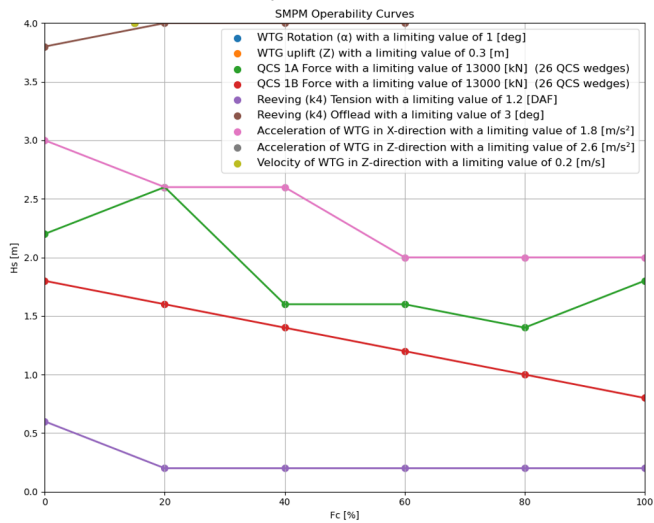
2. However, a prerequisite for this was that the load transfer up to this point could be executed in a stable manner. Therefore, plots similar to those above shown for Situation 3 were made, only without the addition of QCS Wedges. What is striking about these figures (shown in Figure 6.7), is that it shows that no QCS is required for low significant wave heights. Since this is contradictory to the preliminary assessment, this is further investigated. It turns out that the wind loading on the blades is governing for the stability of the WTG during the load transfer phase. If the preliminary assessment is reassessed with the definitive wind load, it is indeed shown that it remains stable for certain load cases (low sea states). This is shown in Figure 6.6b. As can be seen from the graphs, the stability is less affected by a crane tip offset for the low wind load scenario, than for the high wind load scenario. This means that for low wind loads and a small crane tip offset, load transfer could be possible without a QCS. However, the chance that this occurs is considered to be small, as no DP drift and optimal wind loading is considered in this analysis.



(a) Operability for Situation 3 without HC.

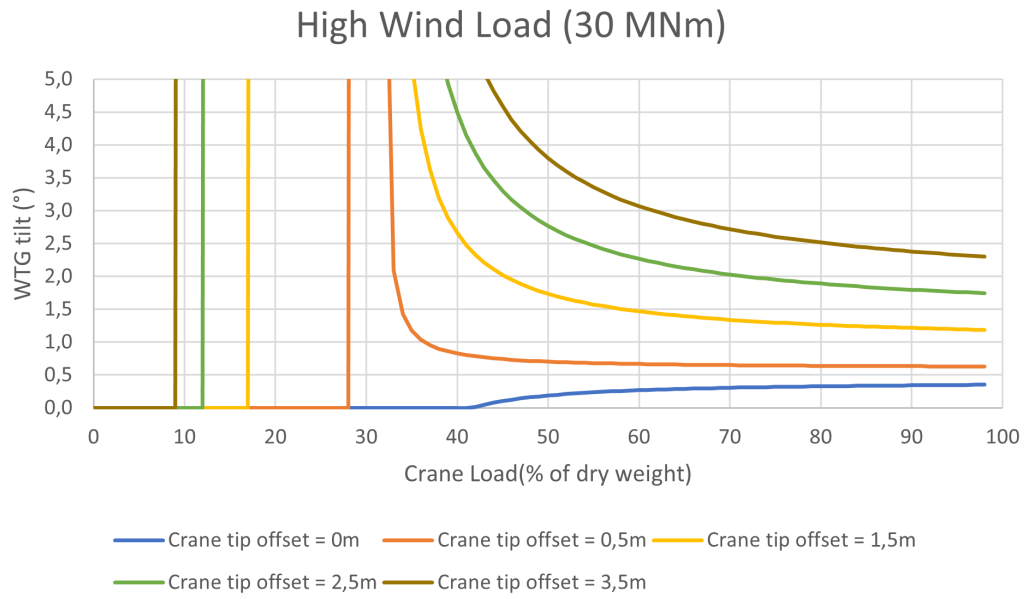


(b) Operability for Situation 3 with HC.

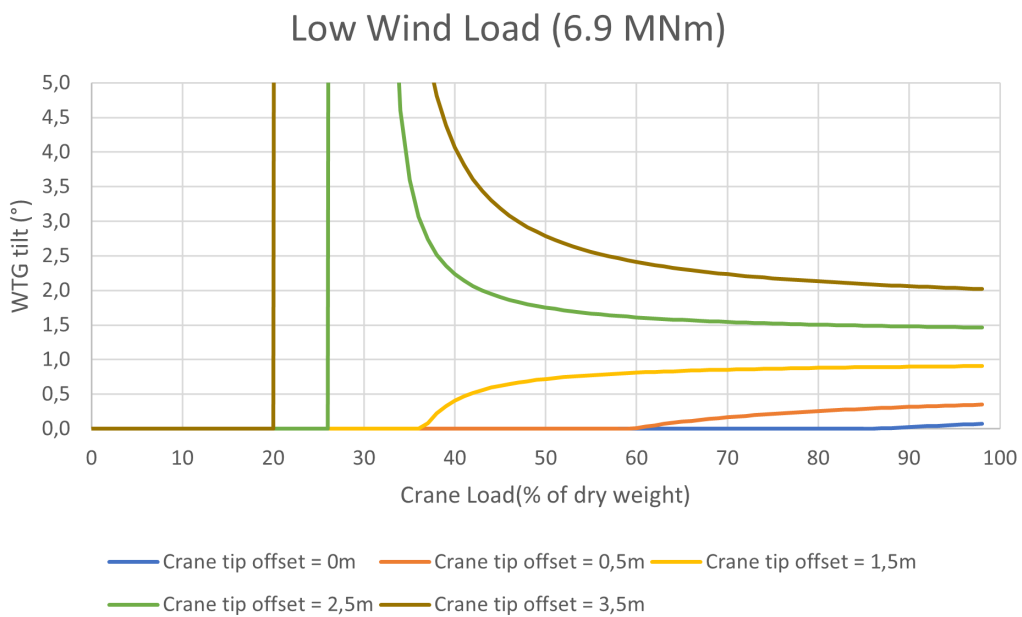


(c) Operability for Situation 3 without Tower Bending nor HC.

Figure 6.5: Various Operability's for Situation 3. F_c is the percentage of the WTG mass that is supported by the crane in static state. For T_p a constant value of $10s$ is used.



(a) Preliminary WTG Stability Assessment



(b) Final WTG Stability Assessment

Figure 6.6: Stability assessment of WTG during load transfer phase. Here, the WTG tilt is given as a function of the load transfer.

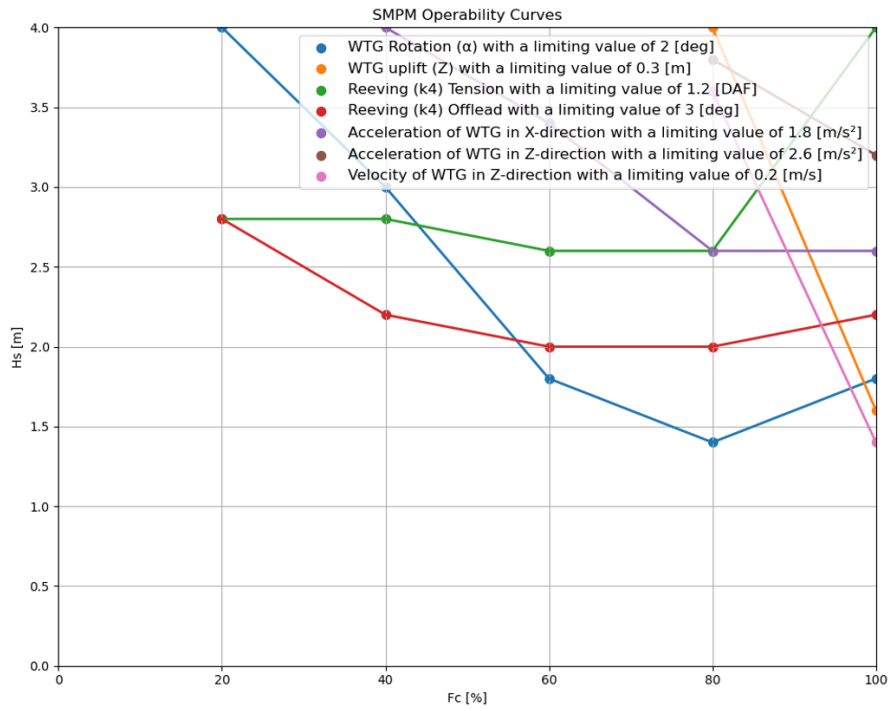
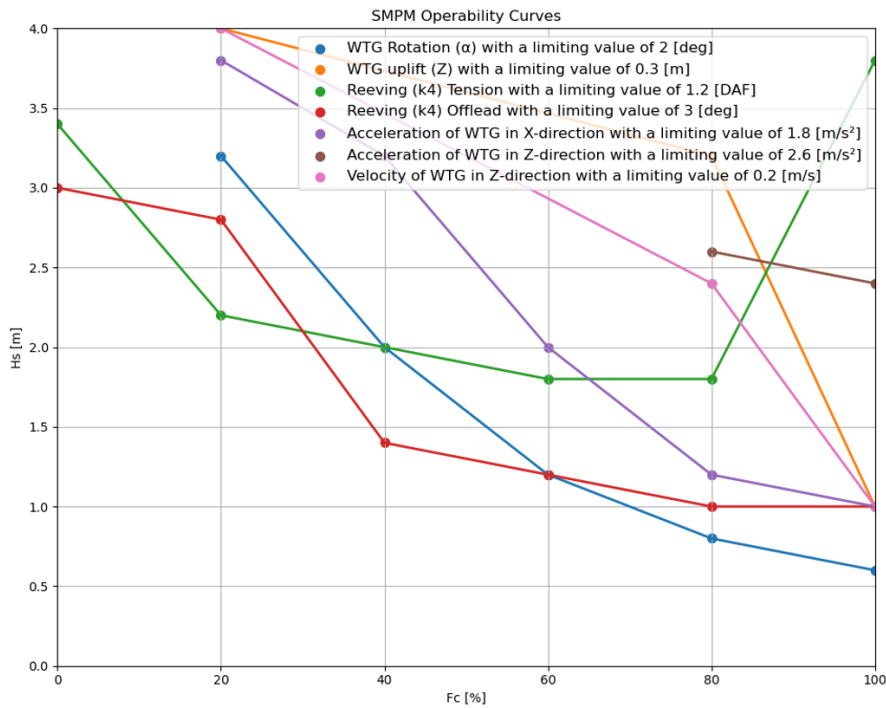
(a) Operability for $T_p = 10s$ (b) Operability for $T_p = 12s$

Figure 6.7: Optimised operability for Situation 3 with HC with 0 QCS Wedges. F_c is the percentage of the WTG mass that is supported by the crane in static state. For T_p a constant value is used. For values of T_p lower than $10s$, no limiting criteria were found. In general, a larger T_p reduces the operability as these are closer to the eigen periods of the vessel. Note that a larger WTG rotation limit of 2° is used.

6.3. Sensitivity Study and Optimisation of Operability

For the sensitivity study, simulations were rerun with different input parameters or limiting parameter values. The goal of these variations was twofold: 1) to verify the output. Check if logical trends exist for different inputs. 2) to optimise the operability. Which design changes are important to make in order to achieve an optimal operability. The most important findings are shown and discussed below.

6.3.1. Sensitivity of Limiting Parameters

As Situation 2 is the critical installation activity, most variations are carried out for Situation 2. First, the sensitivity of the simulations without HC is checked, to see if there is any potential in this option. This is done for the four most restricting limiting parameters and shown in Figure 6.8.

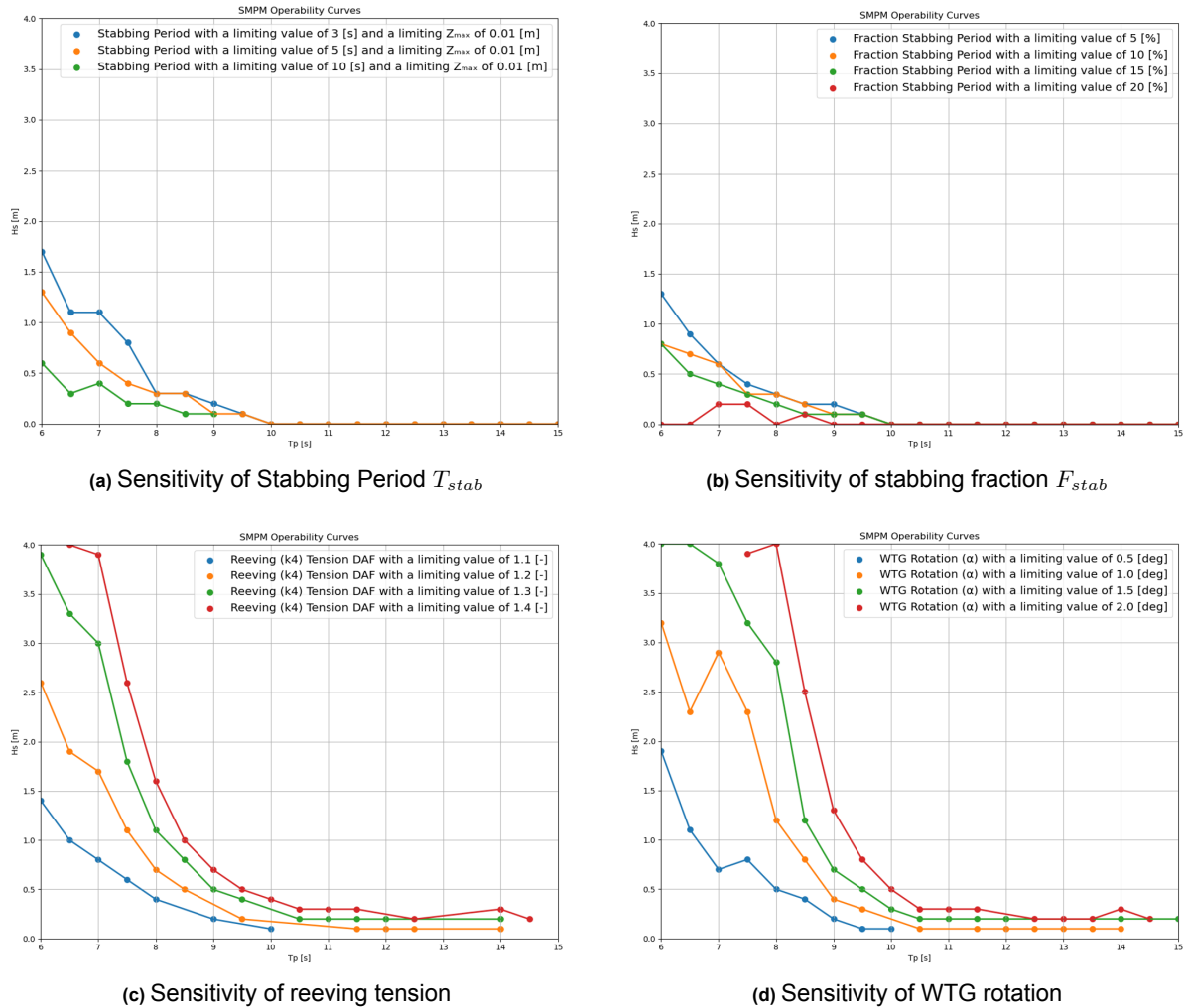
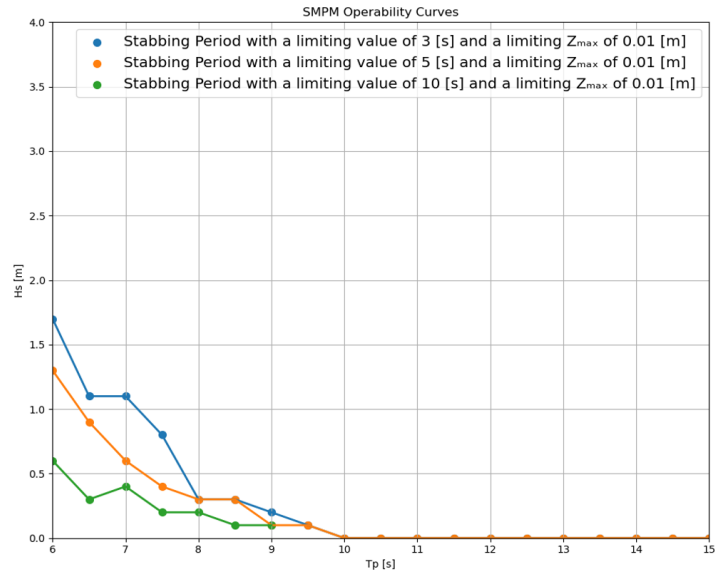
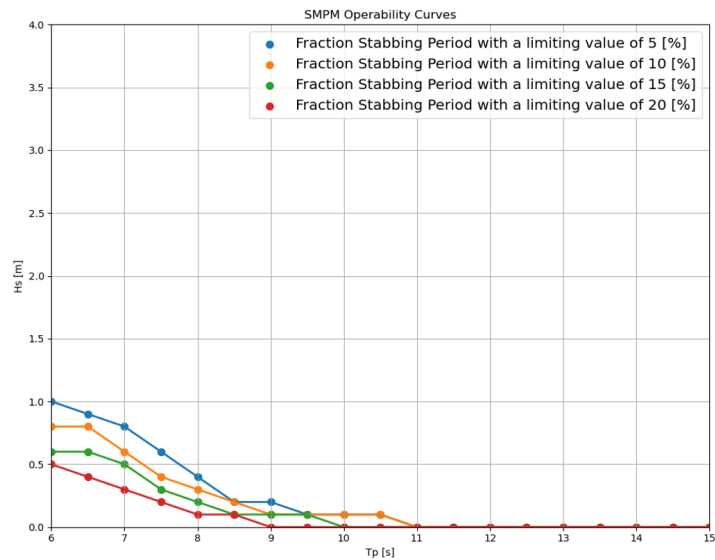


Figure 6.8: Sensitivity of the four most restricting limiting parameters for Situation 2 without HC.

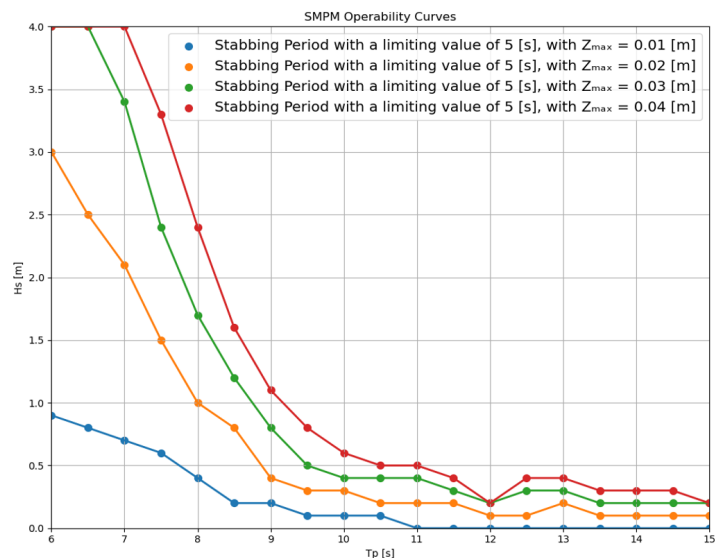
As expected, the operability for each limiting parameter increases if the values are relaxed (lower T_{stab} and F_{stab} required or larger reeving tension and WTG rotation allowed). For shorter peak periods (6-10s), the largest improvements are achieved. For longer peak periods, almost no improvements are achieved. Although, there is improvement of operability for lower peak periods, the improvement is still limited. Limiting parameters such as reeving tension and WTG rotation could be reduced potentially by increasing sling WLL and adding tugger winches to the rigging configuration. However, this is not the case for the limiting parameters T_{stab} and F_{stab} . Even if a F_{stab} equal to 5% is deemed acceptable for Situation 2, the operability is still limited to situation with $H_s > 1m$ for all short peak periods. Therefore, an installation without HC is deemed infeasible from an operability point of view.



(a) Sensitivity of Stabbing Period T_{stab}



(b) Sensitivity of Stabbing Fraction F_{stab} .



(c) Sensitivity of maximum uplift for stabbing Z_{max} .

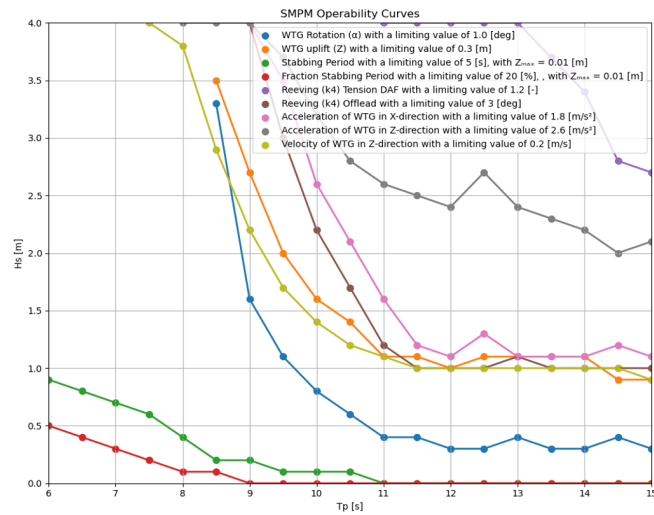
Figure 6.9: Sensitivity of the most restricting limiting parameters for Situation 2 with HC.

The sensitivity of the limiting parameters for Situation 2 with HC are presented in Figure 6.9. As reeving tension and WTG rotation were not close to governing, only the sensitivity of T_{stab} and F_{stab} are presented. Furthermore, the sensitivity of Z_{max} is added.

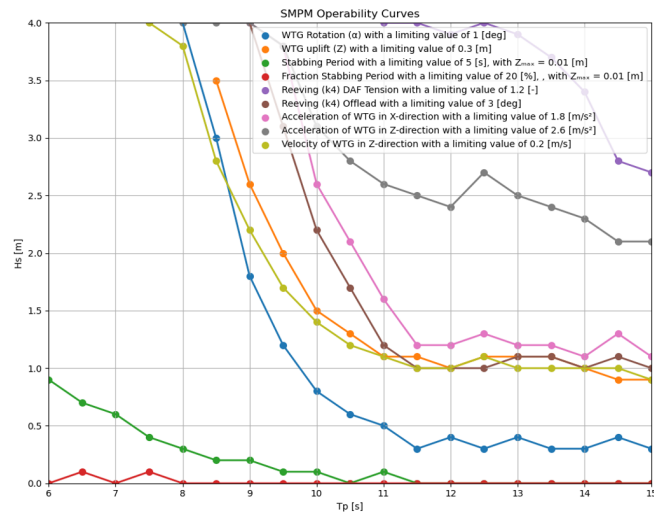
For Situation 2 with HC, the operability can only increase limited by changing T_{stab} or F_{stab} . However, if the limiting WTG uplift during the stabbing period is increased (increase of Z_{max}), the operability is increased much more. This parameter is a design parameter of the C1 Wedge Connection flanges. Therefore, caution should be taken with increasing this parameter as the C1 Wedges will require a larger stroke if the slots are heightened.

6.3.2. Sensitivity of Input Parameters

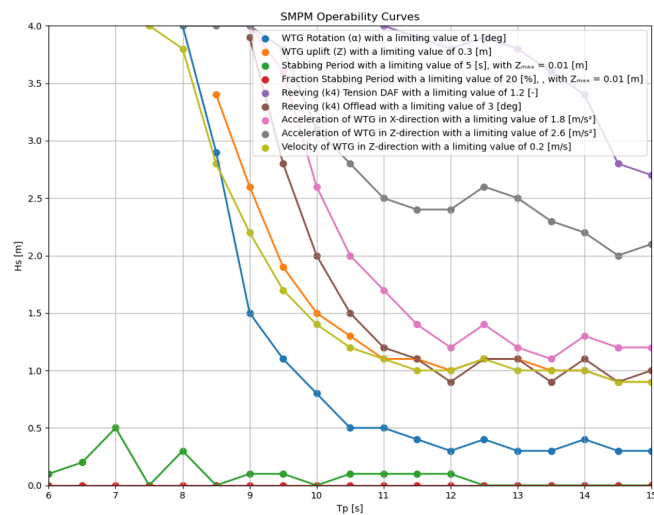
Next to variation of limiting parameters, also some variations of input parameters have been simulated. As this required completely new simulations per variation, this process was very time consuming and only a limited number of variation were simulated. As Situation 2 is the critical installation activity, almost all variation were applied to Situation 2. First the wind load was varied by simulating mean wind speeds of 12 and 14 m/s. The results for the sensitivity of the operability to the mean wind speed are shown in Figure 6.10. Although most limiting parameters are insensitive to a change in mean wind speed, T_{stab} and F_{stab} are reduced even further towards zero for higher mean wind speeds. This means the operability is sensitive to the wind speed or less optimal wind heading, as expected.



(a) Operability for $V_{mean} = 10\text{m/s}$ (base case)



(b) Operability for $V_{mean} = 12\text{m/s}$



(c) Operability for $V_{mean} = 14\text{m/s}$

Figure 6.10: Sensitivity of mean Wind Speed simulated in Situation 2 with HC.

The second variation of input parameters is a change in stiffness of the Heave Compensator. This is shown in Figure 6.12. Here it should be noted that the stated stiffness is per HC system. Since two are used in parallel, the presented values should be doubled to obtain the total equivalent stiffness. What can be observed is that for a different HC stiffness, the operability changes. This is seen for the limiting parameters T_{stab} and F_{stab} . Almost all other limiting parameters stay constant for each variation in HC stiffness. Only the reeving DAF becomes stricter for stiffer models. This can be expected as the HC is the softest component in the rigging setup. The trend towards higher operability for T_{stab} and F_{stab} is confirmed when looking at the spectral density graphs for the vertical motion of the WTG (Figure 6.11). As the vertical motion of the WTG influences T_{stab} and F_{stab} this is an important parameter that can clarify the difference in excitation. Looking at the graphs, it can be seen that the base case stiffness model is excited more over the full frequency range. Also, around the eigenfrequency of the WTG pendulum mode ($0.06944Hz$), the 400 kN/m case is excited most. Although the difference is relatively small, it is sufficient to change the limiting values of T_{stab} and F_{stab} as they are extremely sensitive parameters because Z_{max} is ridiculously small.

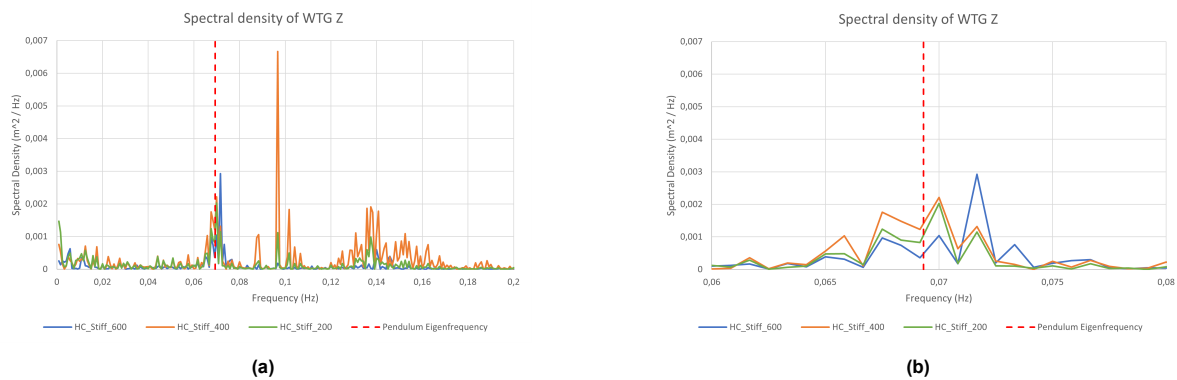
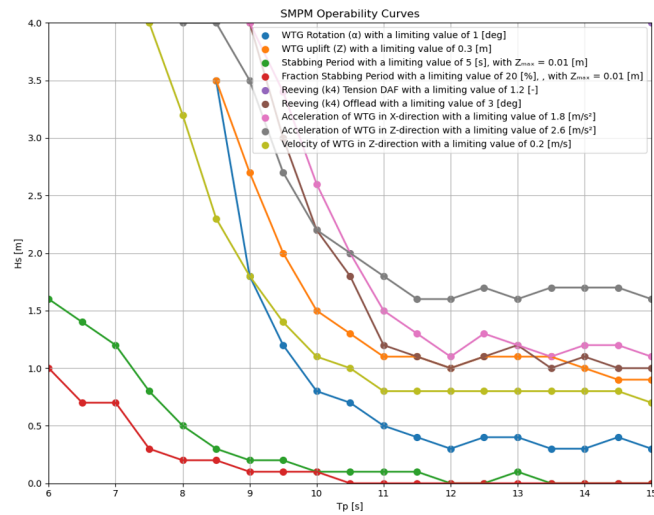
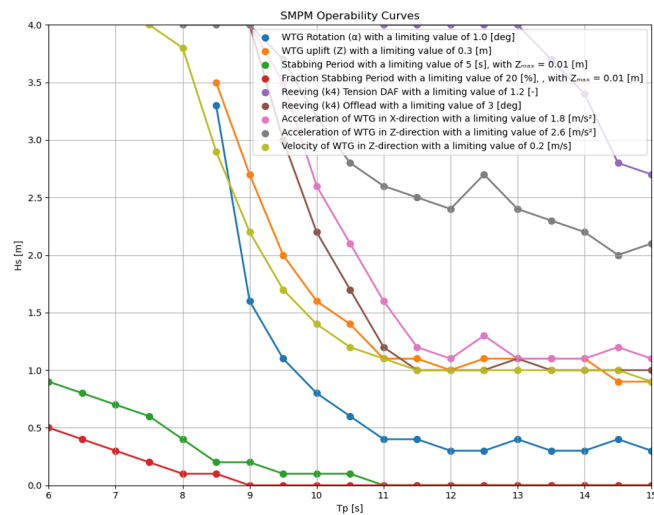


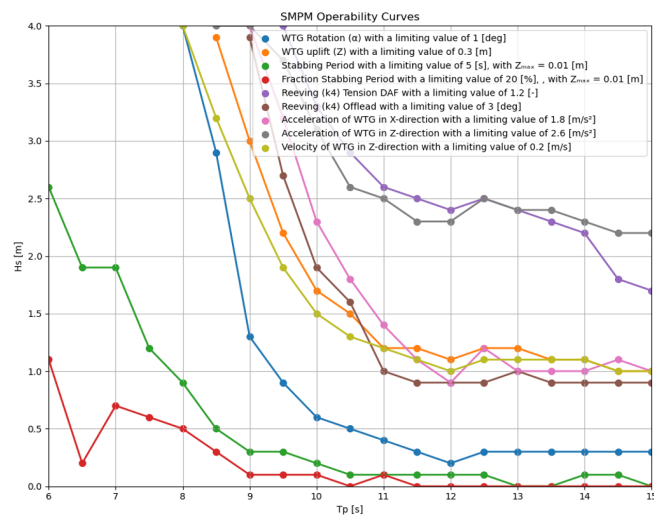
Figure 6.11: Spectral density for WTG Z motion for the varies Heave Compensation stiffnesses. Figure b) is the zoomed in version of Figure a) around the pendulum eigenfrequency. These Power Spectral Densities are directly calculated from the time domain simulations for $T_p = 7.0s$ and $H_s = 0.8m$ by taking the Fourier transform of the time history result.



(a) Operability for HC Stiffness $k_{HC} = 200mT/m$



(b) Operability for HC Stiffness $k_{HC} = 400mT/m$ (base case)



(c) Operability for HC Stiffness $k_{HC} = 600mT/m$

Figure 6.12: Sensitivity of Heave Compensator stiffness simulated in Situation 2 (with HC).

As announced in Chapter 5, the optimal initial load transfer percentage is determined for Situation 2. The results of this variation are presented here (see Figure 6.13). As can be seen from the graphs, the operability increases as the crane load percentage F_c is decreased. This effect seems to level off from 80% initial load in the crane, see Table 6.1. Here, it is best to use the highest initial load percentage as the stability decreases for lower percentages. Therefore, an optimal value of 80% initial crane load is used for situation 2.

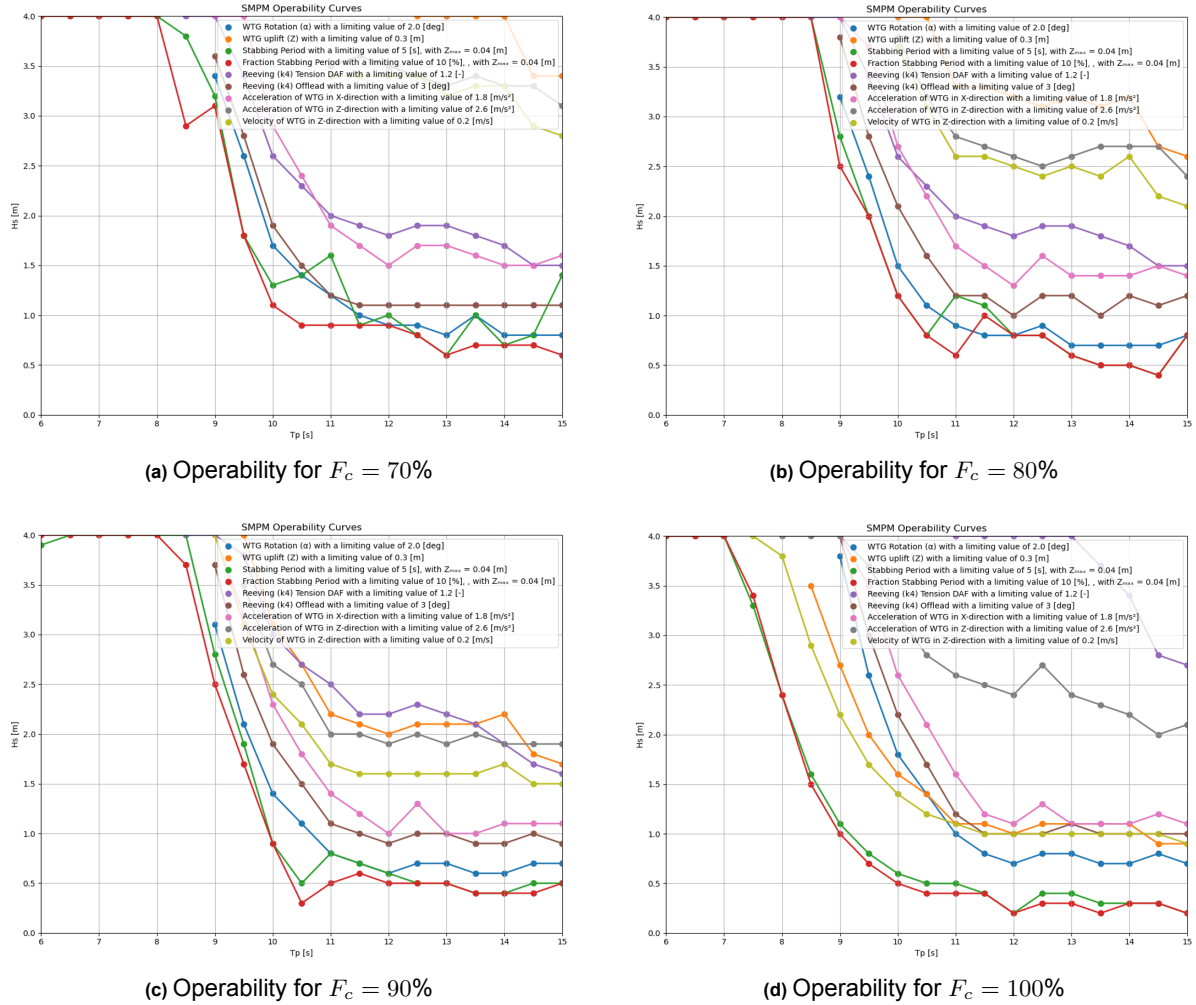


Figure 6.13: Sensitivity of the initial crane load percentage F_c . The increase in operability levels of for $F_c = 80\%$ and lower.

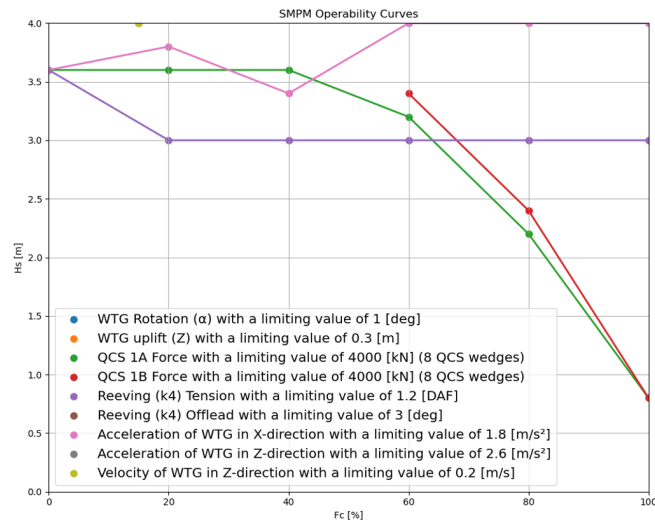
Crane load F_c	Operability Area Fraction
70 %	47.6 %
80 %	47.2 %
90 %	43.8 %
100 %	31.4 %

Table 6.1: Fraction of area under operability graph for Situation 2 as a measure for operability as a function of initial crane load percentage F_c . The increase in operability levels of for $F_c = 80\%$ and lower.

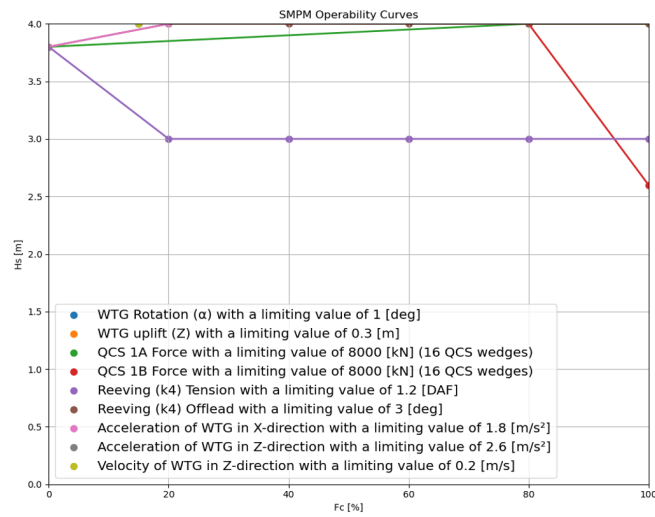
The last variation that was simulated was the variation in the number of QCS Wedges that are stabbed during the QCS activation. This number should be reduced as far as possible to reduce cost and complexity while still providing sufficient restoring moment to keep the WTG upright and having sufficient capacity to withstand any pulling forces from the crane tip motion. Above results (Section 6.2) show that the operability is much better when HC is included in Situation 3. Therefore, only Situation 3

with HC is considered. The results for varying the amount of QCS Wedges is shown in Figure 6.14.

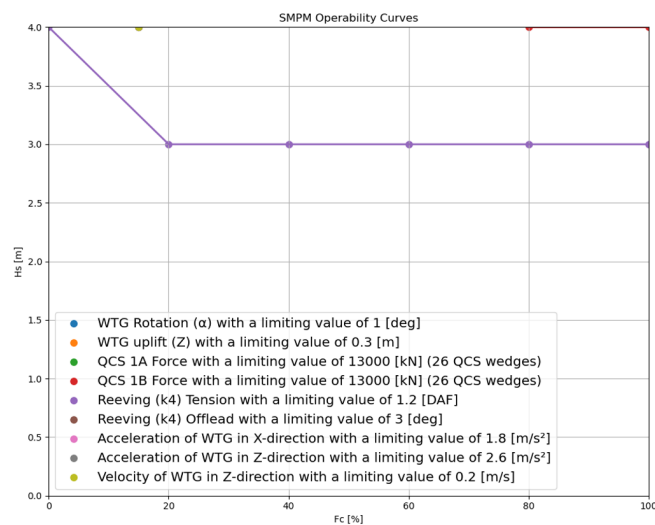
For Situation 3, two additional limiting parameters are added: a maximum force in the QCS on the equivalent right (A) and left (B) side of the WTG tower. These limits are added to make sure the loads in the QCS do not exceed the pretension of the QCS wedges during the simulation. Two limits are added instead of one to ensure the induced overturning moments lie within the limits as well. This maximum force is dependent on the amount of QCS Wedges used in the simulation, as can be seen in the legends of Figure 6.14. As expected, the operability reduces when the number of QCS Wedges is reduced. In the cases with 8 and 16 Wedges the forces in the Wedges are the limiting parameters during the load transfer. Here, the largest loads can be expected when the majority of the WTG load is still in the cranes. This can be explained by looking at the contact force between the WTG and the support structure. As more load is transferred to the support structure, a sudden uplift of the WTG (due to crane tip movement) will first reduce the contact force, before loading the QCS Wedges. Therefore, the more load transferred to the support structure, the less restricting the QCS loading limiting parameter will become. For the operability presented in Figure 6.2, 16 QCS Wedges should suffice to make Situation 3 not the governing critical installation activity with respect to Situation 2 with HC.



(a) Operability for 8 QCS Wedges



(b) Operability for 16 QCS Wedges



(c) Operability for 26 QCS Wedges

Figure 6.14: Sensitivity of the number of QCS Wedges used for Situation 3 with HC.

6.3.3. Optimised Operability

When taking all the above into account, an optimisation of the operability can be achieved by altering some installation procedure and lifting configuration design elements that were used as a starting point for the assessment of the operability (as stated in Section 4.1). First, a Passive Heave Compensator (PHC) could be integrated in the rigging arrangement to reduce the rigging snap loads and the WTG rotation. Second, the C1 Wedge Connection design could be changed in such a way, to be able to activate the QCS under an as large as possible uplift/rotation of the WTG. Thereby, focus could be put on increasing the limiting parameter Z_{max} . Third, the installation procedure could be adjusted. Monitoring phase 5, could be incorporated into monitoring phase 1. Furthermore, phase 4 (lowering the WTG until the C1 flanges overlap) and phase 6 (initial landing of the tower on the support structure) could be executed in one go. This reduces the chance of re-impact during the installation. The "small portion" of the WTG load transferred to the support structure prior to QCS activation, taken 1-2% as the base case in this thesis, could be increased to around 20% (equivalent to $F_c = 80\%$ as described in Subsection 6.3.2), to increase operability, as described above. Adapting this percentage does make the WTG rotation one of the governing limiting parameters. However, this is acceptable as this limiting parameter has some clearance from the governing parameters as shown in Figure 6.2.

Taking these three points into account and reevaluating the operability for Situation 2 and 3, an optimised operability can be achieved for the floating single-lift installation of a WTG equipped with a C1 Wedge Connection as shown in Figure 6.15. Here, some of the limiting parameters have been relaxed to improve operability. Combined, these relaxations form the set of design adaptations required. Whether a C1 Wedge Connection design with a Z_{max} of 0.04m is technically feasible should be checked. Also, an F_{stab} of 10% is relatively low from an operational point of view, although the F_{stab} value increases rapidly as it moves away from the governing limit. For peak periods below 8s, F_{stab} is 50-90%.

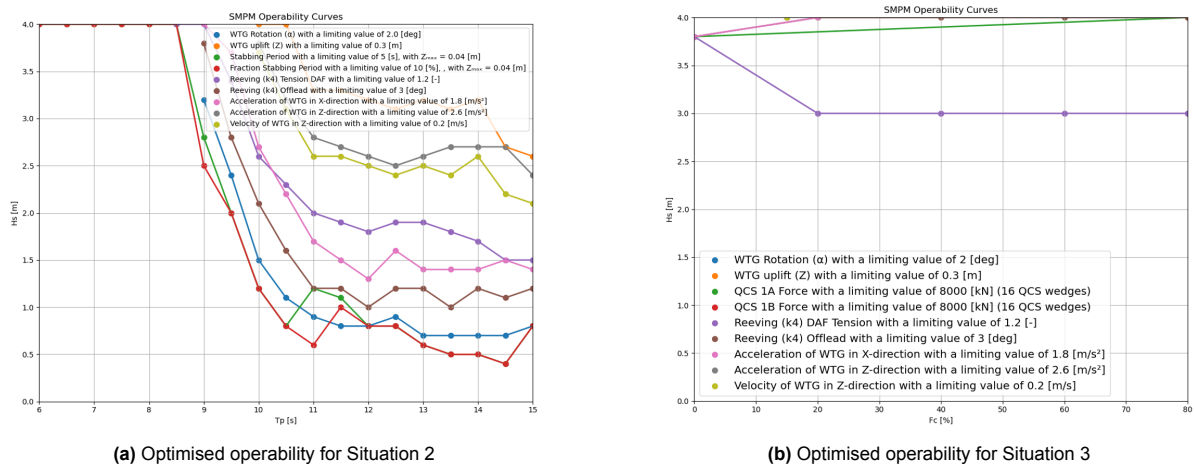


Figure 6.15: Optimised operability for Situation 2 and 3 with HC, a maximum WTG rotation of 1.5° , a Z_{max} of 0.04m, a F_{stab} of 10% and 16 QCS Wedges.

6.4. Validity and Reliability

The quality of the results presented in this Chapter depend on the reliability of the model. This Section discussed the validity of the results for three main influencing parts of the research: the model, the limiting parameters, and the operability plots. The limitations of the results are presented. These are complementary to the limitations mentioned in Section 5.4.

6.4.1. Enhanced OrcaFlex Model

The model is limited to simulating in-plane motions. Therefore, not all physical phenomena are captured in the model. This could lead to misinterpretation of the results. The results can be reliable for this model but are not necessarily applicable to reality. T. Lengkeek mentions in his thesis that the WTG

pendulum and double pendulum mode are excited in the longitudinal plane (the plane assessed in this thesis) but also significant coupling was found for a combination of vessel roll and WTG pendulum mode in the transverse plane (not seen in the model in this thesis) [64]. This does not automatically imply that the transverse plane should have been incorporated in the present study as the lifting set-up and vessel differ significantly.

Limitation to in-plane motions further implies that the effect of directionality of wind and waves is not incorporated in the model. Which combination of these is favourable or should be avoided at all costs? Is it restrictive to have a predetermined installation orientation of the WTG? How does this influence the wind load on the blades? In the model, no wind loading on the blades is incorporated, as it is negligible for optimal wind direction (180°) and blade pitching (minimal drag). However, a sub-optimal combination of these parameters can create significant wind loading on the blades.

Another modelling effect that contains some uncertainty is the contact modelling between the WTG and the support structure. As described in Chapter 5, the procedure advised by Orcina was followed to model this contact. This models the contact as two surfaces in contact. However, the effect of local contact pressure peaks and flatness on the integrity of the C1 Wedge Connection is not assessed. This could for example lead to neglecting local deformations affecting the lifetime performance of the connection.

The allowable rotation of the tower is restricted to one degree, to prevent jamming and bending of the C1 flanges, although a rotational clearance of two degrees is incorporated in the design of the C1 Wedge Connection that can be upgraded if required. The conservative choice for one degree as limiting parameter is made to incorporate the probability of exceeding of the SMPM value, which is 63% by default.

One of the simplifications in the model was the combination of the lifted object components into one rigid body. The main simplification here, is that the vertical translation of the USF due to elongation of the slings between the LLT and USF is ignored. As the stiffness of these four slings combined is actually around $28.4GN$ with a length of around $100m$ (USF to bottom WTG) and carrying all the WTG weight, the static elongation of these slings is $8.6cm$. Since this elongation is relatively minor compared to the overall rigging setup and the sling stiffness, the elongation is not expected to influence the model results. With respect to the stiffness, the consequences of this simplification differ per model situation. In the case with HC, the stiffness of the HC is two orders of magnitude lower than that of these slings. Therefore, the stiffness is not expected to influence the overall behaviour of the model. However, in the case without HC, the softest part in the rigging set-up is formed by the hoisting wires, closely followed by the LLT-USF slings. Then, the simplification does not seem valid as the stiffness would influence the overall behaviour. It is therefore advised to include these slings in the model in a new iteration of the model situation without HC.

6.4.2. Limiting Parameters

Most of the limiting parameters are design choices. This means they can be chosen as seen fit and do not determine the uncertainties in the model. However, they do heavily influence the simulation results. Some parameters are based on experience, such as the impact velocity, or structural limits like the rigging tension. A rigging limiting parameter is the rigging tension. Since it is hard to simulate high-frequent effects, it is hard to estimate peak loads in the rigging. For conservatism, a DAF of the rigging of 1.2 is set as the limiting value instead of a maximum capacity value of 1.5.

A difficulty with the structural limit for the maximal offlead angle is that no pure offlead is calculated in the model. As the model is limited to in-plane motions and the cranes are positioned out-of-plane due to their slew angles the true offlead angles could be larger than the calculated offlead angles. Furthermore, since the model is limited to in-plane motions, not all relevant limiting parameters could be incorporated. Omitted limiting parameters are crane-nacelle clearance, rotation around the X-axis, etcetera. This is all due to the main limitation of the model that only in-plane motions are simulated.

The limiting value for the impact velocity is chosen through comparison with other studies. However, there is a span of impact velocity limits used in literature, ranging from 0.1-0.5 m/s [64, 7], due to different failure events identified. The lower bound is found for maximal accelerations in the RNA, while the upper bound is found for stress levels in the structural steel. In this thesis a value of 0.2 m/s is deemed sufficient for the installation. For the installation of TPs, Acera et al. found that the impact velocity was governing for the installation [1]. The optimised operability plot (Figure 6.15) shows that the impact velocity is not governing for the installation in this thesis. Furthermore, a sensitivity analysis on the impact velocity limiting parameter shows that even with a limiting value of 0.1 m/s, the impact velocity is not governing for the operability.

6.4.3. Operability Plotting

The operability curves are derived from a combination of the scatter tables and the limiting parameter values. The values in the scatter tables are the statistical SMPM values derived from the simulation with a specific combination of H_s and T_p values. As described in Section 5.2, this value is directly derived from the simulation standard deviation of the assessed parameter. Assumptions in this short-term statistical derivation are that the crest height of the 20min assessed sea-state is Rayleigh distributed and that the response can be described as a random process with a Gaussian distribution. Literature states that the assumption that the surface elevation is a stationary, Gaussian process is usually valid for the duration of a wave record of typically 15-30 minutes. The validity of the assumption that the crest height has a Rayleigh distributed PDF, is dependent on the spectral width, defined by Cartwright and Longuet-Higgins [46] as

$$\epsilon = \left(1 - \frac{m_2^2}{m_0 m_4}\right)^{\frac{1}{2}} \quad (6.1)$$

Here, narrow spectra ($\epsilon \rightarrow 0$) approach the Rayleigh distribution, whereas wide spectra ($\epsilon \rightarrow 1$) approach a Gaussian distribution. For the model, the limiting parameters have different spectral widths. The crane tip displacement and WTG rotation are examples of narrow spectra, while the WTG vertical motion has a relatively wide spectrum. Therefore, the validity of the SMPM value is questionable for some limiting parameters. However, the accuracy of the spectral width parameter is also doubted. The value of the fourth-order moment m_4 is dominated by the upper limit of the integration scheme due to the shape of the tail of the spectrum for ocean waves. Furthermore, m_4 is rather sensitive to high frequent noise or the presence of nonlinear effects. This means that the value of ϵ also depends to a high degree on the upper cut-off frequency, errors in the model and nonlinear distortions. Therefore, it is advised to use the spectral width parameter ϵ with great care. To assess this uncertainty, other distributions could be fitted to the data. Examples of these that OrcaFlex facilitates are the Weibull and generalised Pareto distributions, which are both fitted using a maximum likelihood method. The extremes of the data are selected using the peaks-over-threshold method. It is expected that application of these distributions will lead to a lower operability for limiting parameters with a wide spectrum, such as the WTG uplift and combinations of multiple parameters, such as T_{stab} and F_{stab} .

Another point that should be noted regarding the SMPM values is that the probability of exceedance of this value is 0.63. This means there is a probability of 63% that the actual maximum crest height exceeds the most probable value. However, the absolute exceedance is low if the PDF is narrow. If a lower probability of exceedance is required, a risk parameter, as proposed by Ochi, can be specified for the SMPM value in OrcaFlex [74]. This is not included in the current model but could be implemented in a new update of the model.

The ultimate point worth mentioning regarding the reliability of the operability graphs of Situation 2 is that some unexpected results were obtained for the optimisation of the load transfer prior to QCS activation. The SMPM values for the limiting parameters T_{stab} and F_{stab} did not consequently decrease for higher significant wave heights H_s while keeping the peak period T_p constant. Instead, while still overall decreasing, they sometimes gradually increase. Decreasing the simulation time step or increasing the simulation duration helped to oppose these effects, although this significantly increased the required

time for simulation. Therefore, this was only done partially, to keep the simulation time acceptable. It is remarkable that this effect mainly occurred for the limiting parameters T_{stab} and F_{stab} , which are the only limiting parameters for which the standard deviation is not directly taken from the simulation files because computation of the stabbing periods is required first by the post-processing Jupyter script.

For Situation 3, it was decided to simulate each load case (a combination of sea-state and crane load) for 20 minutes. Another option here was to transfer the crane load in one single simulation, where the hoisting wire load was reduced over a pre-set duration. As the wave component phases are randomly distributed, this would make the wave loading during the load transfer a matter of chance. To obtain statistically significant results, the simulation would have to be run many times. By simulating a specific crane load for 20 minutes, the results would already be statistically relevant, and the number of different crane load cases could be chosen. This was done to increase the reliability of the results. One of the consequences of this choice is that the actual crane load varies throughout the simulation, especially for the load cases with higher H_s and T_p values. This for example could cause slack rigging during simulations where the initial crane load was 20%. Therefore, it is advised to also run sufficient simulations with the crane transfer included in the simulation duration before applying this installation methodology to practice.

6.4.4. Comparison to Similar Research

The final part of the validity discussion is directed at comparing the results with other research in the field of WTG installations. As all studies have assessed different installations, the main differences or similarities for the results are also provided.

One of the research projects with most similarities [92] showed that their model was sensitive to swell dominated sea states with wave periods above 7.8s, due to the WTG natural pendulum period but less sensitive to wind dominated sea states. As the operability for wind-dominated seas is not quantified, no argumentative statement can be made about the similarity of the results. Furthermore, it is stated that the second most limiting parameter (aside from Nacelle-Crane clearance, which is not relevant for this thesis) is the vertical motion between tower and support structure. This limit could be addressed to ensure that the tower is always supported horizontally by a bumper and does not glide over it. This limit is best compared to the WTG uplift limit for Situation 2 without HC. However, this limit was by far not governing in this research. For this situation, the reeving DAF would be limiting (if the QCS limits are ignored). However, this limit is not assessed in the reference research.

Another reference research thesis includes a heave compensation system and also concludes that HC is particularly important to reduce the impact velocity and can reduce it from 0.18 m/s to 0.01 m/s [64]. In this thesis, looking at the most comparable load case, a reduction from 0.05 to 0.04 m/s is achieved. It must be said here that the HC is not optimised in this thesis, although a motion reduction of 95%, as in the reference case, is not expected to be achieved.

Another reference case within HMC assessed the wind loads on the RNA during lifting [72]. Here, it was also found that for an optimal wind direction, the wind force perpendicular to the blades (global X-direction) is negligible. It was found that the moment around the global X-axis was largest. However, this DOF is not included in this thesis. The influence of these loads on the WTG behaviour requires further research and a model expansion.

7

Conclusions and Recommendations

HMC wants to explore the possibilities of floating single-lift installations of WTGs. This thesis focuses on the dynamics of the WTG due to vessel responses and wind loading on the WTG. The operability of the mating operation for activation of the C1 quick connection system is determined. Furthermore, the sensitivity of the limiting parameters and design (input) parameters is assessed and options for optimising the installation procedure are proposed. The main findings of this thesis are presented in Section 7.1 and recommendations for further research are given in Section 7.2.

7.1. Conclusions

The conclusions are structured by answering each research sub-question separately. At the end, the main research conclusion is stated for the research goal.

What effect do wind and waves have on the dynamics of a WTG after the alignment phase of the installation?

The mean wind speed induces a load on the WTG creating an overturning moment. If this overturning moment is larger than the restoring moment due to the transferred weight, a QCS is required during the load transfer phase of the installation (Situation 3). For minimal wind loads (optimal direction + blade pitching), no QCS is required. Therefore, the wind loading on the blades is governing for the stability of the WTG during the load transfer installation phase. Wave loading determines the behaviour of the crane tip due to the vessel characteristics. Here, the significant wave height H_s influences the amplitude of the motion and the peak-period T_p influences the amplitude and the frequency of the motion. Increases in amplitude and/or period have a negative effect on the operability of the installation. The wave loading is mainly governing before the QCS activation (Situation 2). Only the first pendulum mode of the WTG lies in the excitation range of the wind & wave loads.

Is a QCS required to keep the WTG stable during the load transfer phase?

The need for the QCS depends on the wind and wave conditions. Here the wind load is the dominant factor. As the assessed situation is under minimal wind load (combination of wind direction and blade pitch), the WTG load transfer phase could be completed without the QCS under relatively calm sea states ($H_s < 1.4m$ and $T_p < 10s$) and a mean wind speed $V_w = 10m/s$. Here, it should be noted that no DP drift is accounted for, no longitudinal (global x-direction) wind speed variations are included, optimal wind heading is used, and only in-plane effects are assessed (3 DOF directions).

What is the operability of the activation of the QCS during a single-lift WTG installation?

Situation 2 is the governing limiting activity (with respect to Situation 3) if at least 16 C1 QCS Wedges are used. The operability is poor (almost negligible) in Situation 2 for the base case setup. Heave Compensation is required to reduce the dynamic reeving tension and the loading of the C1 QCS. An installation without HC is deemed infeasible from an operability point of view.

Is the stabbing window a limiting factor for the application of the QCS?

T_{stab} and F_{stab} are the governing limiting parameters in all assessed cases. This is mainly due to the extremely strict limit of C1 flange slot alignment Z_{max} . If this limit is relaxed to for example $4cm$, the operability is increased substantially.

How do the support structure, WTG, rigging, and crane interact after the QCS is deployed?

The crane tip motion increases the horizontal rigging tension inducing loads on the QCS due to the overturning moment. Vertical motions of the crane tip influence the load on the support structure. This motion is less relevant for the operability as this only causes contact force variations. The effect of the QCS on the vessel cannot be investigated fully with this model as the vessel is not included in the model and DP offset is not accounted for. However, most effect is expected for the vessel pitch and incorporation of heave compensation relaxes the peak load in the rigging.

How does the C1 QCS perform compared to alternative connections during installation?

The C1 QCS has some advantages such as: the LLT can be hung off on the upper flange, it can be remotely activated, and the rigging can be slacked and disconnected after C1 QCS activation. The main components for the QCS are already standard incorporated in the connection, so limited costs are associated with the system. The pretension force in the C1 QCS is almost double compared to FCT for the L-flange, resulting in less QCS Wedges required which reduces the cost and increases the reliability. The Slip Joint is expected to be superior regarding operability and simplicity. However, the implementation of the Slip Joint is held back by other limits, such as extra required lifting height. Installation duration of the connections is estimated to be comparable if the operations are optimised.

What design improvements are required, if any, to make the C1 Wedge Connection suitable for a single-lift WTG installation?

The relaxation of the Z_{max} limit is most important. Furthermore, the maximum WTG rotation should be increased to 2 degrees, which is still within the rotational clearance of the C1 Wedge Connection. An F_{stab} of 20% is optimistic for sea states with a peak period $T_p > 8s$. The operability is not overly sensitive to a reduction of T_{stab} .

How to optimise the operability of a floating single-lift installation of a Wind Turbine Generator (WTG) with a quick connection system (QCS)?

The standard lifting configuration has an extremely low operability. Operability can be improved with lifting aids such as heave compensation and design adaptations as relaxation of the Z_{max} limit. Including these alternations, plus increasing the pre-QCS activation load transfer to 20%, a feasible operability can be achieved for peak periods $T_p < 9s$ and significant wave heights $H_s < 2m$. For higher sea-states the operability is limited by multiple limiting parameters, such as T_{stab} , F_{stab} and the WTG rotation. Here, it should be noted that this is under optimal wind loading conditions and a set of assumptions such as zero DP drift. Under these conditions, the load transfer phase is expected to be stable for relatively calm sea-states ($H_s < 1.4m$ and $T_p < 10s$) and a mean wind speed $V_w = 10m/s$.

7.2. Recommendations

Based on the findings of the thesis, a number of recommendations are formulated for future research. The recommendations proposed here, are split into two categories; those that regards a form of model expansions and those that do not. This second category includes a diverse range of recommendations next to the model's goal.

7.2.1. Model Expansions

As the final model used in this thesis to generate results is built on a set of assumptions, the validity of these assumptions is crucial for the results generated by the model. Some of the assumptions were conservative, while others were progressive with respect to reality. As these progressive assumptions could overestimate the operability, it is advisable to further research these. Two main expansions proposed, are the DP drift and the wind loading on the WTG. DP drift is the phenomenon of vessel motion in surge, sway, and yaw direction due to the imperfect working of the DP system. Similarly to a HC system, a DP system is unable to keep the vessel exactly at the desired location. Disturbances of the DP

system come in many forms: internal errors, external errors, measurement errors, etc. The vessel motion due to these variations affects the motion of the crane tips and thus of the WTG during installation. The impact of DP drift on the operability of the WTG installation requires additional research. It is expected that this will reduce the operability to some level depending on the functioning of the DP-system.

Wind loading on the RNA is extraordinarily complex and should therefore be investigated extensively to assess the correct load on the WTG during an installation. Many factors, such as wind velocity, direction, spatial variations, blade design, orientation, and rotational speed heavily influence the loading. In this thesis, minimal loading on the blades is assumed. However, in reality, weather can vary from time to time, influencing the wind conditions possibly to suboptimal conditions. Therefore, it is advised to research the influence of wind variation on the wind loading on the WTG, especially on the blades. If sub-optimal wind loading on the blades is incorporated, it is expected that the stability during the load transfer phase will decrease up to a level as predicted in Figure 6.6a. This would highlight the importance of a QCS and the desire to keep the initial load transfer as low as possible. As it is expected that wind direction variation will increase the motions of the WTG, implementation of tugger winches to control the WTG motions is also interesting to research. In order to do all of the above properly, a model should be used containing all 6 DOF directions. This can be done by expanding the current model. If a model containing all DOFs is developed, the operability dependency to wave directionality can also be determined. By incorporating all 6 directions the influence of yaw, sway and roll motions is also incorporated into the model. The influence of the sway motions on the operability is expected to be limited, as these motions are similar to the surge motions for the WTG behaviour, and the bottom of the WTG is also constrained in sway direction. However, the roll motions of the tower are expected to reduce the operability as the eigenmodes for the WTG roll are expected to be in the frequency range of the excitation. The yaw forces and moments on the WTG are also expected to be considerable, as was shown in the thesis of A.N. Versnik [103]. However, the C1 Wedge Connection's G&B system contains rotational locking pins which could take on the yaw moment if these are designed accordingly. Overall, the expansion to 6 DOF directions could reduce the simulated operability considerably. Fortunately, such a model also provides opportunities to investigate the impact of additional stabilising measures to enhance operability. It would make the model a closer representation of the real-world dynamics and contribute to a deeper foundation of installation design.

Another subject that requires further investigation is variation of stiffnesses in the model. Although a general variation of the Heave Compensator was executed, a more thorough investigation could explain why the operability was truly minimal for the base case stiffness and whether this is a solid argument to change the HC stiffness. Furthermore, a sensitivity was performed on the contact stiffness between the WTG and the support structure. Because the support structure was assumed a rigid body fixed to the seabed, the relative motions between the WTG and support structure increased for softer contact stiffnesses. This led to a lower operability, since the T_{stab} and F_{stab} require as least motion between the WTG and support structure as possible. As this is counterintuitive to reality and the shortcoming of the model is identified, these results are excluded from the report. To properly model these variations, it is advised to include some degree of freedom to the TP/MP and or model it as a compliant tower.

7.2.2. Elaborations besides Installation Modelling

Based on the operability graphs presented in the results (Chapter 6), the economic feasibility of single lift WTG installations can be further researched. In what areas of the world do these operability curves generate sufficient workability to minimise WoW and optimise installation cycle time? Is there a good business case to implement this methodology for WTG installations? These are truly relevant questions, as economic viability determines the adoption of technology. In Chapter 2, three logistical strategies are discussed. These three scenarios could be used in such a study. Here, it should be noted that this research is focused on bottom-founded support structures. However, other studies found that a floating TLP support structure does not influence the operability significantly [92]. Some floating support structures require a larger crane boom radius with respect to MPs, for example, as their diameter is multiple times larger than bottom-founded support structures. This reduces the lifting capacity and lifting height of the cranes. The consequences of these alternations on the operability of the installation will depend on the assessed scenario.

Furthermore, it is interesting to verify whether the proposed design alterations to the flanges of the C1 Wedge connection and QCS could be incorporated into the design of the connection. This mainly consists of increasing the C1 flange slot alignment Z_{max} that is required. Also, the development of Active Heave Compensation to the required capacity of 1600 mT is an interesting installation aid improvement that could improve the operability of the installation operation.

References

- [1] Wilson Guachamin Acero, Zhen Gao, and Torgeir Moan. "Methodology for assessment of the allowable sea states during installation of an offshore Wind turbine transition piece structure onto a monopile foundation". In: *Journal of Offshore Mechanics and Arctic Engineering* 139.6 (Dec. 2017). ISSN: 1528896X. DOI: 10.1115/1.4037174. URL: https://www.researchgate.net/publication/319254672_Methodology_for_Assessment_of_the_Allowable_Sea_States_During_Installation_of_an_Offshore_Wind_Turbine_Transition_Piece_Structure_onto_a_Monopile_Foundation.
- [2] "Active Heave Compensation". In: *Ocean Drilling Program* (2010). URL: <http://www-odp.tamu.edu/publications/tnotes/tn31/pdf/ahc.pdf>.
- [3] Dang Ahn et al. "Comparative evaluation of different offshore wind turbine installation vessels for Korean west-south wind farm". In: *International Journal of Naval Architecture and Ocean Engineering* 9.1 (Jan. 2017), pp. 45–54. DOI: 10.1016/j.ijnaoe.2016.07.004. URL: <http://dx.doi.org/10.1016/j.ijnaoe.2016.07.004>.
- [4] V. D. Angelis. "Comparison study of electric, electro-hydraulic, and hydraulic drive science winches." In: *11th European Research Vessel Operators Meeting*. Canadian Coast Guard, May 2009. URL: [https://www.ervo-group.eu/np4/%7B\\$clientServletPath%7D/?newsId=13&fileName=CCG_ERVO_Presentation_May_2009.pdf](https://www.ervo-group.eu/np4/%7B$clientServletPath%7D/?newsId=13&fileName=CCG_ERVO_Presentation_May_2009.pdf).
- [5] Piet Bastiaanssen. *Modelling the dynamic behaviour of a rotor nacelle assembly during the installation using a floating vessel*. Tech. rep. Delft: TU Delft, Sept. 2020. URL: [http://repository.tudelft.nl/..](http://repository.tudelft.nl/)
- [6] John H. Bickford. *Introduction to the Design and Behavior of Bolted Joints*. 4th ed. Boca Raton: CRC Press, 2008.
- [7] Ruben Blom. *Allowable Wind Turbine Set-down Impact*. 2022. URL: <https://repository.tudelft.nl/islandora/object/uuid%3Aa3e14327-0d64-46b7-9730-0d1803cd7e9c>.
- [8] Job Bokhorst and Maarten Burger. *EG-515 Weather Risk Assessment*. Tech. rep. Leiden: HMC, Nov. 2023.
- [9] Mariska Buitendijk. *Huisman launches floating installation of wind turbines with Windfarm Installation Vessel*. Apr. 2022. URL: <https://swzmaritime.nl/news/2022/04/22/huisman-launches-floating-installation-of-wind-turbines-with-windfarm-installation-vessel/>.
- [10] Adrijana Buljan. *BP and Equinor Terminate Empire Wind 2 Offtake Agreement, Await 'New Offtake Opportunities'*. Jan. 2024. URL: <https://www.offshorewind.biz/2024/01/04/bp-and-equinor-terminate-empire-wind-2-offtake-agreement-await-new-offtake-opportunities/>.
- [11] BVG Associates. *Long-term outlook on developments in foundation technology*. Tech. rep. TKI Wind op Zee, Aug. 2022. URL: www.tki-windopzee.nl.
- [12] C1 Connections. *The C1 Wedge Connection*. 2022. URL: <https://c1connections.com/>.
- [13] Alessandro ; Cabboi et al. "Vibration-assisted installation and decommissioning of a slip-joint". In: *Engineering Structures* 209 (Apr. 2020), p. 109949. ISSN: 0141-0296. DOI: 10.1016/J.ENGSTRUCT.2019.109949. URL: <https://repository.tudelft.nl/islandora/object/uuid%3A1a45f6a9-9416-4645-b18e-d9d14fbf8f15>.
- [14] Cadeler. *Wind Scylla*. URL: <https://www.cadeler.com/vessels/seajacks-scylla>.
- [15] Cadeler. *Wind-Peak-Technical-Specification*. Sept. 2023.

- [16] D. Cannell et al. "Adaptive Passive Heave Compensation Systems - The Next Generation". In: *Offshore Technology Conference Asia 2016, OTCA 2016* (Mar. 2016), pp. 94–107. DOI: 10.4043/26544-MS. URL: <https://dx.doi.org/10.4043/26544-MS>.
- [17] Lu Cheng et al. "FE-assisted investigation for mechanical behaviour of connections in offshore wind turbine towers". In: *Engineering Structures* 285 (June 2023), p. 116039. ISSN: 0141-0296. DOI: 10.1016/J.ENGSTRUCT.2023.116039.
- [18] Lu Cheng et al. "The C1 wedge connection in towers for wind turbine structures, tensile behaviour of a segment test". In: *Engineering Structures* 282 (May 2023), p. 115799. ISSN: 0141-0296. DOI: 10.1016/J.ENGSTRUCT.2023.115799.
- [19] J. Chung and G. M. Hulbert. "A Time Integration Algorithm for Structural Dynamics With Improved Numerical Dissipation: The Generalized- α Method". In: *Journal of Applied Mechanics* 60.2 (June 1993), pp. 371–375. ISSN: 0021-8936. DOI: 10.1115/1.2900803.
- [20] Cranemaster. *Mudmat and manifold installation with limited rigging height*. URL: <https://cranemaster.com/references/mudmat-and-manifold-installation-western-australia-with-limited-rigging-height/>.
- [21] Cranemaster. *SWL 1200 ton and above*. 2023. URL: <https://cranemaster.com/units/swl-1200t-and-above/>.
- [22] Koen Erwin Yvonne Creusen et al. "Introducing the C1 Wedge Connection". In: *Steel Construction* 15.1 (Feb. 2022), pp. 13–25. ISSN: 18670539. DOI: 10.1002/STCO.202100039.
- [23] DEME Group. *Orion*. URL: <https://www.deme-group.com/technologies/orion#>.
- [24] DNV AS. *DNV ST-0054 Transport and installation of wind power plants*. Tech. rep. Nov. 2021.
- [25] DNV AS. *DNV-RP-C205 Environmental Conditions and environmental loads*. Tech. rep. Sept. 2019.
- [26] DNV AS. *DNV-RP-N103*. Tech. rep. Sept. 2021.
- [27] DNV AS. *DNV-ST-0126 Support structures for wind turbines*. Tech. rep. DNV, Dec. 2021.
- [28] DNV AS. *DNV-ST-N001 Marine operations and marine warranty*. Tech. rep. DNV, Dec. 2023. URL: <https://standards.dnv.com/explorer/document/F3547C048BFD4125823EE8ADA20394BB/5>.
- [29] David Fidalgo Domingos, Peter Wellens, and Jan Willem van Wingerden. "Frequency-domain framework for floating installation of wind-turbine towers". In: *Ocean Engineering* 297 (Apr. 2024), p. 116952. ISSN: 0029-8018. DOI: 10.1016/J.OCEANENG.2024.116952.
- [30] DOT. *Slip Joint*. 2022. URL: <https://dotpower.nl/innovation/slipjoint/>.
- [31] *EchoBolt: A Sound Innovation for Offshore Wind Turbine Maintenance*. July 2021. URL: <https://ore.catapult.org.uk/stories/a-sound-innovation-for-wind-turbine-maintenance/>.
- [32] Thijs Eijkhout and Jovana Jovanova. "Active heave compensation of a floating crane using electric drive". In: *IEEE/ASME International Conference on Advanced Intelligent Mechatronics, AIM 2021-July* (July 2021), pp. 1089–1094. DOI: 10.1109/AIM46487.2021.9517502.
- [33] Energy Facts Staff Writer. *Van Oord Successfully Installs World's First Submerged Slip Joint*. Apr. 2020. URL: <https://www.energyfacts.eu/van-oord-successfully-installs-worlds-first-submerged-slip-joint/>.
- [34] Energy Institute. *Case study on reducing manual handling and ergonomics related incidents in the offshore wind industry*. Feb. 2020. URL: <https://www.gplusoffshorewind.com/?a=699447>.
- [35] K. Feyrer. "Wire ropes: Tension, endurance, reliability". In: *Wire Ropes: Tension, Endurance, Reliability* (2007), pp. 1–322. DOI: 10.1007/978-3-540-33831-4/COVER.
- [36] GROW. *Bolt & Beautiful*. Sept. 2022. URL: <https://grow-offshorewind.nl/project/bolt-beautiful>.

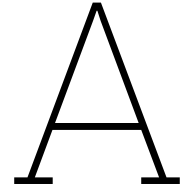
- [37] Peter Gu et al. "Modeling, simulation and design optimization of a hoisting rig active heave compensation system". In: *International Journal of Machine Learning and Cybernetics* 4 (Feb. 2012), pp. 85–98. DOI: 10.1007/s13042-012-0076-x. URL: <https://link-springer-com.tudelft.idm.oclc.org/article/10.1007/s13042-012-0076-x>.
- [38] Peter Gu et al. "Modeling, simulation and design optimization of a hoisting rig active heave compensation system". In: *International Journal of Machine Learning and Cybernetics* 4.2 (Apr. 2013), pp. 85–98. ISSN: 18688071. DOI: 10.1007/S13042-012-0076-X.
- [39] Wilson Guachamin Acero et al. "Methodology for assessment of the operational limits and operability of marine operations". In: *Ocean Engineering* 125 (Oct. 2016), pp. 308–327. ISSN: 00298018. DOI: 10.1016/J.OCEANENG.2016.08.015. URL: https://www.researchgate.net/publication/307478131_Methodology_for_assessment_of_the_operational_limits_and_operability_of_marine_operations.
- [40] Klaus Hasselmann. "Measurements of wind-wave growth and swell decay during the Joint North Sea Wave Project (JONSWAP)". In: (Jan. 1973). URL: https://www.researchgate.net/publication/256197895_Measurements_of_wind-wave_growth_and_swell_decay_during_the_Joint_North_Sea_Wave_Project_JONSWAP.
- [41] Heerema. *History*. 2022. URL: <https://www.heerema.com/history>.
- [42] Heerema Marine Contractors. *Heerema installs first wind turbine using novel RNA method*. Nov. 2022. URL: <https://www.heerema.com/news/heerema-installs-first-wind-turbine-using-novel-rna-method>.
- [43] Heerema Marine Contractors. *LiftDyn Validation Based on Model Tests*. Tech. rep. Leiden, May 2017.
- [44] Heerema Marine Contractors. *Successful Installation of 24 Arcadis Ost 1 Turbines*. 2023. URL: <https://www.heerema.com/news/successful-installation-of-24-arcadis-ost-1-turbines>.
- [45] Heerema Marine Contractors B.V. *LiftDyn Theory Manual*.
- [46] Leo Holthuijsen. *Waves in Oceanic and Coastal Waters*. 2009th ed. Vol. 3. New York: Cambridge University Press, 2007. DOI: 10.2277/0521860288. URL: https://www.researchgate.net/publication/253127661_Waves_in_Oceanic_and_Coastal_Waters.
- [47] Fengrui Hou Jiaoyi; Zhang and Dayong Ning. "Design and Simulation of a Passive Heave Compensator with Adaptive Damping Regulation for 600 Meters Shipwreck Salvaging Claw". Ottawa, June 2023.
- [48] J. Hoving. "Linearization of elongations in kinematic elements". Delft, 2024.
- [49] Sophie van Hoytema and Bob Meijer. *De Toekomst van Offshore Windturbines: Groei, Optimalisatie en Standaardisatie*. May 2022. URL: <https://www.youtube.com/watch?v=TYk9qJL8v5U&list=TLGGIbJGE0rt2Wcx0DAxMjAyNA>.
- [50] Huisman. *Installatieschip voor windmolenparken*. 2024. URL: https://www.huismanequipments.com/nl/products/renewables/offshore_wind/windfarm-installation-vessel.
- [51] *Inflation Reduction Act Guidebook*. Sept. 2023. URL: <https://www.whitehouse.gov/cleanenergy/inflation-reduction-act-guidebook/>.
- [52] International Electrotechnical Commission. *Wind Energy Generation Systems - Electromagnetic Compatibility (EMC) - Requirements and test methods*. Tech. rep. 2024. URL: https://www.iec.ch/dyn/www/f?p=103:30:713698002236708:::FSP_ORG_ID,FSP_LANG_ID:1282,25?q=tc%2088.
- [53] International Renewable Energy Agency. *Future of wind : deployment, investment, technology, grid integration and socio-economic aspects (A Global Energy Transformation paper)*. Abu Dhabi, Oct. 2019, p. 87. ISBN: 9789292601553.
- [54] IQIP. *Pipe Flange Clamp Tool*. URL: <https://iqip.com/products/handling-equipment/flange-clamp/>.

- [55] Zhiyu Jiang. "Installation of offshore wind turbines: A technical review". In: *Renewable and Sustainable Energy Reviews* 139 (Apr. 2021), p. 110576. ISSN: 1364-0321. DOI: 10.1016/J.RSER.2020.110576.
- [56] Zhiyu Jiang et al. "A parametric study on the final blade installation process for monopile wind turbines under rough environmental conditions". In: *Engineering Structures* 172 (Oct. 2018), pp. 1042–1056. ISSN: 0141-0296. DOI: 10.1016/J.ENGSTRUCT.2018.04.078.
- [57] Pat Jones. *Maximizing Hydraulic Efficiency*. May 2012. URL: <https://www.design-engineering.com/features/maximizing-hydraulic-efficiency/>.
- [58] J M J Journée and W W Massie. "Offshore hydromechanics". In: (2001).
- [59] Jelle Joustra, Bas Flipsen, and Ruud Balkenende. "Structural reuse of wind turbine blades through segmentation". In: *Composites Part C: Open Access* 5 (July 2021), p. 100137. ISSN: 2666-6820. DOI: 10.1016/J.JCOMC.2021.100137.
- [60] Koninklijk Nederlands Elektrotechnisch Comité. *NEN-EN-IEC 61400-1 Wind energy generation systems - Part 1: Design requirements*. Tech. rep. Delft: NEN, Apr. 2019.
- [61] Sebastian Kuchler et al. "Active control for an offshore crane using prediction of the vessels motion". In: *IEEE/ASME Transactions on Mechatronics* 16.2 (Apr. 2011), pp. 297–309. ISSN: 10834435. DOI: 10.1109/TMECH.2010.2041933.
- [62] M. Kurstjens and S. Erents. *Considerations when moving to TP-less*. Tech. rep. SIF, Aug. 2022.
- [63] Nikolai M. Kuznetsov. "Stability of Shock Waves". In: *Handbook of Shock Waves* (2001), pp. 413–454. DOI: 10.1016/B978-012086430-0/50009-9.
- [64] Thijs Lengkeek. *Floating installation of offshore wind turbines in a single lift*. 2018. URL: <https://repository.tudelft.nl/islandora/object/uuid%3A3fa2d392-5c74-4348-bdea-e2fefb7a3115>.
- [65] Sharda Lochan, Ali Mehmanparast, and John Wintle. "A review of fatigue performance of bolted connections in offshore wind turbines". In: (2019). DOI: 10.1016/j.prostr.2019.08.037. URL: www.sciencedirect.comwww.sciencedirect.com.
- [66] Timothée Macquart, Duygu Kucukbahar, and Bob Prinsenn. *Dutch Offshore Wind Market Report 2023*. Tech. rep. Utrecht: RVO, Apr. 2023.
- [67] C. A. Madsen et al. "Analytical and numerical investigation of bolted steel ring flange connection for offshore wind monopile foundations". In: *IOP Conference Series: Materials Science and Engineering* 276.1 (Dec. 2017). ISSN: 1757899X. DOI: 10.1088/1757-899X/276/1/012034. URL: https://www.researchgate.net/publication/321775525_Analytical_and_numerical_investigation_of_bolted_steel_ring_flange_connection_for_offshore_wind_monopile_foundations.
- [68] Naunidh Mangat et al. *Optimal offshore wind turbine size and standardisation study*. Tech. rep. Utrecht: TKI Wind op Zee, May 2022. URL: www.tki-windopzee.nl.
- [69] Adnan Memija. *Ørsted Cancels Two Wind Projects Offshore New Jersey, Clears Revolution Wind for Takeoff*. Nov. 2023. URL: <https://www.offshorewind.biz/2023/11/01/orsted-cancels-two-wind-projects-offshore-new-jersey-clears-revolution-wind-for-takeoff/>.
- [70] G. Meskers. *Rigging stiffness and damping*. Leiden, 2023.
- [71] A.V. Metrikine. *Lecture Notes CT 4145 - CIE4140 Structural Dynamics (2021/22 Q3)*. URL: <https://brightspace.tudelft.nl/d2l/le/content/399214/viewContent/2588747/View>.
- [72] mocean. *RNA Installation Analysis*. Tech. rep. Aug. 2022.
- [73] Adelaide Nespoli et al. "The high potential of shape memory alloys in developing miniature mechanical devices: A review on shape memory alloy mini-actuators". In: *Sensors and Actuators A* 158 (2010), pp. 149–160. DOI: 10.1016/j.sna.2009.12.020.
- [74] Michel K. Ochi. *Ocean Waves*. Cambridge University Press, Mar. 1998. ISBN: 9780521563789. DOI: 10.1017/CB09780521563789.

- [75] Orcina. *OrcaFlex documentation*. 2024. URL: <https://www.orcina.com/resources/documentation/>.
- [76] Orcina. *OrcaFlex literature*. 2024. URL: <https://www.orcina.com/resources/literature/>.
- [77] Orcina. *OrcaFlex technical notes: Modelling contactguide*. May 2023. URL: <https://www.orcina.com/resources/papers-and-technical-notes/>.
- [78] Tom Pawson. *Why do cranes (and loads) fall over?* Jan. 2022.
- [79] E.L. Petersen et al. "Wind power meteorology". In: *Risø National Laboratory for Sustainable Energy* (1998). ISSN: 10991824. URL: <https://findit.dtu.dk/en/catalog/537f101b74bed2fd2100870d>.
- [80] Willard J. Pierson and Lionel Moskowitz. "A proposed spectral form for fully developed wind seas based on the similarity theory of S. A. Kitaigorodskii". In: *Journal of Geophysical Research* 69.24 (Dec. 1964), pp. 5181–5190. ISSN: 01480227. DOI: 10.1029/JZ069i024p05181.
- [81] Zhengru Ren et al. "Active tugger line force control for single blade installation". In: *Wind Energy* 21.12 (Dec. 2018), pp. 1344–1358. ISSN: 10991824. DOI: 10.1002/WE.2258.
- [82] *REPowerEU*. May 2022. URL: https://commission.europa.eu/strategy-and-policy/priorities-2019-2024/european-green-deal/repowereu-affordable-secure-and-sustainable-energy-europe_nl.
- [83] RVO Nederland. *Inflation Reduction Act Rapport*. Tech. rep. Den Haag: RVO, Jan. 2023.
- [84] Scaldis. *Groen - Beatrice Demonstrator Project*. July 2007. URL: <https://www.scaldis-smc.com/en/projects/groen-2007-jul-beatrice/>.
- [85] Sebastian Schreier. *Floating Substructures & Moorings*. Oct. 2022.
- [86] Seaqualize. *The Seaqualize Heave Chief*. 2023. URL: <https://www.seaqualize.com/>.
- [87] Christopher Sexton, Benjamin Stokes, and Vincent McCarthy. *Multi-functional clamp system and method for the installation of a wind turbine on an offshore substructure*. July 2020.
- [88] Sif Group. *Start of steel construction*. July 2023. URL: <https://sif-group.com/en/news/start-of-steel-construction/>.
- [89] J.M.J. Spijkers, A.W.C.M. Vrouwenvelder, and E.C. Klaver. *Lecture Notes on Structural Vibrations - CIE4140 Structural Dynamics (2021/22 Q3)*. Jan. 2005. URL: <https://brihtspace.tudelft.nl/d21/1e/content/399214/viewContent/2588745/View>.
- [90] *Spinergie*. URL: <https://www.spinergie.com/>.
- [91] *Spyder IDE*. 2024. URL: <https://www.spyder-ide.org/>.
- [92] Quint van Suijlen. *Floating to floating installation of a full 15 MW wind turbine on a tension leg platform with a semi-submersible crane vessel: A parametric sensitivity study*. 2023. URL: <https://repository.tudelft.nl/islandora/object/uuid%3A2ca9baa7-55f4-4f67-a3a0-d0c5a8a1e4d6>.
- [93] Sander Suur and Ferdy Hengeveld. "Borssele V slip joint connection: design, certification and installation of the world's first full-size submerged slip joint". In: *Steel Construction* 15.3 (Aug. 2022), pp. 152–159. ISSN: 18670539. DOI: 10.1002/STCO.202100038. URL: https://www.researchgate.net/publication/359896198_Borssele_V_slip_joint_connection_design_certification_and_installation_of_the_world's_first_full-size_submerged_slip_joint.
- [94] J. van der Tempel. *Slip Joint Offshore Research project (SJOR)*. Dec. 2019. URL: <https://grow-offshorewind.nl/project/sjor>.
- [95] *The Stability Frame, Hywind Scotland*. 2024. URL: <https://www.istructe.org/structural-awards/projects/2018/the-stability-frame,-hywind-scotland/>.
- [96] TIOBE. *TIOBE Index*. 2024. URL: <https://www.tiobe.com/tiobe-index/>.
- [97] Bartolomej Tomic. "You're Gonna Need A Bigger Crane...". Aug. 2023. URL: <https://www.marinelink.com/news/youre-gonna-need-a-bigger-crane-507647>.

- [98] Bartolomej Tomic. *PHOTO: Boskalis Tows First of Five 9.5MW Turbines for Kincardine Floating Wind Farm*. Dec. 2020. URL: <https://www.oedigital.com/news/483774-photo-boskalis-tows-first-of-five-9-5mw-turbines-for-kincardine-floating-wind-farm>.
- [99] Yehezkiel Tumewu, Petrone Crescenzo, and Mettupalayam Sivaselvan. "Numerical Simulation of the Influence of Platform Pitch Motion on Power Generation Steadiness in Floating Offshore Wind Turbines". In: *International Journal of Environmental Science & Sustainable Development*. 2.1 (July 2017), p. 92. ISSN: 2357-0849. DOI: 10.21625/ESSD.V1I2.39.
- [100] Susanna Twidale. *Vattenfall Stopping Norfolk Boreas Offshore Wind Farm in UK North Sea*. July 2023. URL: <https://www.oedigital.com/news/506672-vattenfall-stopping-norfolk-boreas-offshore-wind-farm-in-uk-north-sea>.
- [101] Ramon van der Valk. *Hoist and boom wire dynamics during offshore heavy lifting*. 2017. URL: <https://repository.tudelft.nl/islandora/object/uuid%3Af347a0c0-98aa-45e7-881d-fee5ce5ab0f4>.
- [102] H. F. Veldkamp and J. Van Der Tempel. "Influence of wave modelling on the prediction of fatigue for offshore wind turbines". In: *Wind Energy* 8.1 (2005), pp. 49–65. ISSN: 10954244. DOI: 10.1002/WE.138.
- [103] Ana Versnik. *Analysis of loads encountered during a single lift operation of offshore wind turbines*. Leiden, July 2023. URL: <https://repository.tudelft.nl/islandora/object/uuid%3A647b0473-946c-4a8b-9ea6-93bd78157a77>.
- [104] Kees Vuik et al. "Numerical Methods for Ordinary Differential Equations". In: *TU Delft OPEN Textbooks* (Feb. 2023). DOI: 10.5074/T.2023.001. URL: <https://doi.org/10.5074/t.2023.001>.
- [105] Vuyk Engineering. *Gulliver*. URL: <https://vuykrotterdam.com/projects/gulliver>.
- [106] Wout Weijtjens et al. "Bolted ring flanges in offshore-wind support structures-in-situ validation of load-transfer behaviour". In: (2020). DOI: 10.1016/j.jcsr.2020.106361. URL: <https://doi.org/10.1016/j.jcsr.2020.106361>.
- [107] David Weston. *Hywind turbines complete foundation installation*. June 2017. URL: <https://www.windpowermonthly.com/article/1437693/hywind-turbines-complete-foundation-installation>.
- [108] Rebecca Williams, Feng Zhao, and Joyce Lee. *GLOBAL OFFSHORE WIND REPORT 2022*. Tech. rep. Brussels: GWEC, June 2022. URL: www.gwec.net.
- [109] WindEurope. *Europe invested €17bn in new wind in 2022, the lowest since 2009*. Mar. 2023. URL: <https://windeurope.org/newsroom/press-releases/europe-invested-e17bn-in-new-wind-in-2022-the-lowest-since-2009/>.
- [110] WindEurope. *Offshore wind investments recovering but still "way to go" – including on supply chain*. Aug. 2023. URL: <https://windeurope.org/newsroom/news/offshore-wind-investments-recovering-but-still-way-to-go-including-supply-chain/#>.
- [111] J K Woodacre, R J Bauer, and R A Irani. "A review of vertical motion heave compensation systems". In: (2015). DOI: 10.1016/j.oceaneng.2015.05.004. URL: <http://dx.doi.org/10.1016/j.oceaneng.2015.05.004>.
- [112] Michiel Zaaijer and Axelle Viré. *Introduction to wind turbines - Reader - AE4W02TU Introduction to Wind Turbines: Physics and Technology (2022/23 Q2)*. Sept. 2022. URL: <https://brightspace.tudelft.nl/d2l/le/content/498962/viewContent/2911594/View>.
- [113] Michiel Zaaijer, Axelle Viré, and Pim van der Male. *OWFD-Aerodynamic loading - Reader - OE44120 Offshore Wind Farms Design (2021/22 Q4)*. Apr. 2020. URL: <https://brightspace.tudelft.nl/d2l/le/content/401379/viewContent/2643829/View>.
- [114] Yuna Zhao et al. "Numerical study on the feasibility of offshore single blade installation by floating crane vessels". In: *Marine Structures* 64 (Mar. 2019), pp. 442–462. ISSN: 09518339. DOI: 10.1016/J.MARSTRUC.2018.12.001.

-
- [115] Linbo Zhu, Abdel Hakim Bouzid, and Jun Hong. "Numerical and Experimental Study of Elastic Interaction in Bolted Flange Joints". In: *Journal of Pressure Vessel Technology, Transactions of the ASME* 139.2 (Apr. 2017). ISSN: 15288978. DOI: 10.1115/1.4035316.



Heerema Marine Contractors

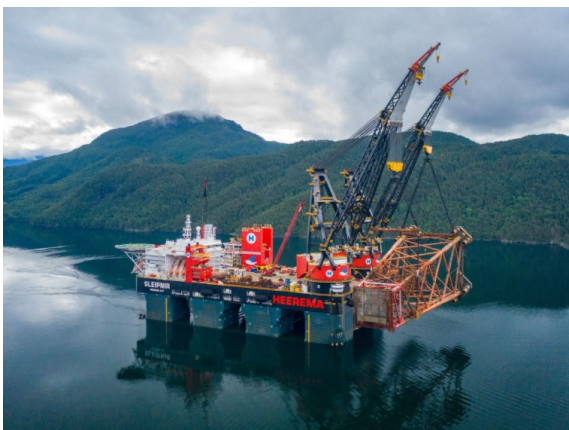
A.1. History

Constructora Heerema was established in 1948 in Venezuela [41]. The company constructed and installed drilling platforms for oil companies operating on Lake Maracaibo. In 1962, Heerema Engineering Services was founded, focusing on the North Sea. In 1978, Heerema commissioned the world's first semi-submersible crane vessels (SSCVs): the Balder and Hermod. Low oil prices in the mid-1980s forced Heerema and McDermott, an engineering and construction company, to start a joint venture called HeereMac (1989). The year 1997 was a turning point: HeereMac was terminated, and operations continued under the name of Heerema Marine Contractors (HMC). HMC acquired SSCV "Thialf" (ex DB-102) from McDermott, causing HMC to own and operate three of the world's five SSCVs. In 2013, HMC introduced the DCV Aegir. The vessel was designed for capability of executing complex infrastructure and pipeline projects in ultra-deep water. In 2018, Heerema pivoted away from pipelay towards the renewables market. Modifications were made to the Aegir and the organisation was reorganised. In 2019, Heerema introduced the largest SSCV in the world: the Sleipnir. The vessel is designed for a 20,000 metric ton lifting capacity.

A.2. Fleet

Sleipnir

The newest vessel of HMC's fleet is the SSVC Sleipnir. The vessel is equipped with two 10,000 tonnes revolving cranes. The large deck area makes it suitable for transporting jackets, topsides, or modules. The transit speed is over 10 knots, and the vessel has the capacity to run on LNG.



(a) SSCV Sleipnir.

Main data

Construction Year	2019
Lift Capacity	20,000 metric tons
Dimensions	
Length	220 m
Width	102 m
Draft	12 - 32 m

(b) Sleipnir main specifications

Figure A.1: HMC's Sleipnir

Aegir

The Aegir's combination of heavy lifting and high sailing speed offers a unique opportunity for offshore transport, installation, and removal operations. The vessel was introduced in 2013 as a pipe-laying vessel but was retrofitted after a strategy switch of the company in 2018. The vessel has a single crane with a lifting capacity of 5,000 tonnes, and the option to use a split main crane block to upend tall structures and long piles, similar to the dual crane vessels.



(a) DCV Aegir.

Main data

Construction Year	2012
Lift Capacity	5,000 metric tons

Dimensions

Length	211 m
Width	46 m

Draft

Operating draft	9 - 11 m
Transit draft	8 m

(b) Aegir main specifications

Figure A.2: HMC's Aegir

Thialf

Thialf was built in 1985 and is equipped with two revolving cranes capable of a tandem lift of 14,200 tonnes. The vessel has a class III dynamic positioning system, making it suitable for the installation of foundations, moorings, SPARs, TLPs and integrated topsides.



(a) SSCV Thialf.

Main data

Construction Year	1985
Lift Capacity	14,200 metric tons

Dimensions

Length	201.6 m
Width	88.4 m
Depth to work deck	49.5 m
Draft	11.9 - 31.6 m

(b) Thialf main specifications

Figure A.3: HMC's Thialf

Balder

Balder is the world's first SSCV and was built in 1978 in Japan. In guyed mode, the cranes are capable of executing a tandem lift of 6,300 tonnes. The vessel is multi-functional with its depth reach lowering capability as well as its heavy lift capacity to install topsides. Balder has been involved in the installation and decommissioning of over 100 projects worldwide. Due to the vessel's extensive history, it is the ideal choice for decommissioning structures.



(a) SSCV Balder.

Main data	
Construction Year	1978
Lift Capacity	6,300 metric tons
Dimensions	
Length	154 m
Width	86 m
Width of Deck	105 m
Draft	
Draft	14 m and deeper
Draft incl. thrusters	4.5 m under hull

(b) Balder main specifications

Figure A.4: HMC's Balder

Supporting fleet

HMC's fleet also consists of two tugs; Bylgia and Kolga, and ten barges supporting the offshore operations. Bylgia and Kolga are used for towing, anchoring and mooring operations. The barges are used for transportation, jacket launches, and float-over operations.



(a) Tugs Bylgia and Kolga.

Main data	
Construction Year	2013
Summer draft	7.37 m
Dimensions	
Length	72 m
Width	18 m
Bollard pull	
Bylgia	200 t
Kolga	212 t

(b) Bylgia's and Kolga's main specifications

Figure A.5: HMC's Bylgia and Kolga

A.3. Present day

Nowadays Heerema Group consists of three companies: Heerema Marine Contractors (HMC), Heerema Fabrication Group (HFG), and Heerema Engineering Solutions (HES). HFG operates two fabrication yards: one in Vlissingen (NL) and one in Opole (POL). HES offers custom engineering and consultancy services to developers, contractors, and suppliers within the offshore renewable industry, including, but not limited to HMC. HMC is currently broadening its focus from the Oil & gas (T&I and decommissioning) business to also incorporate the offshore wind business.

B

LiftDyn description leaflet

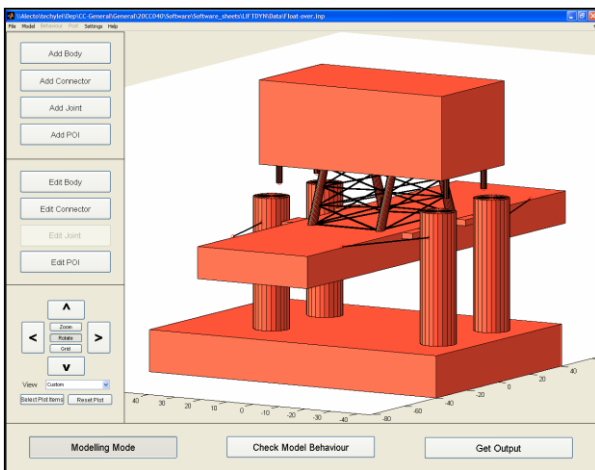


LIFTDYN

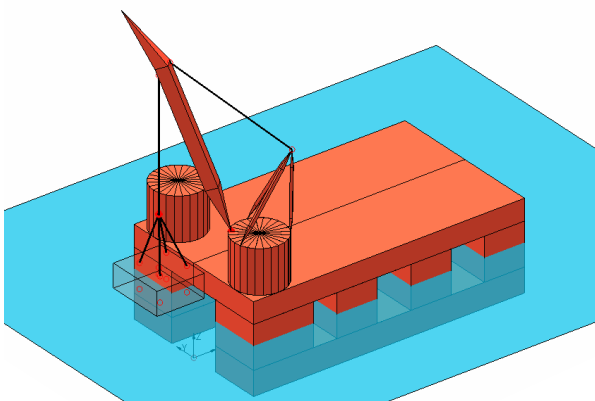
Multibody hydro-dynamic analysis in the frequency domain

The possible risks and the workability of an offshore operation in a particular sea condition are determined by the motion response of the crane vessel, the lifted object and the cargo barge during various stages of the lift procedure. In addition, the forces in the hoisting arrangement or the possible impact between the lifted object and the cargo barge might be limiting the lift operation.

LIFTDYN is an in-house developed computer code that is designed to model and solve general linear hydrodynamic problems in the frequency domain. The program features a graphical user interface enabling visual checking options.



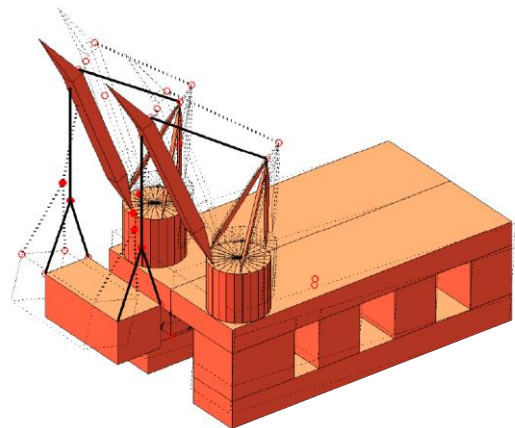
The program can solve systems consisting of rigid bodies connected to each other or to the earth by springs, dampers and hinges. In this way, all linear dynamic systems can be modeled irrespective of the number of bodies or connectors.



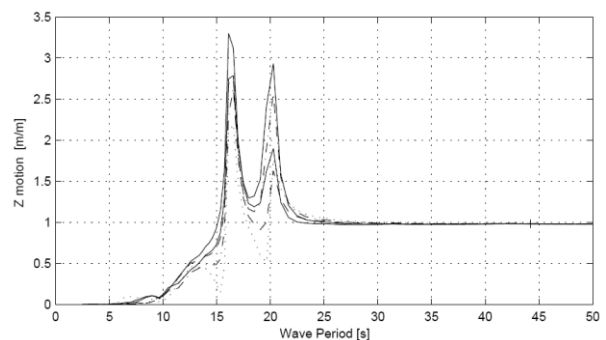
The bodies may have frequency dependent (added) mass and damping, and frequency

dependent exciting forces, which can be calculated with any diffraction code. Linear damping may be added to represent the viscous damping not calculated by the diffraction analysis code.

The calculation procedure includes animation of the all structural mode shapes, which give insight in the hydrodynamic behavior of the system and can be used to optimize lift arrangements, etc.



The resulting Response Amplitude Operators (RAO) calculated by LIFTDYN can be post-processed to a motion, velocity or acceleration RAO at any desired point relative to any other point. A RAO of the force in a connector can also be generated. A generated RAO can be used to produce the significant response in a specific seastate. Furthermore, limiting criteria can be defined to obtain operability curves indicating the maximum allowable wave height as a function of the spectral period.



The results of LIFTDYN can be exported imported in other applications, i.e. to perform a weather downtime assessment taking into account actual motion limits, or for motion prediction during the offshore execution.



Literature Analysis

The sources used in this literature research are the foundation upon which the thesis is built. This appendix analyses the used sources briefly and presents some visualisations of the used data.

C.1. Qualitative analysis

During the literature review, a systematic strategy was used to determine the relevant parts of literature documents. First the title, author and year were checked. If these seemed relevant, the abstract and conclusion were read or scanned. If any interesting aspects appeared, these parts, or sometimes the whole paper was read. After reading, any interesting references would be noted down for later review. Through subject titles, fields of interest and advice of supervisors (or their colleagues) a set of literature was found, which was reviewed piece by piece. The set was updated throughout the research to filter out irrelevant subjects and add new subjects.

The literature used in this literature review was aimed to be diverse, in-depth, and up to date. Sources were used from different disciplines, time periods and types (papers, books, theses, etc.). News articles were used to sketch an image of the current offshore wind energy market and its trends and goals. In-depth, technical papers were used to assess topics relevant to the subject. And finally, sources from several industry perspectives were used to summarize discussions and form conclusions regarding the literature review.

C.2. Quantitative analysis

In total, 103 diverse sources were referenced in this literature review. Of these 103, 12 were used solely as reference to figures used in the thesis. The other 91 were used for the contents of the literature research. Please note that more sources were used in the overall duration of the project, but only these 93 were selected to reference to. Figure C.1 shows a Pareto chart of the date-dependency of the sources referenced to. As can be observed, almost all sources originate in the 21st century. A majority of the sources is even from the current decade. This shows that the literature used is up-to-date and most state-of-the-art knowledge is implemented. Since almost all of the latest sources are based on previous work, it is not to be expected that main principles of physics are left unaccounted for.

Figure C.2 shows a bar chart of the various categories of sources. It can be noticed that a lot of sources concern the categories 'Connections', 'General'¹, or 'Heave Compensation (HC)'. The main reason for this is that in these categories, a lot of developments are still ongoing. Therefore, a lot of diverse sources with different points of view are considered in the literature review. Other categories like 'Structural Dynamics' or 'Hydromechanics' contain less sources, since less has changed regarding the offshore industry in these categories, in other words, a more general consensus has been reached on their application to the offshore industry. A category that shows few sources but is still quite popular or relevant is the 'Installation Methodology' category. The reason for having so little sources is due to

¹General' here means no technical content. The content of these sources is for example concerning the wind energy market.

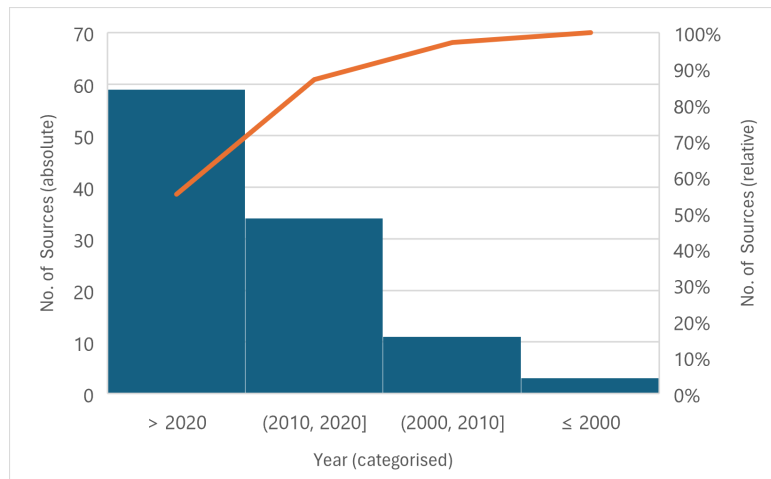


Figure C.1: Pareto chart of sources used in the literature research ordered per decade.

the fact that 'Installation Methodology' is mentioned in many sources but is often not considered the 'main' category of the source and therefore not taken into account in the figure.

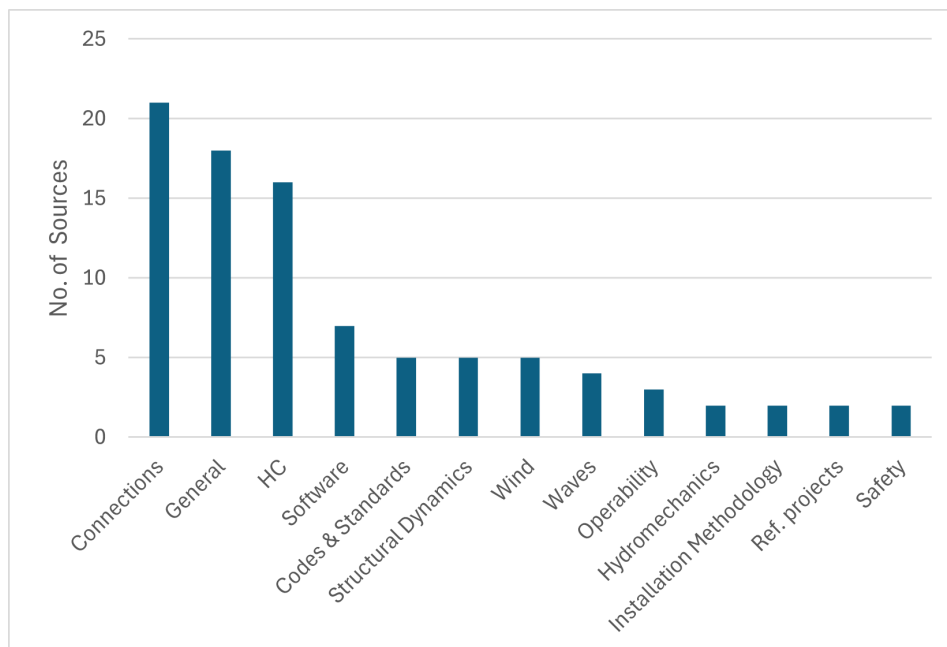


Figure C.2: Sources used in the literature research categorised by subject. Please note that the number of sources used is not directly correlated to the extent to which the subject is discussed.

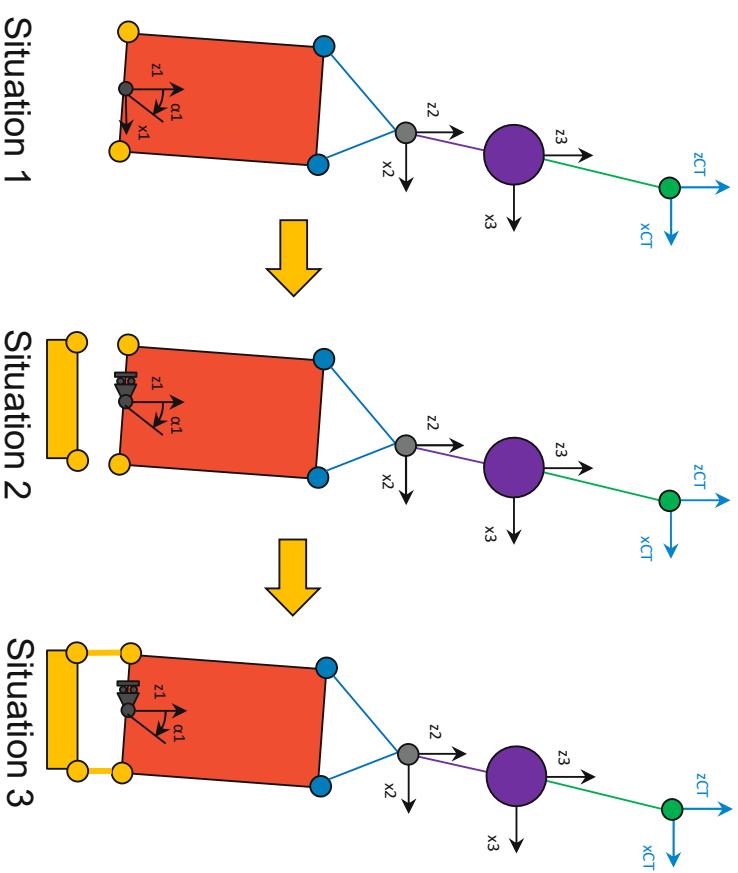
D

Equation of Motion Python Model

Model Situations

1. Free hanging
2. X-motion WTG restricted; impact; **no** QCS* stiffness
3. X-motion WTG *restricted*; impact; **incl.** QCS* stiffness

- SIT_1 not modeled in Python
- SIT_2 is most important: determines if QCS* can be activated.



*QCS: Quick Connection System

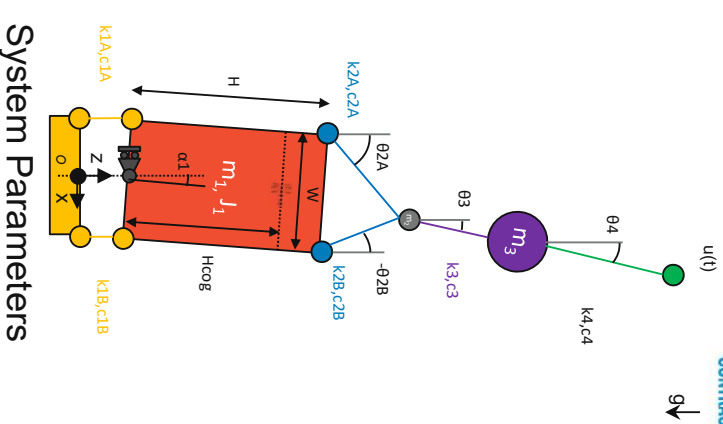
Python Model Equations Of Motions



- Situation 3 as starting point; situation 2 = situation 3 + k1=0
- Lagrangian approach: $\frac{d}{dt} \left(\frac{\partial T}{\partial \dot{q}_s} \right) + \frac{\partial V}{\partial q_s} = 0, \quad s = 1 \dots 6$
- U(t) motion as external force
- Small elongation linearization

$$T = \sum_{s=1}^6 \frac{1}{2} m_s v_s^2 + \frac{1}{2} J_s \omega_s^2$$

$$V = \sum_{s=1}^6 \frac{1}{2} \hat{k}_s e_s^2 + m_s g h_s, \quad \hat{k}_s = k_s + \frac{d}{dt} c_s$$



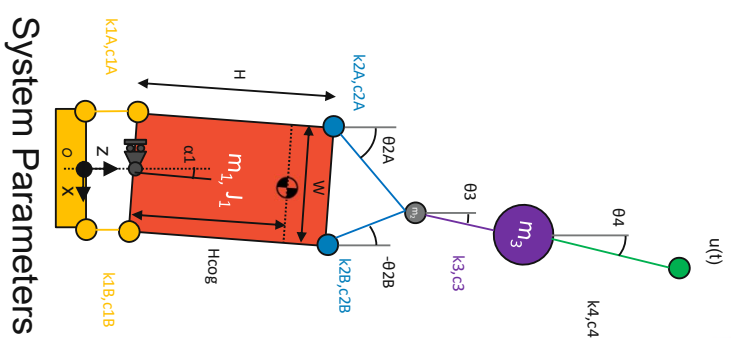
System Parameters

Python Model Equations Of Motions



- K, C and M matrices (6x6)
- F vector (6x1)

$$M = \begin{bmatrix} m_1 H_{cog}^2 + J_1 & 0 & 0 & 0 & 0 & 0 \\ 0 & m_1 & 0 & 0 & 0 & 0 \\ 0 & 0 & m_2 & 0 & 0 & 0 \\ 0 & 0 & m_2 & m_2 & 0 & 0 \\ 0 & 0 & 0 & 0 & m_3 & 0 \\ 0 & 0 & 0 & 0 & 0 & m_3 \end{bmatrix}$$



System Parameters

Python Model EOM implementation



MARINE CONTRACTORS

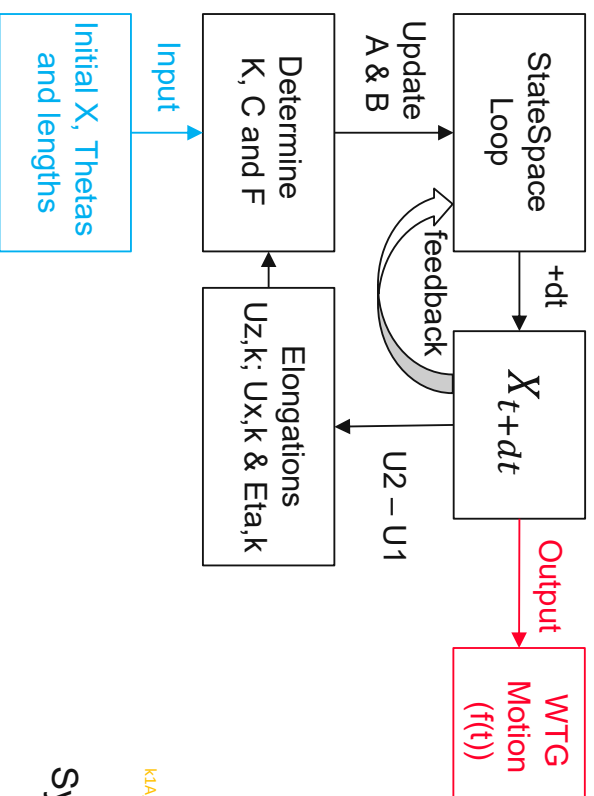
- Angles used for K-/C-matrix and F-vector definition
- StateSpace formulation for loop in time:

$$X_{t2} = X_{t1} + dt * (A^{-1}(F - BX_{t1}))$$

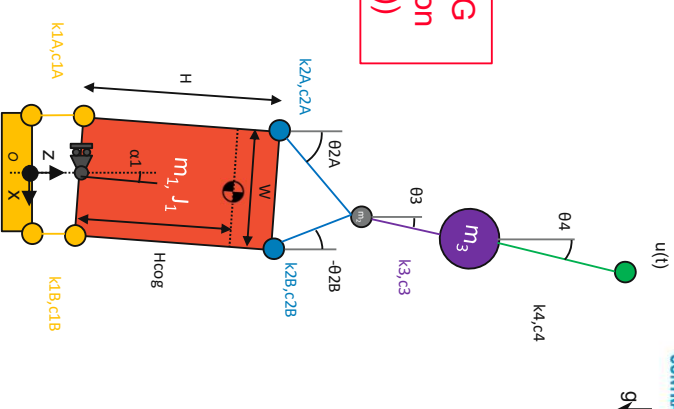
$$A = \begin{bmatrix} M & 0 \\ 0 & I \end{bmatrix}$$

$$B = \begin{bmatrix} C & K \\ -I & 0 \end{bmatrix}$$

$$X_t = \begin{pmatrix} v_t \\ p_t \end{pmatrix}$$



System Parameters



E

LiftDyn input model

The crane tip input signal is derived from the crane tip RAOs, that are calculated in a separate LiftDyn model. Here, a brief description of this model is given.

E.1. Model Input

For the model, an existing vessel model of the Sleipnir is used with the configuration as described in Table 4.3. The WTG and rigging are simplified to one rigid body and one sling per crane. The same WTG properties are used as described in Table 4.2. For the rigging, a stiffness of 2.7 GN and a length of 16m is used. The hoist wires have a length of 32m and a stiffness of 3.4 GN.

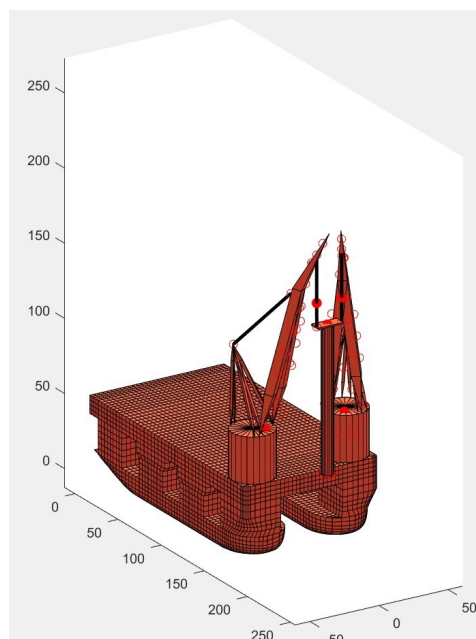


Figure E.1: Visualisation of LiftDyn model used to generate Crane Tip motion RAOs.

E.2. Model Output

Then the model calculates the model behaviour; the Mode Shapes. These are animated and checked, before the output is generated. Output can be generated in many forms: RAOs, responses or operability curves. As only the RAOs are required, these are obtained for the crane tip motion. The X motion and Z motion RAOs are generated in the global axes system and exported to an Excel file. This file is later on imported in the OrcaFlex and Python models.

Nomenclature

Definitions

- **Balance of Plant:** includes all civil and electrical works that are part of a wind farm, such as inter array cables, export cables, foundations, grid connection, and substations. Everything excluding the wind turbines.
- **Offshore Wind Turbine:** Structure converting wind energy into electric energy consisting of a Wind Turbine Generator (WTG) and its support structure.
- **Stability:** If upon releasing a structure from a virtually displaced state, the structure returns to its original configuration, then the structure is in stable equilibrium. The structure is in a stable position.
- **Outlining Phase:** During the outlining phase of an installation operation the component to be installed is positioned above its final position. In other words; the X and Y coordinate of the component are matching with the final position. After the alignment phase, the component only has to be lowered to its landing position. The component is constrained from moving in the horizontal plane during the final lowering operation.

Abbreviations

Abbreviation	Definition
AHC	Active Heave Compensator
ALARP	As Low As Reasonably Possible
APHC	Adaptive Passive Heave Compensation
CAGR	Compound Annual Growth Rate
CAPEX	Capital Expenditures
CoG	Centre of Gravity
DCV	Deepwater Crane Vessel
DOF	Degree of Freedom
DP	Dynamic Positioning
DNV	Det Norske Veritas
EOM	Equation of Motion
EU	European Union
FCT	Flange Clamping Tool
FD	Frequency Domain
FEM	Finite Element Method
FID	final investment decision
FLS	Fatigue Limit State
FWT	Floating Wind Turbine
G&B	Guides and Bumpers
GBF	Gravity Based Foundation
GBS	Gravity Based Structure
HC	Heave Compensation
HES	Heerema Engineering Solutions
HSE	Health, Safety and Environment
HFG	Heerema Fabrication Group
HLV	Heavy Lift Vessel
HMC	Heerema Marine Contractors
LCOE	Levelized Cost Of Electricity
LLF	Lower Lifting Frame

Abbreviation	Definition
MP	Mono-pile
MPC	Model Predictive Control
MRU	Motion Reference Unit
MWL	Mean Water Level
NHA	Nacelle Hub Assembly
ODE	Ordinary Differential Equations
OEM	Original Equipment Manufacturer
OWT	Offshore Wind Turbine
OWF	Offshore Wind Farm
PDF	Probability Density Function
PHC	Passive Heave Compensator
PLC	Programmable Logic Controller
QCS	Quick Connection System
RAO	Response Amplitude Operator
RNA	Rotor Nacelle Assembly
SMPM	Single Most Probable Maximum
SSCV	Semi-Submersible Crane Vessel
SWL	Safe Working Load
TD	Time Domain
TP	Transition Piece
UK	United Kingdom
US	United States
USF	Upper Stabilising Frame
ULS	Ultimate Limit State
VIV	Vortex Induced Vibrations
WLL	Working Load Limit
WTG	Wind Turbine Generator
WoW	Waiting on Weather

Symbols

Symbol	Definition	Unit
A	Area	[m ²]
A_γ	normalizing factor	[-]
a	amplitude	[m]
C	Compression ratio	[-]
C_D	drag coefficient	[-]
C_L	lift coefficient	[-]
c	Damping	[Ns/m]
d	Water depth	[m]
E	Young's Modulus	[Pa]
e	elongation	[m]
E_f	variance density spectrum	[m ² s]
F	force	[N]
F_c	crane load as part of static WTG weight	[%]
F_{stab}	percentage of the time in which the activation of the C1 QCS is possible (see Table 5.3)	
f	frequency	[Hz]
$G(f)$	peak enhancement function	[-]
g	gravitational acceleration	[m/s ²]
H	(wave) Height	[m]
I	(wind) Intensity	[-]
K	Kinetic energy	[J] OR
K	stiffness matrix	[N/m]
k	Stiffness	[N/m]
L	Lagrangian function	[J]
L	Length	[m]
m	mass	[kg]
mT	metric Ton (1000 kg)	[kg]
P	Potential energy	[J]
p	pressure	[Pa]
S	Spectrum	[m ² s]
s	stroke	[m]
T	Wave period	[s]
T_{stab}	time required to activate the C1 QCS (see Table 5.3)	
t	time	[s]
U	Wind Speed	[m/s]
u	displacement	[m]
V	Velocity	[m/s]
W	Watt	[J/s]
X	model state	[rad], [m], [rad/s], or [m/s]
x	horizontal (fore - aft) coordinate	[m]
y	horizontal (starboard - port side) coordinate	[m]
z	height or vertical coordinate	[m]
Z_{max}	maximum vertical misalignment of the C1 Connection stabbing slots (see Table 5.3)	
α	rotation of WTG around y	[°]
γ	peak enhancement factor	[-]
ϵ	spectral width	[-]
ζ	critical damping ratio	[-]
η	water surface elevation	[m]
η_i	motion of a rigid body in direction i	[rad] or [m]

Symbol	Definition	Unit
θ	rotation of wire ropes around y	[rad]
λ	Wavelength	[m]
μ	expected value	[m]
ρ	Density	[kg/m ³]
σ	standard deviation	[m/s]
ϕ	phase shift	[rad]
ω	frequency	[rad/s]

List of Figures

1.1	Selection of the offshore wind industry heavy lift crane vessel capacity. The vessels in the green area are estimated to be able to install 15MW turbines.	2
1.2	Total installed WTG capacity, in megawatts, in Northern Europe between 2016 and 2024. Note that the 2024 data are not complete, since not all 2024 data is available [90].	2
1.3	New offshore installations, global, in megawatts [108].	3
1.4	Render of dual crane whole WTG installation with SSCV Sleipnir	5
2.1	Schematic of the Mono-pile, gravity-based and jacket offshore wind turbine support structures [55].	8
2.2	Support structure type versus maximum development water depth and installation date, for global projects excluding China. The bubble area is approximately proportional to installed capacity [11].	9
2.3	Schematic of spar, semi-submersible and tension leg platform floating wind turbines.[55].	10
2.5	Offshore Wind Turbine Installation Methodologies and the number of critical lifts associated with them [55].	12
2.6	The lifting configuration used for the installation of the Hywind Pilot Project. The clamping device indicated by number 7 is patented by SAIPEM and is a type of Lower Lifting Frame (LLF). The numbers 40 represent the crane's blocks. Part 11 is the Upper Stabilising Frame (USF) [87].	13
2.7	The lifting configuration used for the installation of the Beatrice Wind Farm Demonstrator Project [84].	14
2.8	Examples of the three considered transport strategies.	15
2.9	Windfarm Installation Vessel (WIV) concept by Huisman [9].	16
2.10	Caption	17
2.11	Tensile bar [89].	17
2.12	Three connection types used in offshore wind turbines [31, 30, 12].	18
2.13	Bolted ring flange connection and equivalent single bolt segment [67].	19
2.14	Flange Clamp Tool (FCT) from IQIP	19
2.15	The Slip Joint working principle of a friction-based connection.	20
2.16	The C1 Wedge Connection working principle [12].	21
2.17	Quick Connection System (QCS) [12].	22
2.18	Standard PHC & equivalent Spring-Mass-Damper Model [16].	23
2.19	Bode diagrams showing an uncompensated (or poorly compensated) system operating within the wave spectrum and a compensated system with the damped natural frequency lower than the wave frequency spectrum [111].	24
2.20	AHC Electro-mechanical system [32].	24
2.21	An example of the behaviour of a MPC system [111].	25
2.22	An example of an APHC model. Here, controlling the valve opening determines the stiffness parameter [47].	26
3.1	Wind speed energy per frequency. The 'Spectral Gap' represents the relatively low spectral density around a frequency of 1.0 cycle/hr [112]. The short-term effects are relevant for this thesis and a mean wind speed is incorporated to capture the long-term effects.	28
3.2	Lift and drag forces on a wind turbine air foil (blade cross-section) [99].	30
3.3	Schematic representation of a 5MW blade, showing air foils and their changing cord lengths and orientation [59].	31
3.4	31
3.5	Variance density spectrum showing the variance of (a part of) the spectrum can be obtained with integration [46].	32

3.6	PM and JONSWAP spectral shapes [102].	34
3.7	Definition of vessel motions in 6 DOF's [58].	34
3.8	RAO with frequency areas [58].	35
3.9	General methodology to establish allowable operational limits [39].	37
3.10	Stable and unstable mechanical systems (gravity is presumed to act downward here). A small displacement of the ball away from its equilibrium position will (a) be opposed by the action of gravity and the object will move back toward its equilibrium location (top-left) ; (b) be enhanced by the action of gravity and the object will move away from its equilibrium location (top-right) ; (c) not produce a new force (bottom-left) ; or (d) possibly place the ball beyond its region of stability, depending on the displacement (bottom-right) [63].	38
3.11	Lost working day incidents in 2018 [34].	40
4.1	Visualization of the clamping of the Lower Lifting Tool (blue part) on the C1 Wedge Connection upper flange.	45
4.2	Visualization of the Sleipnir model [92].	46
4.3	Vessel definitions [92].	46
4.4	Wind and wave headings definition.	46
4.5	Parameters used to describe the elongation of a spring element between particles a and b for small elongations.	49
4.6	Lumped element model used to develop the Python model. The masses M1, M2 and M3 represent the WTG, Rigging Shackle and Crane Block, respectively. The green element is the Crane Tip, and its motion is considered an input signal to the model.	49
4.7	Eigen periods and eigenmodes of Python Model. The modes are ranked from low to high eigenfrequencies. Each row represents a single DOF of the system, with the letters referring to the direction of the DOF and the numbers referring to the body of the DOF. Z2, for example, is the vertical motion of the Shackle (Mass 2). Alpha is the rotation of the WTG. The mode shapes (eigenvectors) are scaled such, that the largest contributing DOF has a value of 1.0.	50
4.10	Visualisation of the Fundamental OrcaFlex model. The left figure shows a general model view with the components labelled. The right figure shows the shaded graphics view including the DOFs of the modelled masses (green DOFs are enabled, red DOFs are disabled).	53
4.11	Eigen periods and eigenmodes of Fundamental OrcaFlex Model. The modes are ranked from low to high eigenfrequencies. Each row represents a single DOF of the system, with the letters referring to the direction of the DOF and the numbers referring to the body of the DOF. Z2, for example, is the vertical motion of the Shackle (Mass 2). Alpha is the rotation of the WTG. The mode shapes (eigenvectors) are scaled such, that the largest contributing DOF has a value of 1.0.	54
5.1	Visualisation of the Enhanced OrcaFlex model. The left figure shows a general model view with the components labelled. The right figure shows the shaded graphics view including the DOFs of the modelled masses (green DOFs are enabled, red DOFs are disabled).	59
6.1	Operability for Situation 2 without Heave Compensation and $F_c = 100\%$	68
6.2	Operability for Situation 2 with Heave Compensation ($k_{HC} = 400mT/m$) and $F_c = 100\%$	68
6.3	Scatter Table with SMPM Values for impact velocity in Situation 2 with HC (raw output). The darker the background colour, the larger the SMPM value.	69
6.4	Operability without Tower Bending incorporated for Situation 2 with Heave Compensation.	70
6.11	Spectral density for WTG Z motion for the varies Heave Compensation stiffnesses. Figure b) is the zoomed in version of Figure a) around the pendulum eigenfrequency. These Power Spectral Densities are directly calculated from the time domain simulations for $T_p = 7.0s$ and $H_s = 0.8m$ by taking the Fourier transform of the time history result.	79
6.15	Optimised operability for Situation 2 and 3 with HC, a maximum WTG rotation of 1.5° , a Z_{max} of 0.04m, a F_{stab} of 10% and 16 QCS Wedges.	84

A.1	HMC's Sleipnir	99
A.2	HMC's Aegir	100
A.3	HMC's Thialf	100
A.4	HMC's Balder	101
A.5	HMC's Bylgia and Kolga	101
C.1	Pareto chart of sources used in the literature research ordered per decade.	105
C.2	Sources used in the literature research categorised by subject. Please note that the number of sources used is not directly correlated to the extent to which the subject is discussed.	105
E.1	Visualisation of LiftDyn model used to generate Crane Tip motion RAOs.	112

List of Tables

2.1	Comparison of PHC and AHC. The type(s) mentioned possess the described positive functionality.	25
4.1	Lifting configuration overview. Both the situation without as the situation with Heave Compensation is addressed. Visualisations of the rigging arrangement with and without HC are given in Figure 5.1 and 4.10.	44
4.2	Wind Turbine Generator (WTG) Parameters	45
4.3	Additional Sleipnir Installation Parameters	45
5.1	Static Wind Load in global X-direction with a mean wind speed of $10m/s$. Here, the unpitched blades are loaded with maximal drag forces while the pitched blades are loaded with minimal drag forces.	60
5.2	Passive Heave Compensation Parameters	61
5.3	Critical Events and Limiting Parameters	62
5.4	Hoist wire lengths for Situation 3 simulations	63
5.5	Main modelling Choices and Argumentation	66
6.1	Fraction of area under operability graph for Situation 2 as a measure for operability as a function of initial crane load percentage F_c . The increase in operability levels of for $F_c = 80\%$ and lower.	81